Structural Behavior of Reinforced Concrete Deep Beams Strengthened in Flexure with CFRP

by

Mustafa Mohammed Raheem

B.S., University of Babylon, Babylon, 2010
M.S., University of Technology, Baghdad, 2012
M. Eng, The University of Kansas, Lawrence, 2017

AN ABSTRACT OF A DISSERTATION

submitted in partial fulfillment of the requirements for the degree

DOCTOR OF PHILOSOPHY

Department of Civil Engineering
College of Engineering

KANSAS STATE UNIVERSITY
Manhattan, Kansas

2019

Abstract

This research presents an analytical and experimental investigation for the use of flexural CFRP sheets as a strengthening technique to improve the shear capacity of reinforced concrete deep beams. The analytical work presents a new analysis method that is developed to predict the response of reinforced concrete deep beams with and without flexural CFRP strengthening. The method utilizes the truss analogy approach that is extended from the Strut-and-Tie Model (STM) for unstrengthened beams. In contrary to STM, the new method is used to capture the full structural response of unstrengthened beams by modeling a single truss. On the other hand, the new method is used to predict the entire response of strengthened beams by assuming the beam to be composed of two parallel compatible trusses. The first truss has its lower chord member composed of the steel bars while the second truss has its lower chord member composed of the flexural CFPR sheets. By imposing the compatibility condition of a statically indeterminate truss, the contribution of each truss is realized. The experimental work was conducted on three deep beam specimens with identical rectangular cross-sectional area. The first beam was tested as a control beam, and the other two beams were strengthened in flexure with four layers of flexural CFRP sheets anchored by two different flexural anchorage devices. The first strengthened beam was anchored with GFRP patches applied to both sides of the beam. The second strengthened beam was anchored with side GFRP bars inserted longitudinally to both sides of the beam. The comparison between the analytical and experimental results showed reasonable agreement and asserted the validity of the analytical approach and methodology developed in this study.

Structural Behavior of Reinforced Concrete Deep Beams Strengthened in Flexural with CFRP

by

Mustafa Mohammed Raheem

B.S., University of Babylon, Babylon, 2010
M.S., University of Technology, Baghdad, 2012
M. Eng, The University of Kansas, Lawrence, 2017

A DISSERTATION

submitted in partial fulfillment of the requirements for the degree

DOCTOR OF PHILOSOPHY

Department of Civil Engineering
College of Engineering

KANSAS STATE UNIVERSITY
Manhattan, Kansas

2019

Approved by:

Major Professor
Hayder A. Rasheed

Copyright

Abstract

This research presents an analytical and experimental investigation for the use of flexural CFRP sheets as a strengthening technique to improve the shear capacity of reinforced concrete deep beams. The analytical work presents a new analysis method that is developed to predict the response of reinforced concrete deep beams with and without flexural CFRP strengthening. The method utilizes the truss analogy approach that is extended from the Strut-and-Tie Model (STM) for unstrengthened beams. In contrary to STM, the new method is used to capture the full structural response of unstrengthened beams by modeling a single truss. On the other hand, the new method is used to predict the entire response of strengthened beams by assuming the beam to be composed of two parallel compatible trusses. The first truss has its lower chord member composed of the steel bars while the second truss has its lower chord member composed of the flexural CFPR sheets. By imposing the compatibility condition of a statically indeterminate truss, the contribution of each truss is realized. The experimental work was conducted on three deep beam specimens with identical rectangular cross-sectional area. The first beam was tested as a control beam, and the other two beams were strengthened in flexure with four layers of flexural CFRP sheets anchored by two different flexural anchorage devices. The first strengthened beam was anchored with GFRP patches applied to both sides of the beam. The second strengthened beam was anchored with side GFRP bars inserted longitudinally to both sides of the beam. The comparison between the analytical and experimental results showed reasonable agreement and asserted the validity of the analytical approach and methodology developed in this study.

Table of Contents

List of Figures viii
List of Tables x
Acknowledgements xi
Dedication xii
Chapter 1 - Introduction 1
1.1 General 1
1.2 Deep Beams 2
1.2.1 Deep Beam Failures 3
1.3 Fiber Reinforced Polymer Strengthening System 6
1.3.1 Fiber Materials 7
1.3.2 Matrix 8
1.4 CFRP Strengthening in RC Members 9
1.5 Debonding Problems in CFRP Strengthened RC Beams 11
1.6 Objective 12
1.7 Dissertation Layout 12
1.8 References 13
Chapter 2 - Literature Review 15
2.1 Introduction 15
2.2 Available Experimental Studies on Reinforced Concrete Deep Beams 15
2.3 Existing Models and Shear Theories of Reinforced Concrete Deep Beams 18
2.3.1 Tooth Model 18
2.3.2 The Modified Compression Field Theory (MCFT) 19
2.3.3 Strut-and-Tie Model (STM) 21
2.3.3.1 Strut-and-Tie Model According to ACI 318 25
2.3.4 Finite Element Method (FEM) 28
2.4 Available Studies on Nonlinear Analysis of Reinforcement Concrete Deep Beams 29
2.5 Available Experimental and Analytical Studies on RC Beams Strengthened by FRP 32
2.6 References 38
Chapter 3 - Experimental Work and Test Results 43

3.1 General 43
3.2 Material Properties 43
3.2.1 Concrete 43
3.2.2 Steel Reinforcement 44
3.2.3 Fiber Reinforced Polymer (FRP) 46
3.2.4 Bonding Materials 47
3.3 Deep Beam Specimens 48
3.4 Test Setup and Instrumentation 53
3.5 Test Results and Discussion 56
3.6 References 64
Chapter 4 - Analytical Work and Prediction Results 65
4.1 General 65
4.2 Assumptions and Analytical Procedure 65
4.3 Confirmation Examples 72
4.3.1 Beams from Experimental Program 72
4.3.1.1 Beam (CON) 73
4.3.1.2 Beam (CSW-GSP) 77
4.3.2 Beams from Literature 82
4.3.2.1 Unstrengthened Beam (Control) 83
4.3.2.2 Strengthened Beam (S1) 84
4.4 References 87
Chapter 5 - Conclusions and Recommendations 88
5.1 General 88
5.2 Conclusions 88
5.2.2 Conclusions from Experimental Work 88
5.2.2 Conclusions from Analytical Work 89
5.3 Limitations of The Study 89
5.4 Recommendations for Future Work 90

List of Figures

Figure 1-1 Example of a deep beam [5] 3
Figure 1-2 Crack patterns for beams with $2.5 < L_a/d < 4$ 4
Figure 1-3 Modes of failure of deep beams [8] 6
Figure 1-4 Typical composition of FRP material [9] 7
Figure 1-5 Stress-strain relationship of fibers and steel [10] 8
Figure 1-6 Stress-strain curves of fibers, FRP and matrix [11] 9
Figure 1-7 Applications of CFRP for strengthening an actual bridge 10
Figure 1-8 Debonding failure modes of RC beam strengthened with CFRP in flexural [13] 11
Figure 2-1 Kani's tooth model [9] 19
Figure 2-2 Diagram used in Rahal's method [15] 20
Figure 2-3 STM for a deep beam 22
Figure 2-4 STM nodes [18] 23
Figure 2-5 Type of STM struts 24
Figure 2-6 Reinforcement crossing a strut [7] 26
Figure 2-7 One-and two-panel truss models [7] 28
Figure 2-8 Park and Kuchma strut-and-tie model for a deep beam [27] 31
Figure 2-9 End anchorage made of steel plates and bolts [41] 36
Figure 2-10 New flexural anchorage techniques [43] 37
Figure 3-1 Compression testing of the concrete cylinders 44
Figure 3-2 Steel tensile test 45
Figure 3-3 Stress-strain relationship for steel reinforcing bars 46
Figure 3-4 FRP sheets 46
Figure 3-5 Bonding Materials (a) Parts A and B of the epoxy; (b) Mixing of the epoxy 47
Figure 3-6 History of the tested deep beam specimens 49
Figure 3-7 Geometry and reinforcement of the tested deep beam specimens 50
Figure 3-8 Geometry and details of specimen (CSW-GSP) 52
Figure 3-9 Geometry and details of specimen (CSW-GSB) 53
Figure 3-10 Introduction of notches on the CFRP sheets 54
Figure 3-11 Laboratory test setup 55

Figure 3-12 Location of side FRP strain gages of specimen (CSW-GSP) 56
Figure 3-13 Cracks pattern of beam specimen (CON) 56
Figure 3-14 Load vs. mid-span deflection for beam specimen (CON)..... 57
Figure 3-15 Cracks pattern of beam specimen (CSW-GSP) 58
Figure 3-16 Load vs. mid-span deflection for beam specimen (CSW-GSP)..... 59
Figure 3-17 Load vs. mid-span FRP strain for beam specimen (CSW-GSP)..... 59
Figure 3-18 Load vs. GFRP patch strain at the failure for beam specimen (CSW-GSP)..... 60
Figure 3-19 Cracks pattern of beam specimen (CSW-GSP) 61
Figure 3-20 Load vs. mid-span deflection for beam specimen (CSW-GSP)..... 62
Figure 3-21 Load vs. mid-span FRP strain for beam specimen (CSW-GSP)..... 62
Figure 3-22 Load vs. mid-span deflection for all tested deep beam specimens 63
Figure 4-1 Concrete stress-strain curve 66
Figure 4-2 Steel bilinear stress-strain relationship..... 67
Figure 4-3 Flowchart of proposed approach for unstrengthened deep beam..... 68
Figure 4-4 Two parallel trusses for a deep beam strengthened in flexure with CFRP 69
Figure 4-5 Flowchart of proposed approach for strengthened deep beam..... 72
Figure 4-6 Truss model of specimen beam (CON)..... 73
Figure 4-7 Top nodal zone of specimen beam (CON)..... 75
Figure 4-8 Load-deflection comparison of beam specimen (CON) 77
Figure 4-9 Truss 1 (concrete + steel) model of beam specimen (CSW-GSP)..... 78
Figure 4-10 Truss 2 (concrete + CFRP) model of beam specimen (CSW-GSP) 78
Figure 4-11 Load-deflection comparison of beam specimen (CSW-GSP) 81
Figure 4-12 Typical beam dimensions of the literature beams..... 82
Figure 4-13 Load-deflection comparison of unstrengthened beam (Control) 84
Figure 4-14 Load-deflection comparison of strengthened beam (S1) 86

List of Tables

Table 1-1 Comparison between ordinary beams and deep beams 3
Table 1-2 Properties of concrete, steel and CFRP [10] 10
Table 2-1 ACI 318-14 stress limits and strength reduction factors 26
Table 3-1 Concrete mix properties of test beams 43
Table 3-2 Test results of reinforcement bars 44
Table 3-3 Mechanical properties of FRP sheets 47
Table 3-4 Technical properties of bonding materials 48
Table 3-5 Designation of the tested beam specimens 51
Table 3-6 Summary of results of the tested beam specimens 63
Table 4-1 Prediction and experimental results of experimental program beams 81
Table 4-2 Prediction and experimental results of literature beams 87

Acknowledgements

Foremost, I thank God, who gave me health and the necessary strength to carry out the present research. **I** wish to express my gratitude and sincere appreciation to my sponsor, The Higher Committee for Education Development in Iraq, for the scholarship provided to me to pursue my graduate study in the United States. **I** wish to express my grateful thanks to my family and all my friends for their encouragement and unending support at all times. **I** would like to express my deep thanks to my supervisor Prof. Hayder A. Rasheed for his encouragement, valuable guidance, helpful advice and efforts during the preparation of this work. **F**inally, special thanks to the research technologists, Cody Delaney and Ben Thurlow, at the structural laboratory at Kansas State University for their valuable support.

Mustafa M. Raheem

2019

Dedication

I dedicate this work to…

My mother for her love and care

My family for their interest and love

My friends for their support and encouragement

Chapter 1 - Introduction

1.1 General

It is well known that concrete is an excellent building material that offers many superior advantages as a construction material. However, it is also known to have high compressive strength and weak tensile strength. A concrete beam without any form of reinforcement will crack and fail when subjected to a relatively small load. The failure occurs in a sudden brittle manner. The most common way to reinforce a concrete member is to use steel reinforcement wherever concrete is anticipated to respond in direct tension or shear. Since a concrete structure usually has a very long design life, it is not unusual for the demands on the structure to change over time. The structure may have to carry larger loads at a later date, or fulfil new standards. In some cases, a structure will have to be repaired after being subjected to an extreme load event. Another reason for a need to strengthen can be due to errors that have been made during the original design or construction phase. If any of these situations should arise, it needs to be determined whether it is more economical to strengthen the existing structure or to replace it. In comparison to building a new structure, strengthening an existing one is often more limiting, since the conditions are already set **[1]**.

There are many different ways to repair or strengthen a concrete structure. There is often a possibility to use a section enlargement technique to change the physical appearance of a member and in that way giving it improved properties in strength and stiffness. However, this also means that the member needs more space which is not always possible **[1]**. In recent decades, using carbon fiber reinforced polymer (CFRP) laminates or sheets has proven to be an effective means of strengthening reinforced concrete (RC) members. One advantage with this technique is that there are no large physical changes in the size of the member, high strengthening levels can be achieved.

However, premature failures such as laminate peeling and separation can significantly limit the capacity of the retrofitted members from being attained. Laminate peeling or separation may occur due to the high longitudinal shear and transverse normal stresses at the ends of the laminates resulting from the abrupt curtailment of the laminates **[2]**.

Although many structural applications include the use of reinforced concrete deep beams, there has been very limited research into the behavior of such beams with external strengthening. Moreover, most design guidelines were developed for typical shallow beams with external FRP materials.

1.2 Deep Beams

Reinforced concrete deep beams have always been a subject of considerable interest in structural engineering applications. A deep beam in general, has an effective span to depth ratio much smaller than expected for typical beams. The ACI code defines deep beams as those, which have clear span to overall depth less than four, and should be loaded on the top face and supported on the bottom face of the beam. To facilitate compression struts being developed between the loads and support points **[3]**.

Reinforced concrete deep beams consist of a major component in the superstructure of bridges. They have been used in tall buildings, offshore structures, foundation walls, floor diaphragms, transfer girders, and bent caps **[4]**. A typical bent cap is shown in Figure 1-1.

The force transfer mechanism in deep beams differs from ordinary beams because the strain and stress pattern is nonlinear. Hence, the classical elastic beam theory of bending is not applicable to problem of deep beams. A deep beam exhibits a very complicated stress state that can be described by the strut and tie action since the mechanical behavior of deep beam is governed by shear. Accordingly, the materials and techniques used to upgrade the shear capacity of deteriorated and

defective deep beams should be well investigated **[6]**. A comparison between deep beams and ordinary beams is listed in Table 1-1.

Figure 1-1 Example of a deep beam [5]

Table 1-1 Comparison between ordinary beams and deep beams

No.	Ordinary beam	Deep Beam
1	Plane sections before bending remain plane sections after bending.	Plane sections before bending do not remain plane sections after bending.
2	Shear deformation is neglected.	Shear deformations become significant compared to pure flexure.
3	The strain profile can be considered linear until ultimate stage.	The strain profile is nonlinear even at elastic stage.
4	State of stress is simplified to one dimension.	Two dimensional state of stress is considered.

1.2.1 Deep Beam Failures

The shear span to effective depth ratio of deep beams determines the failure mode of such beams. Fundamentally, four modes of failure or their combinations can occur **[7]**:

1. Flexural failure;

2. Diagonal tension failure;
3. Shear-compression failure; and
4. Splitting failure (pure shear failure).

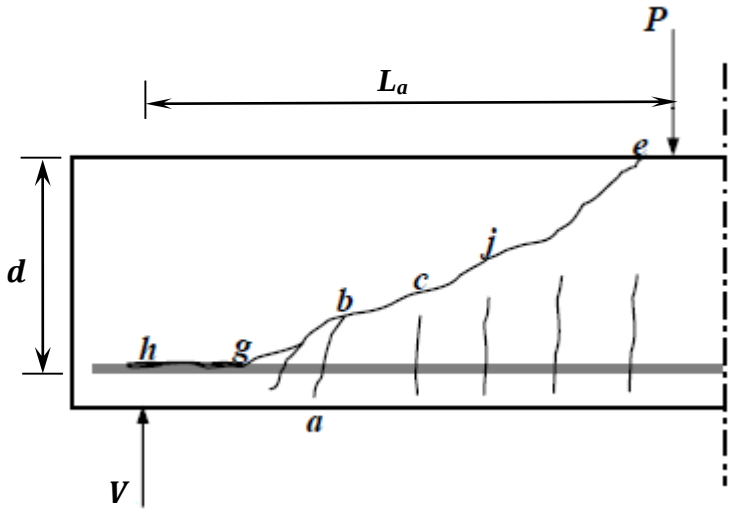

Figure 1-2 Crack patterns for beams with $2.5 < L_a/d < 4$

For beams with $2.5 < L_a/d < 4$:

Beams with (L_a/d) ratio lower than four tend to fail in shear, as shown in Figure 1-2. The flexural crack (a-b) would propagate towards the loading point gradually becoming an inclined crack, which is known as flexural-shear crack. With increasing shear force, failure usually occurs in one of two modes. If (L_a/d) ratio is relatively high, the diagonal crack would rapidly spread to (e), resulting in a collapse by splitting the beam into two pieces. This mode of failure is often called diagonal-tension failure. If (L_a/d) ratio is relatively low, the diagonal crack tends to stop somewhere at (j), and a number of random cracks may develop in the concrete around the longitudinal tension reinforcement. As the shear force is increased, the diagonal crack widens and propagates along the level of the tension reinforcement, see (Figure 1-2 crack g-h). This failure

mode is often called shear-tension failure or shear-bond failure. The ultimate load is not much higher than the diagonal cracking load **[7]**.

For beams with $1.0 < L_a/d < 2.5$:

For (L_a/d) ratio lower than 2.5 and greater than 1.0, the diagonal crack often forms independently. The beam usually remains stable after such cracking. Further increase in the shear force will cause the diagonal crack to penetrate into the concrete compression zone at the loading point, until eventually crushing failure of concrete occurs there. This inclined crack is steeper than that which occurs in flexural-shear case, suddenly develops and proceeds to propagate towards the neutral axis. This failure mode is usually called shear-compression failure. For this mode, the ultimate load is more than twice the diagonal cracking load **[8]**.

For beams with $L_a/d < 1.0$:

Three distinct types of failure can occur in this case. These are illustrated in Figure 1-3.

- Flexural: The beam has a low percentage of bottom steel and fails in tension at mid-span. Such type of failure rarely occurs in practice.
- Flexural-shear: The beam fails in shear, with main cracks propagating upwards from regions close to the support towards the applied load. In this case, there is a moderate amount of bottom steel and the development of shear-crack is normally preceded by flexural cracks at mid-span.
- Diagonal splitting: This is the most common mode of failure. The final shear crack again extends between the applied load and support, but it grows outwards from mid-depth, having been initiated in a more brittle manner than either of other two failure modes **[8]**.

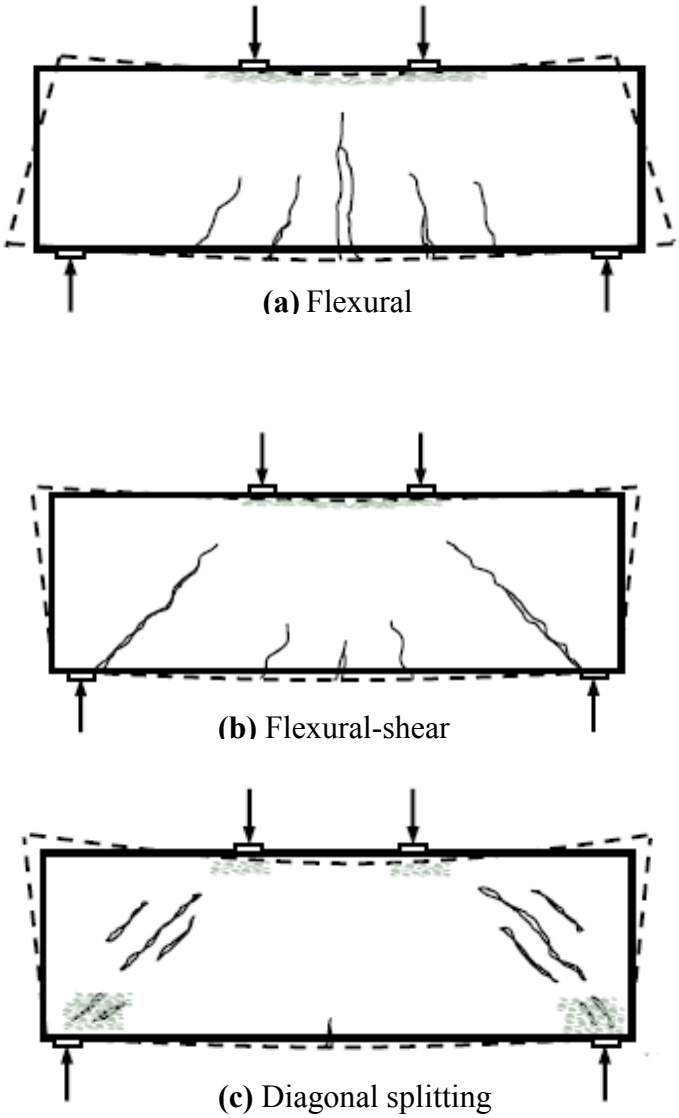

Figure 1-3 Modes of failure of deep beams [8]

1.3 Fiber Reinforced Polymer Strengthening System

The term composite often refers to a material composed of two or more distinct components working together. Often one of the components is harder and stronger, while the other is more of a force transferring material. FRP is an abbreviation of fiber reinforced polymers and is a composite of fibers and adhesive as shown in Figure 1-4. Because of high stiffness to weight ratio, relatively unlimited material length availability, and immunity to corrosion, the use of FRP material presents great advantages to advance the process of externally bonded strengthening **[9]**.

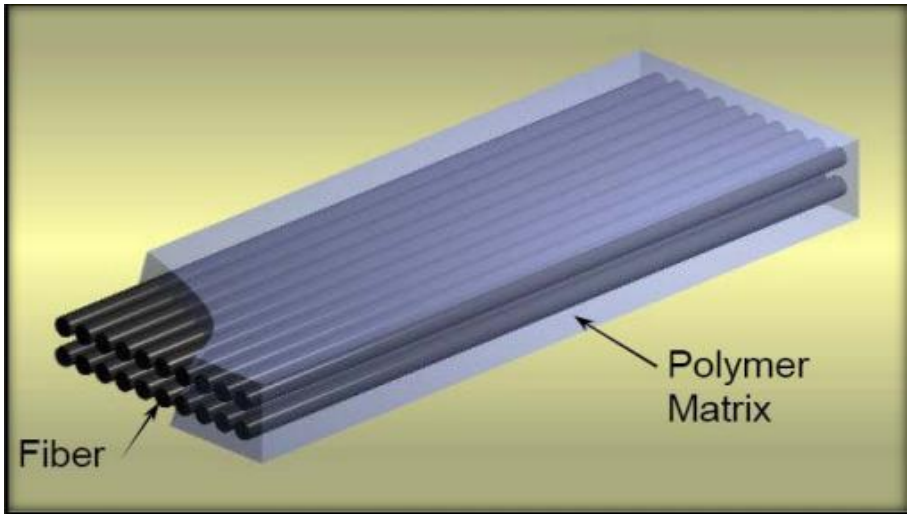

Figure 1-4 Typical composition of FRP material [9]

1.3.1 Fiber Materials

Several materials are available for the fibers, e.g. glass, aramid, carbon. Almost 95 percent of all applications for strengthening purposes in civil engineering are made by carbon fibers. Figure 1-5 demonstrate some typical response of uniaxial loaded fiber materials and steel. HM and HS are abbreviations of high modulus of elasticity and high strength, respectively. Fibers have a linear elastic behavior until failure which is brittle. The fibers are what make the FRP strong and there are three things that control the mechanical properties of the FRP **[1]**:

Constituent materials

As mentioned earlier there is a wide array of different materials to use. It important to note that the choice of fiber materials, together with choice of polymer, determines the quality, properties and behavior the FRP will obtain.

Fiber amount

Regarding the amount of fiber used in the FRP, it is easy to say that the more fiber used, the higher properties will be achieved. This is somewhat true, but with too high of a fiber content there will

be manufacturing problems. If the fibers are tightly packed the matrix will have problems enclosing the fibers which might deteriorate the FRP.

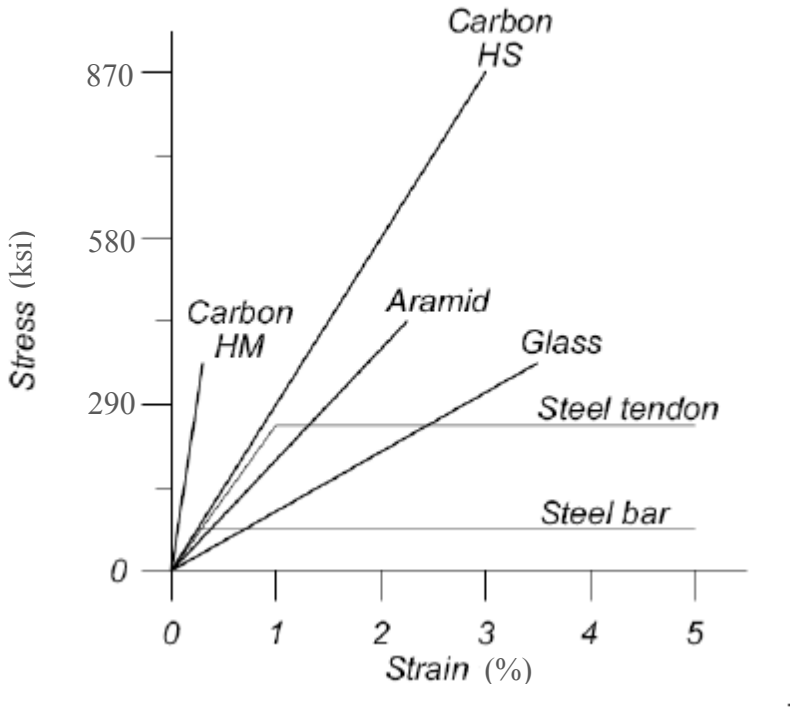

Figure 1-5 Stress-strain relationship of fibers and steel [10]

Fiber orientation

The FRP will be stiffer and stronger in the fiber direction. For example, a rod with all the fibers along its axis is very strong in its fiber direction but, in perpendicular direction, the FRP has not much weaker properties. A typical FRP product for the construction industry has therefore an anisotropic behavior compared to steel which is isotropic.

1.3.2 Matrix

The polymer matrix is used to bind the fibers together and to transfer the stresses between the fibers and to protect the fibers from external mechanical and environmental damage **[11]**. The

shear stresses created between the fibers are limited to the properties of the matrix. The matrix is also the limiting factor when applying forces perpendicular to the fibers. It is important that the matrix must have the capability to sustain higher strains than the fibers as shown in Figure 1-6. If not, there will be cracks in the matrix before the fibers fail and fibers will be unprotected **[9]**.

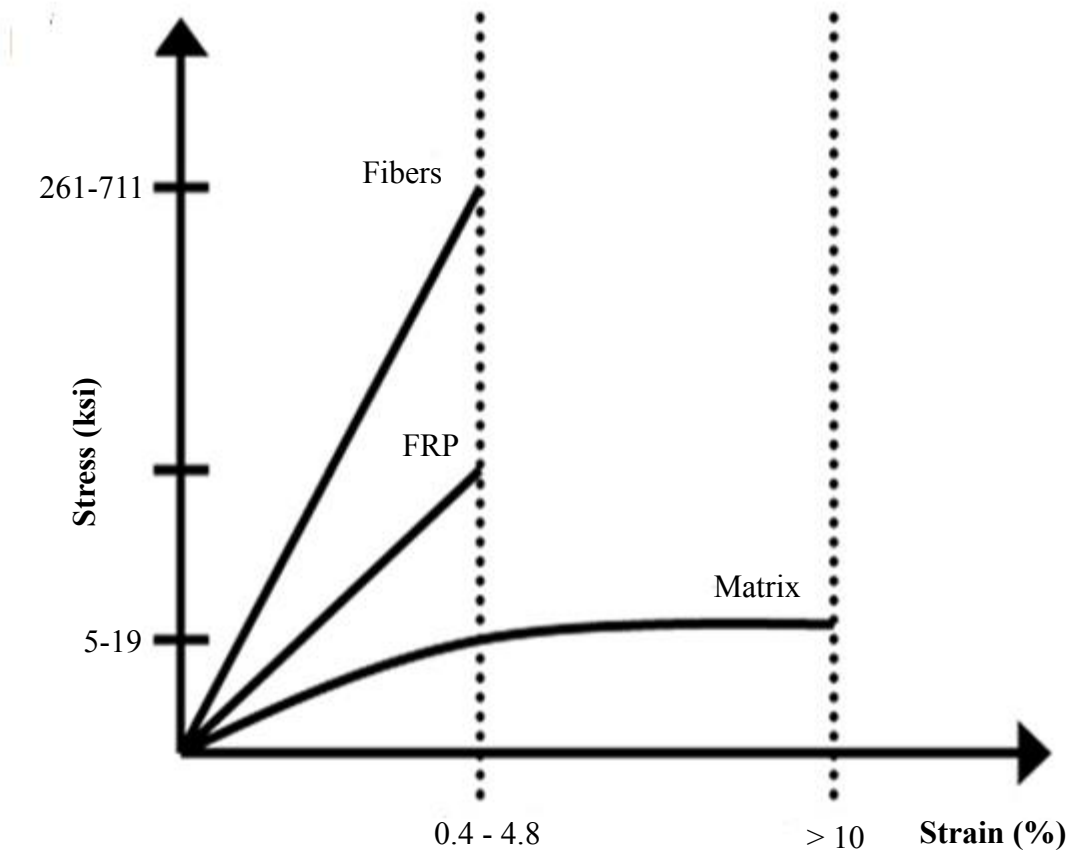

Figure 1-6 Stress-strain curves of fibers, FRP and matrix [11]

1.4 CFRP Strengthening in RC Members

The technique of strengthening reinforced concrete structures by externally bonded Carbon Fiber Reinforced Polymer (CFRP) was started in 1980s and since has attracted researchers around the

world. Strengthening with externally bonded CFRP laminates or sheets has shown to be applicable to many kinds of members and structures. Currently, this method has been applied to strengthen such members as columns, beams, walls, and slabs, see Figure 1-7. The use of external CFRP reinforcement may be classified as flexural strengthening, improving the ductility of compression members through confinement, and shear strengthening.

Figure 1-7 Applications of CFRP for strengthening an actual bridge

Table 1-2 Properties of concrete, steel and CFRP [10]

Material	**E (ksi)**	**Compressive strength (ksi)**	**Tensile strength (ksi)**	**Density (lb/ft^3)**
Concrete	5800	0.75-8.70	0.15-0.44	150
Steel	30458	34.81-100.08	34.81-100.08	487
CFRP	116030	N/A	305-871	110-120

The overall characteristics of strength, stiffness, less susceptibility to creep and fatigue rupture and durability of carbon fibers make it very suitable for strengthening the concrete structures, see Table 1-2.

1.5 Debonding Problems in CFRP Strengthened RC Beams

A CFRP sheet debonding arises due to loss of cohesion in the adhesive interface or crack propagation in the concrete within the concrete cover or at the level of the internal reinforcement. In general, the adhesive interface, epoxy matrix, is very strong compared to concrete and failures within the resin are rare **[12]**. The CFRP failure modes that refer to debonding are **[13]**:

1. Concrete cover detachment;
2. Plate end interfacial debonding;
3. Intermediate flexural crack induced interfacial debonding; and
4. Intermediate flexural-shear crack induced interfacial debonding.

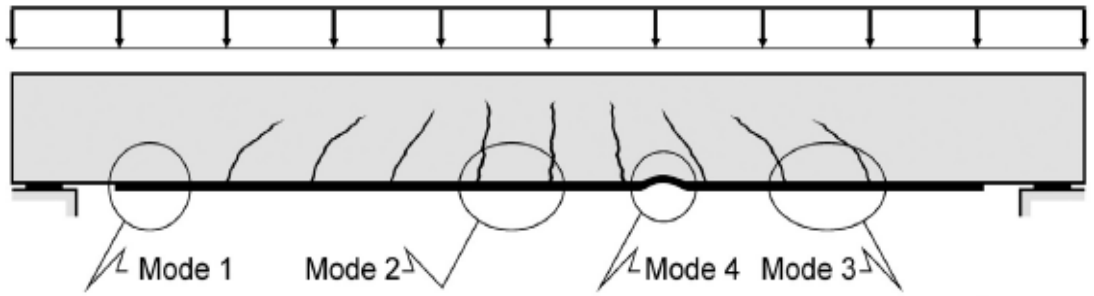

Figure 1-8 Debonding failure modes of RC beam strengthened with CFRP in flexural [13]

The previous debonding failure modes can also be classified into four debonding mechanisms, as shown in Figure 1-8 **[13]**:

1. Sheet end debonding;
2. Intermediate debonding, caused by flexural cracks;
3. Debonding due diagonal cracks; and
4. Debonding caused by irregularities and roughness of concrete surface.

Although the loss of composite action between the CFRP and RC beam is unique and difficult to predict, this failure mode may be limited by using CFRP anchorage devices **[12]**.

1.6 Objective

The objective of the present research is to understand the behavior of reinforced concrete deep beams with and without flexural CFRP strengthening and the effect of innovative anchorage devices on their capacities. The behavior of these beams is indicated by their levels of ultimate shear strength, mid span deflection, FRP reinforcement strain, crack propagation, strut angle, and by their type of failure. Moreover, developing a nonlinear truss analogy approach to predict the capacity of such beams based on the experimental results is intended.

1.7 Dissertation Layout

The dissertation consists of five chapters as follows:

The Chapter 1 presents a general introduction about the behavior of reinforced concrete deep beams, the application of CFRP in strengthening, and the objective of this work. Chapter 2 reviews the available previous studies carried out experimentally and theoretically, which are related to the present study. In Chapter 3, an experimental work, detail of specimens, material properties, test procedure, and experimental results are presented. Chapter 4 presents the analytical work and the prediction results. Chapter 5 shows a summary of the conclusions of the present work and recommendations for further work.

1.8 References

1. Nordin, H., 2003. *Fibre reinforced polymers in civil engineering: flexural strengthening of concrete structures with prestressed near surface mounted CFRP rods* (Doctoral dissertation, Luleå tekniska universitet).
2. Ashour, A.F., El-Refaie, S.A. and Garrity, S.W., 2004. Flexural strengthening of RC continuous beams using CFRP laminates. *Cement and concrete composites*, *26*(7), pp.765-775.
3. ACI Committee, American Concrete Institute and International Organization for Standardization, 2008. Building code requirements for structural concrete (ACI 318-08) and commentary. American Concrete Institute.
4. Zhang, Z., Hsu, C.T.T. and Moren, J., 2004. Shear strengthening of reinforced concrete deep beams using carbon fiber reinforced polymer laminates. *Journal of Composites for Construction*, *8*(5), pp.403-414.
5. Mohamed, K.A., 2015. *Performance and Strut Efficiency Factor of Concrete Deep Beams Reinforced with GFRP Bars* (Doctoral dissertation, Université de Sherbrooke).
6. Eun, H.C., Lee, Y.H., Chung, H.S. and Yang, K.H., 2006. On the shear strength of reinforced concrete deep beam with web opening. *The Structural Design of Tall and Special Buildings*, *15*(4), pp.445-466.
7. Abdel-Razzak, A.A., 2001. *The Effect of Low Shear Span Ratio on the Shear Strength of RC Beams* (Doctoral dissertation, University of Technology, Baghdad).
8. Subedi, N.K., Vardy, A.E. and Kubotat, N., 1986. Reinforced concrete deep beams some test results. *Magazine of Concrete Research*, *38*(137), pp.206-219.

9. Bisby, L.A. and Williams, B.K., 2004. An introduction to FRP strengthening of concrete structures. *ISIS Educational Module*, *4*, pp.1-39.
10. Carolin, A., 2003. *Carbon fibre reinforced polymers for strengthening of structural elements* (Doctoral dissertation, Luleå tekniska universitet).
11. Barecchia, E., 2007. *The use of FRP materials for the seismic upgrading of existing RC structures* (Doctoral dissertation, Tesi di Dottorato XIX ciclo, 197p, Università degli Studi di Napoli Federico II Facoltá di Ingegneria, Italy).
12. Teng, J., Chen J.F., Smith S., and Lam L., 2001. *FRP-Strengthened RC Structures*, John Wiley and Sons, LTD.
13. Bocciarelli, M., di Feo, C., Nisticò, N., Pisani, M.A. and Poggi, C., 2013. Failure of RC beams strengthened in bending with unconventionally arranged CFRP laminates. *Composites Part B: Engineering*, *54*, pp.246-254.

Chapter 2 - Literature Review

2.1 Introduction

In this Chapter, a brief review is carried out on the experimental and analytical methods that investigated the behavior of steel reinforced concrete deep beams. Also, the behavior of reinforced concrete beams strengthened by CFRP laminates is summarized according to main studies in this field.

2.2 Available Experimental Studies on Reinforced Concrete Deep Beams

In 1965, De Paiva and Siess [1] tested 19 simply-supported deep beams. All beams had a constant span of 610 in. and the effective depth of these beams was varied among 6 in., 8 in., and 12 in., which led to (L/d) ratios equal 4, 3, and 2 respectively. The purpose of this study was to present an investigation of the shear strength and behavior of moderately reinforced concrete deep beams. They found that by increasing the percentage of the tension reinforcement, the load capacity of the beam was increased and the mode of failure tends to change from flexural to shear. The increase in the concrete strength had a negligible effect on the ultimate strength of beams failing in flexure but increased the strength and, in some cases, changed the mode of failure of beams failing in shear. Also, it was found that the addition of vertical and inclined stirrups has no effect on the formation of inclined cracks. The addition of vertical stirrups tends to reduce the deflections at ultimate load.

In 1971, Manuel et al [2] investigated 12 reinforced concrete deep beams in which the variables (L_a/d) and (L/d) were systematically varied and other major variables were kept constant. They studied the effects of changes in (L_a/d) and (L/d) ratios on failure. They found that the ultimate strength of reinforced concrete deep beams appears to be significantly influenced by (L_a/d) ratio and insignificantly affected by (L/d) ratio. Furthermore, the diagonal tension cracking capacity of

deep beams is not influenced significantly by (L/d) ratio. The extent of arch action for beams of constant shear span at any level is reduced as the length of beam increases. The influence of (L_a /d) ratio relates to the mode of failure

In 1972, Kong and Singh [3] tested 45 lightweight concrete deep beams. Different types and amounts of web reinforcement were used. The tested beams were divided into three groups. The beams of group A and group B were different in the spacing of the web reinforcement, and the beams of group C were used for a preliminary study of the effect of terminating a longitudinal bar within the shear span. All 45 beams were tested under four-point bending. For all beams, the depth (h) was kept constant while the span and clear shear span were varied to change the (L/h) and (L_a/h) ratios, respectively. An attempt was made to isolate the effects of (L/h) and (L_a /h) on crack control, diagonal cracking loads, and ultimate shear loads. They found that (L/h) ratio has little effect on ultimate loads, diagonal cracking loads, crack widths, which are all strongly dependent on the (L_a/h) ratio. For strength and crack control, the inclined web reinforcement was very effective for all the (L_a/h) ratios studied while the effectiveness of other types of web reinforcement depended on the (L_a/h) ratio. They also found that the addition of a main longitudinal bar, which is terminated within the shear span, would seem to have little harmful effects on maximum crack width, diagonal cracking load, or ultimate load.

In 1982, Smith and Vantsiotis [4] tested 52 reinforced concrete deep beams under four-point bending. The objective was to study the effect of vertical and horizontal web reinforcement and the shear span to effective depth ratio on the ultimate shear strength. The test indicated that the web reinforcement produces no effect on formation of inclined cracks and seems to moderately affect the shear strength. It was noted that web reinforcement contribution to ultimate shear strength never exceeded the limiting value of $1/3\sqrt{f'_c}$ bd. Horizontal web reinforcement appears

to have little influence on the ultimate shear strength, while its influence was more noticeable in the beam with $L_a/d < 1.0$. Also, increasing concrete strength increased the ultimate load capacity when the beam has low L_a/d ratio and seems to diminish as L_a/d ratio, for these deep beams, increases.

In 2003, Yang et al [5] tested 21 deep beams to evaluate whether the ACI equation for deep beams is applicable to high strength concrete deep beams with steel ratio less than 1 %. The design code has been developed for concrete beams without shear reinforcement, and with concrete less than 5.8 ksi in strength, an average overall depth of 17 in. and average reinforcement ratio of 2.22 %. The test variables included concrete strength, shear span to depth ratio and overall depth within the range of 16-40 inches. The high strength concrete deep beams exhibit more remarkable size effects with regard to brittle behavior. It was also shown that ACI equations gave similar safety factors on the shear strength at the first diagonal crack of the high strength-concrete deep beams, but didn't specify a high enough safety factor on their ultimate shear strength due to size effect.

In 2006, Brown and Bayrak [6] examined the amount of transverse reinforcement required to resist the tension developed in a bottle-shaped strut and presented an equilibrium-based approach to determining the necessary amount of transverse reinforcement for a bottle-shaped strut. They concluded that the use of bottle shaped strut without transverse reinforcement should not be permitted regardless of the efficiency factor implemented. A minimum amount of reinforcement should be used to compensate for effects of temperature, restrained shrinkage, and other effects that may not be explicitly taken into account. In addition, the amount of transverse reinforcement required to maintain equilibrium in a bottle-shaped strut is a function of the force applied to that strut. Hence, the efficiency factor affects the required reinforcement **[7]**.

In 2011, Tuchscherer et al [8] evaluated the benefit of distributing stirrups across the web of the deep beams. Six deep-beam specimens were tested with a span-depth ratio (L_a/d) of 1.84. The primary experimental variables were the number of stirrup legs distributed across the web and the amount of web reinforcement. Based on the test results, it can be concluded that distributing stirrup legs across the width of the web of specimens as wide as 36.5 in. had a small influence on the shear capacity and service-level behavior. Due to the fact that web reinforcement distribution across the section web is relatively ineffective in a deep beam, a limitation of stirrup spacing across the web may be inefficient or unnecessary. Nonetheless, it is generally considered good practice to provide intermediate stirrups across the section of very wide beams. Based on the findings of their study, they stated that intermediate stirrup legs are not necessary in deep beams as wide as 36 inches. Also, exterior stirrup legs should be transversely spaced no farther than d from one another, where d is the depth of the beam from the extreme compression fiber to the centroid of the tension reinforcement **[7]**.

2.3 Existing Models and Shear Theories of Reinforced Concrete Deep Beams

2.3.1 Tooth Model

In 1964, Kani [9] tried to explain flexural-shear cracking with a rational model named Kani's tooth model, in which the secondary diagonal cracks were believed to result from bending of concrete. The concrete between two adjacent flexural cracks was considered to be analogous to a tooth in a comb, as shown in Figure 2-1. The concrete teeth were assumed to be free cantilevers fixed in the compression zone of the beams and loaded by the horizontal shear from bonded reinforcement. This model has been developed further by McGregor and Walters (1967) **[10]**, Hamadi and Regan (1980) **[11]**, and Reineck (1991) **[12]**. Moreover, Chana (1987) **[13]** confirmed

the basic mechanisms of the tooth model by extensive measurements of the deformation prior to failure by using Kani's test results.

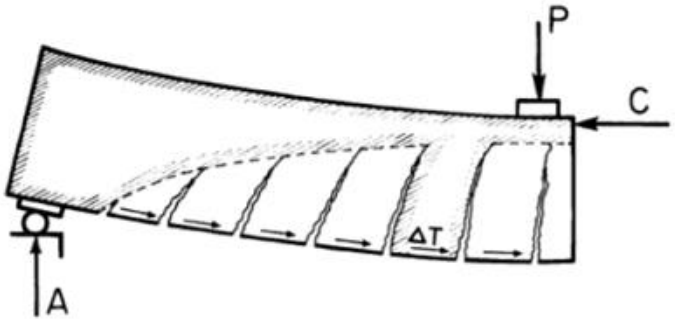

Figure 2-1 Kani's tooth model [9]

2.3.2 The Modified Compression Field Theory (MCFT)

In 1986, Vecchio and Collins [14] defied the original form of the MCFT from the testing of 30 reinforced concrete panels subjected to uniform strain states in a specially built tester. The MCFT was described as a general model for the load–deformation behavior of two-dimensional cracked reinforced concrete elements subjected to shear. It models concrete considering concrete stresses in principal directions summed with reinforcing stresses assumed to be only axial. The concrete stress-strain behavior in compression and tension was derived originally from Vecchio's research. The most important assumption in the model is that cracked concrete in reinforced concrete can be treated as a new material with empirically defined stress-strain behavior. The strains used for these stress-strain relationships are average strains. The calculated stresses are also average stresses in that they implicitly include stresses between cracks, stresses at cracks, interface shear on cracks, and dowel action. The crack check is a critical part of the MCFT and the theories derived from it. The crack check involves limiting the average principal tensile stress in the concrete to a maximum allowable value determined by considering the steel stress at a crack and the ability of the crack surface to resist shear stresses.

In 2000, Rahal [15] proposed a procedure without iteration as a simplification for the MCFT. Rahal's method consists of two equations and the curve in Figure 2-2.

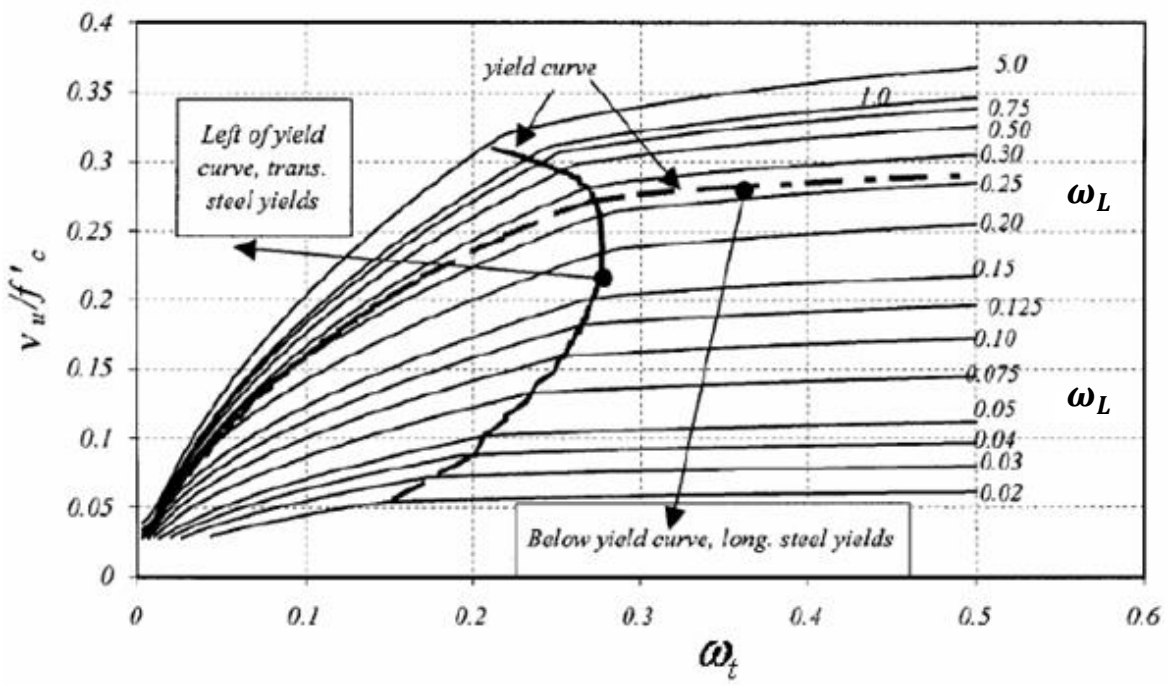

Figure 2-2 Diagram used in Rahal's method [15]

$$\omega_L = \frac{\rho_L * f_{yl}}{\acute{f}_c} = \frac{A_L * f_{yl}}{b_w * d_v * f'_c} \tag{2.1}$$

$$\omega_t = \frac{\rho_t * f_{yt}}{\acute{f}_c} = \frac{A_v * f_{yt}}{b_w * s * f'_c} \tag{2.2}$$

Use of the curve:

1. calculate ω_L and ω_t using equation (2.1) and equation (2.2),
2. Enter Figure 2-2 with ω_L and ω_t values and obtain $\frac{v_u}{f'_c}$, and,
3. If v_u is smaller than the cracking stress, take v_u equal to this cracking stress.

Figure 2-2 shows that for a given level of ω_L and by increasing the index of transverse reinforcement ω_t, the strength increases. The ratio of increase, however, drops beyond a certain

level of ω_t, where crushing in the concrete occurs before yielding of the steel. At low levels of reinforcement (low ω_L and ω_t) the strength is governed by the cracking strength in the concrete, taken as 1/3 $\sqrt{f'_c}$ ksi for members with $7 \leq f'_c$ ksi. This lower limit is not shown in Figure 2-2 because the coordinate axis is a function of f'_c instead of $\sqrt{f'_c}$.

2.3.3 Strut-and-Tie Model (STM)

In 1987, Schlaich et al [16] suggested an approach based on the elastic theory to be the rational and appropriate basis for the design of cracked reinforced concrete beams loaded in bending, shear and torsion. Since all parts of a structure are of similar importance, an acceptable design concept must be valid and consistent for every part of any structure. Furthermore, since the function of the experiment in design should be restricted to verify or dispute a theory but not to derive it, such a concept must be based on physical models which can be easily understood and therefore are unlikely to be misinterpreted. The design of structural concrete was proposed to generalize the truss analogy in order to apply it in the form of strut-and-tie model to every part of any structure. In the elastic stress distribution of deep members, significant shear is transmitted directly to the support by diagonal compression. This means that less redistribution is required after cracking, and it seems reasonable to apply strut-and-tie model to deep beams **[7,17]**.

STM allows for easy visualization of the flow of forces. In addition, these truss models represent all internal force effects and do not require separate flexure and shear models, as is the case for slender members analyzed with sectional approaches. STM is based on the lower-bound theory of plasticity and the capacity of the model is always less than the true capacity if the truss is in equilibrium and has sufficient deformation capacity to allow redistribution of forces into the assumed truss elements **[7]**.

STM was recommended by design provisions and among researchers to design reinforced concrete deep beams. This model reduces complex states of stress of such beams into a truss comprised of simple, uniaxial stress paths. Each uniaxial stress path is considered a member of the STM, see Figure 2-3. Members of the STM subjected to tensile stresses are called ties; and represent the location where reinforcement should be placed. STM members subjected to compression are called struts. The intersection points of truss member are called nodes. Knowing the forces acting on the boundaries of the STM, the forces in each of the truss members can be determined using basic truss analysis **[7]**.

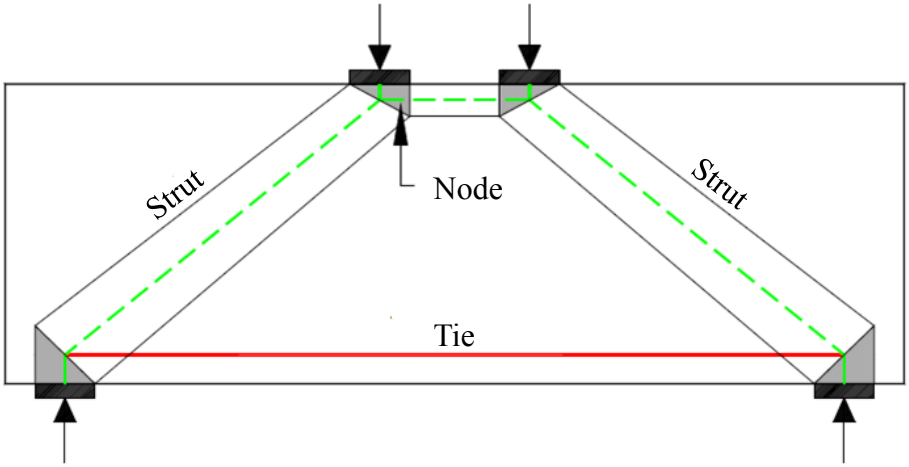

Figure 2-3 STM for a deep beam

Most design specifications recognize three major node types: CCC, CCT, and CTT nodes. Figure 2-4 illustrates the different types of nodes. A node that connects only compressive forces is called CCC node; while CCT is a node under the action of one tension force and two (or more) compression forces. A CTT node connects one compression force and two (or more) tension forces. The regions around the nodes are called nodal zones. An extended nodal zone can be used for the analysis of the stresses in the region, including determination of reinforcement anchorage

requirements. The ACI 318 defines a nodal zone as a portion of a member bounded by the intersection of effective strut and tie widths, see Figure 2-4.

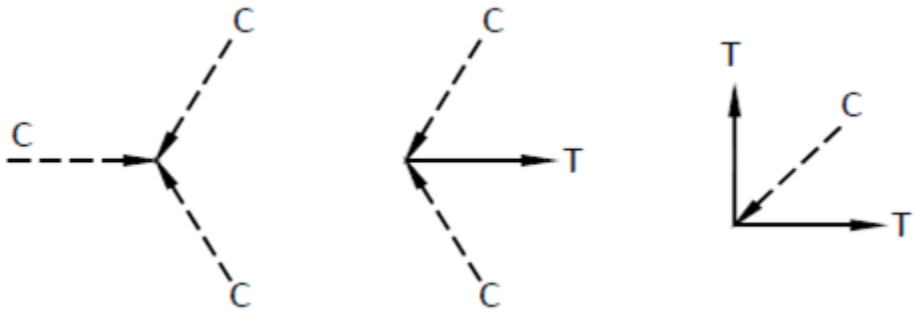

(a) Basic Type of Nodes

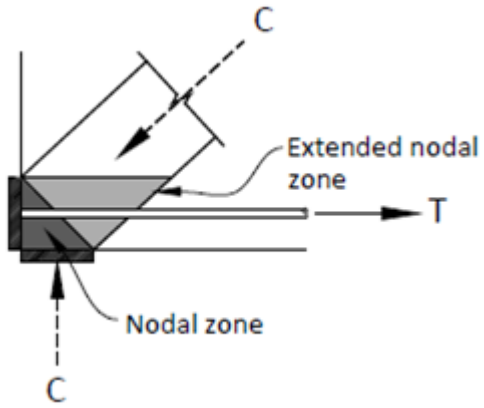

(b) Nodal zone for a CCT node

Figure 2-4 STM nodes [18]

Most research and design specifications specify the limiting compressive stress of a strut as the product of the concrete compressive strength (f'_c), and an efficiency factor. The efficiency factor is often a function of the geometric shape (or type) of the strut and the type of the node. As discussed by Schlaich, J. and Schafer (1991) **[19]**, there are three major geometric shape classes

for struts: prismatic, bottle-shaped, and compression fan as shown in Figure 2-5. Prismatic and bottle shaped struts are the most basic types of a strut, while fan strut is more practical for deep beams with distributed loading. Prismatic struts have uniform cross-sections **[7]**.

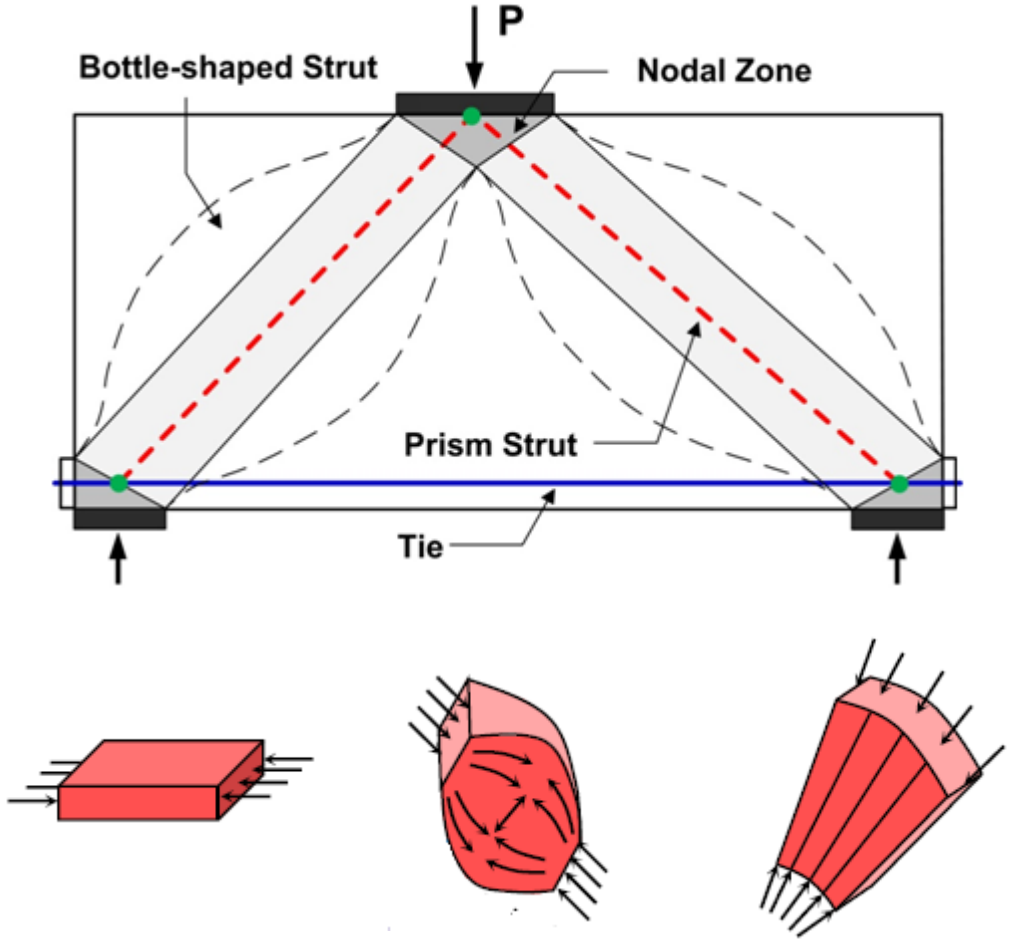

Figure 2-5 Type of STM struts

Typically, prismatic struts are used to model the compressive stress block of a beam element as shown in Figure 2-5. Bottle-shaped struts are formed when the geometric conditions at the end of the struts are well defined, but the rest of the strut is not confined to a specific portion of the structural element. The geometric conditions at the ends of bottle-shaped struts are typically

determined by the details of bearing pads and/or the reinforcement details of any adjoined steel. The best way to visualize a bottle-shaped strut is to imagine forces dispersing as they move away from the ends of the strut, see Figure 2-5 **[7]**.

2.3.3.1 Strut-and-Tie Model According to ACI 318

In 2002, the ACI building code stated that deep beams should be designed using either nonlinear analysis or using the STM. This code provides nominal capacities of the struts of a STM as a fraction of the specified compressive strength of the concrete. Moreover, ACI 318 provides the procedure for calculating the nominal capacities of the elements of the STM, which are the strut, the nodal zone and the tie. The design of the struts, ties and nodal zones are based on: $\varphi F_n \geq F_u$ where F_u is the largest force in that element for all loading cases, F_n is the nominal strength, and φ is a factor specified by the code **[20]**.

There are two types of struts defined in the procedure. The first type of strut has a uniform cross sectional area over its length between the applied load and the support plate. The nominal capacity of a strut is given by $f_{ce} = 0.85\,\beta_s\ f'_c$, where β_s is defined as the efficiency factor. The efficiency factor β_s is the reduction of the ultimate strength of the strut. This factor reflects the ability of the concrete to resist loads at cracking level, develops or transfers compression across cracks in a tension zone. The value of β_s ranges from 0.4 to 1 based on the type of the strut. The nominal capacity of the bottle strut is calculated in the same way as the straight struts, but with a different value for the efficiency factor β_s. For this type of strut, the β_s is taken as 0.75 if f'_c is not greater than 6 ksi and if the web reinforcement satisfies the Equation (2.3) below, see Table 2-1.

$$\sum_{i=1}^{m} \frac{A_{si}}{b_s * S_i} sin\ \alpha_i \geq 0.003 \qquad (2.3)$$

In the above equation, S_i and A_{si} indicate spacing and area of a bar for web reinforcement (horizontal or vertical), and b_s indicates the width of the strut as shown in Figure 2-6 **[20]**.

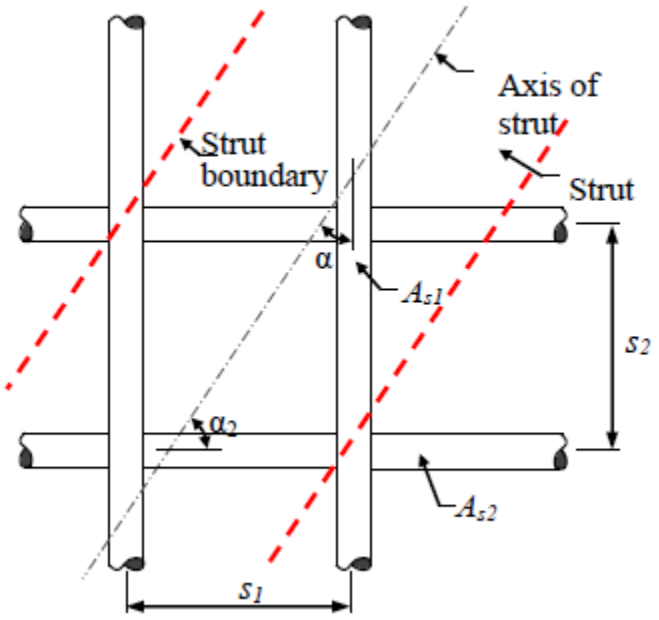

Figure 2-6 Reinforcement crossing a strut [7]

Table 2-1 ACI 318-14 stress limits and strength reduction factors

Strut and node efficiencies ($0.85 f'_c$)		**β_s**
Struts	Strut with uniform cross section over its length	1.00
	Bottle-shaped struts with reinforcement	0.75
	Bottle-shaped struts without reinforcement	0.60
	Struts in tension members	0.40
	All other cases	0.60
Nodes	Nodes bounded by compression or bearing CCC node	1.00
	Nodes anchoring one tie CCT node	0.80
	Nodes anchoring more than one tie CTT and TTT nodes	0.60
Strength reduction factor, φ		
φ = 0.75 for struts, ties, and nodes		

In 2006, **Quintero-Febres et al [21]** have assumed a shallower slope of 6:1 for the spread of the compressive force in the strut to avoid an excessive number of web reinforcement in the case of a high-strength concrete $f'_c > 6$ ksi, where the code does not provide any specific guideline.

In 2008, **Brown et al [22]** have argued that it is not preferable to use the bottle strut since the web reinforcement is less than the required amount and such an amount cannot prevent the diagonal tension crack from growing.

The ACI 318 has suggested a basic concept of STM that satisfies equilibrium and constitutive relationships, and they have allowed the design of reinforced concrete deep beams with a single or one-panel truss model for the beams with a shear span to effective depth ratio L_a/d of less than 2. In addition, the reinforced concrete deep beams with L_a/d of larger than 2 can be designed by using two-panel truss model to avoid compatibility problems and for efficiency. Figure 2-7 shows one and two panel truss models. The angle between the axis of any strut and any tie entering a common node may not be less than 25 degrees. This provision stems from the idea that struts will lose capacity as they approach the direction of a tie. Clearly, a strut that is coincident with a tie will have no compressive capacity. The angle of 25 degrees was chosen to eliminate potential problems with struts that form a slight angle with a tie. They also found that the one-panel truss model is preferred mechanism for resisting loads in deep beams with limited amount of web reinforcement.

In 2009, **Park and Aboutaha [23]** have compared the efficiency factors for different models and have concluded that the results obtained using ACI 318 are not conservative as compared to the experimental results in many cases. However, the code does not specify which type of strut should be used in the design procedure since the procedure may yield multiple solutions.

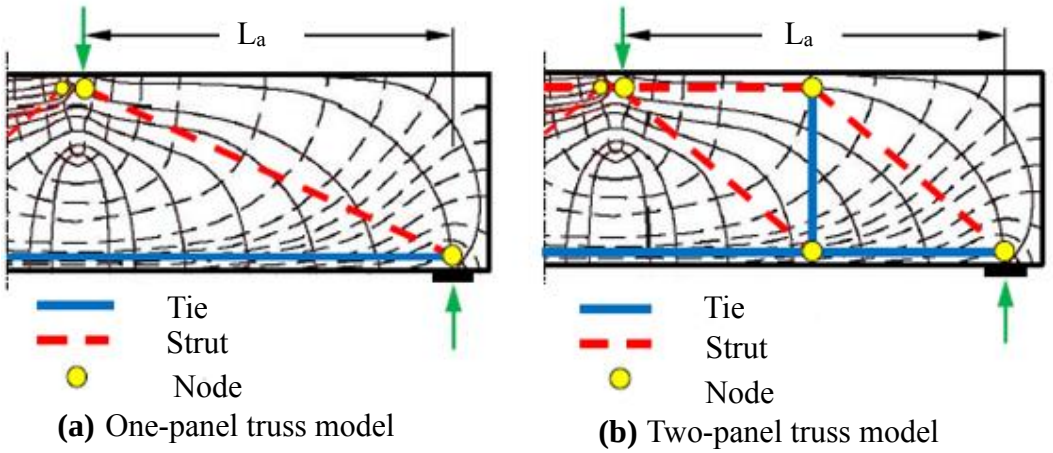

Figure 2-7 One-and two-panel truss models [7]

2.3.4 Finite Element Method (FEM)

In structural applications, most problems are too complicated to analyze exactly and mathematical solutions for their governing equations are obtained only for limited types of structures of simple geometry and load characteristics. The finite element method has been used to obtain approximate solutions for realistic types of problems in engineering. Steady state, transient, linear, or nonlinear problems in stress analysis; heat transfer and fluid flow problems may be analyzed by the finite element method.

During the recent decades and because of the development of relatively powerful analytical techniques implementing state of the art computers and the interest in nonlinear analysis of concrete as a structural material, the use of finite element method has greatly increased. Moreover, this method has many advantages among others such as effectively modeling the nonlinearity in materials and in geometry and both of them. In solving problems in structural engineering, the domain is divided into sub-domains called elements connected with each other at selected points called nodes. In each element, the behavior is described by a separate set of assumed functions representing the element. The element stiffness matrices are assembled to form the stiffness matrix

for the whole structure. Equivalent nodal forces are used to represent the external loads and the boundary conditions can be applied easily to the assembled stiffness matrix of the total structure.

2.4 Available Studies on Nonlinear Analysis of Reinforcement Concrete Deep Beams

In 1986, Mahmood [24] analyzed reinforced concrete deep beams using a nonlinear finite element technique. The nonlinearities included the stress-strain behavior of concrete and its anisotropy under varying biaxial stress conditions, cracking and crushing of concrete, yielding of steel, the nonlinear bond stress-slip phenomenon and the post-cracking shear transfer by aggregate interlock. Concrete was represented by using quadrilateral isoparametric elements, or quadrilateral elements with incompatible modes. Main steel was represented by either using simple truss elements or constant strain triangular elements connected to the concrete nodes by zero length spring linkage elements with proper stiffness to simulate bond and dowel action. The incremental-iterative procedure with variable stiffness matrix was adopted in the nonlinear solution algorithm. Analytical results obtained, such as deflections, crack pattern, ultimate loads and failure mechanism showed reasonable agreements with published experimental and analytical results.

In 1997, Aziz [25] tested 28 reinforced crushed stone concrete deep beams under two equal point loads. Test specimens were divided into three series with and without web reinforcement. The beams were tested for different shear span to depth ratio ranging from 1.05 to 2.22, and different effective span to effective depth ranging from 2.53 to 7.41. The investigation objectives were to study the effect of shear to effective depth ratio, effective span to effective depth ratio, compressive strength of concrete, and web reinforcement. It was found that the ultimate shear stress decreases with increasing shear span to effective depth ratio and maximum size of aggregate, while it increases with increasing compressive strength of concrete and amount of shear reinforcement.

In 2002, Al-Shraify [26] used three dimensional finite element models to simulate the behavior of reinforced concrete continuous deep beams. Concrete was modeled using 20-node isoparametric quadratic elements, while the reinforcing bars were modeled as axial members embedded within the concrete element. Perfect bond between the concrete and steel was assumed to take place. In general, a good agreement between the finite element solution and the experimental work was obtained. From the parametric study, it was found that by increasing compressive strength from 4 to 7 ksi, an increase in shear strength by 23 % was observed. Also, when the clear span to effective depth ratio was decreased by 37 %, the failure load was increased by 46 %.

In 2007, Park and Kuchma [27] proposed a strut-and-tie based method for calculating the strength of reinforced concrete deep beams. A strut and tie statically determinate model, as shown in Figure 2-8, was used for describing the flow of stresses in a deep beam. The model was used in the development of a general approach that considers the compression softening and web splitting phenomena as influenced by transverse tensile straining. The proposed compatibility based strut and tie model procedure uses an iterative secant stiffness formulation, employs constitutive relations for concrete and steel, and considers strain compatibility. The strain compatibility relation used in this study requires that the sum of normal strain in two perpendicular directions is an invariant. Also they assumed that the effective depth of the top horizontal concrete strut will be calculated by: $w_c = kd$, where d is the effective depth of the deep beam and k is derived from the classical bending theory for a singly reinforced beam section as: $(k = \sqrt{(n\rho)^2 + 2n\rho} - n\rho)$. In this case, n is the ratio of steel to concrete elastic modules and ρ is the longitudinal reinforcement ratio. Moreover, this model was compared with the strut-and-tie given in ACI 318-05 code provision in predicting the capacity of 214 deep beams which were tested to failure. The

comparison showed that the proposed method consistently predicts the strengths of deep beams with a wide range of horizontal and vertical web reinforcement ratios, concrete strengths, and shear span to depth ratios (L_a/d) well **[20]**.

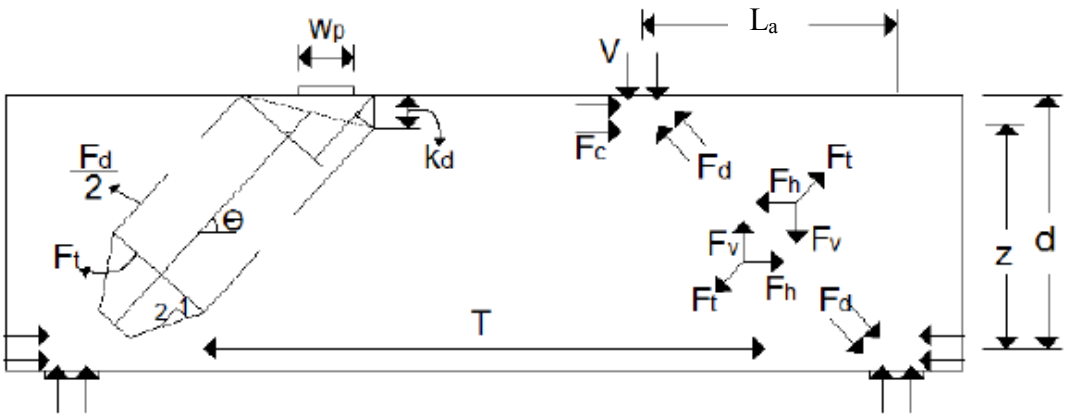

Figure 2-8 Park and Kuchma strut-and-tie model for a deep beam [27]

In 2007, Zhang and Tan [28] proposed a modified strut and tie model for determining the shear strength of reinforced concrete deep beams. The model is a modification to the original model proposed by Tan et al. (2003) **[29]** with a direct STM for pressurized deep beams. The assumption of this model can be summarized in the following: concrete tension–stiffening properties are used instead of concrete tensile strength to improve model prediction consistency. The component force of tension tie in the direction of the concrete diagonal strut is also included in the model for completeness. The softening effect of concrete strength due to the presence of transverse tensile strain is implicitly taken into consideration. The stress distribution factor of this model is derived from the consideration of both force and moment equilibrium. Moreover, the modified model for simply supported deep beams was evaluated using 233 test results and it was shown to be in a better agreement with the experimental results than the original model **[20]**.

2.5 Available Experimental and Analytical Studies on RC Beams Strengthened by FRP

In 1992, Berset [30] performed the first research focusing on shear strengthening of reinforced concrete beam with composites materials, by testing reinforced concrete beams with externally bond (GFRP) laminate. In addition, he proposed a simple analytical method to compute the contribution of external reinforcement to the shear capacity similar to the contribution of stirrups, and based on maximum allowable strain, which is determined from experiments **[31]**.

In 2001, Kachlakev et al [32] produced an ANSYS finite element model to study the effects of shear strengthening by comparing the behavior of two full-scale reinforced concrete beams. Experimental beams replicated the transverse members from the Horsetail Creek Bridge, which were deficient in shear reinforcement. Three-dimensional finite element models were developed using layered elements for the FRP composites. It was found that the general behavior through the linear and nonlinear ranges up to failure of the finite element models show good agreement with observations and data from the experimental full-scale beam tests. The addition of GFRP to the control beam shifts the behavior of the actual beam and model from a sudden shear failure near the ends of the beam to flexure failure by steel yielding at the mid span. This finite element model can be used in additional studies to develop design rules for strengthening reinforced concrete bridge members by using FRP.

In 2004, Zhang el al [33] tested 16 reinforced concrete deep beams without shear reinforcement. They were divided into four groups with four beams in each group. One beam in each group was a control beam, while the others were strengthened by various configuration of CFRP shear reinforcement. The result of the test demonstrated the feasibility of the use of externally applied CFRP system to restore or increase the shear capacity of a deep beam. It was found in a regular beam situation that the shear span to effective depth ratio has large value the anchorage for vertical

CFRP shear reinforcement, which will greatly improved the shear strength. But, when the shear span to effective depth ratio becomes smaller in magnitude, or the beam behaves like a deep beam, the anchorage of the vertical CFRP shear reinforcement will not likely to improve the shear strength as much as a regular beam case. Also, it was noted the effected stresses in the CFRP laminates at the failure did not reach the ultimate tensile stress (fiber rupture) of CFRP laminate.

In 2004, Hwang et al [34] presented experimental and analytical studies related to seismic retrofitting of reinforced concrete frames containing partition walls using the CFRP laminate. The test result indicated that the use of CFRP laminate with sufficient end anchorage was quite effective in enhancing the shear strength of partition walls. The application of the CFRP sheets without anchor system was worthless since they quickly debond. Also, it was found strengthening low-rise walls by vertical CFRP sheet were more effective than the application of horizontal CFRP sheet. Experimental and analytical results indicated that the shear resisting mechanism of reinforced squat walls can be modeled using the strut and tie action.

In 2004, Santhakumar et al [35] presented a numerical study to simulate the behavior of retrofitted reinforced concrete shear beams. The study was carried out on an un-retrofitted RC beam designated as control beam and RC beams retrofitted using CFRP composites with ±45º and 90º fiber orientations. The effect of retrofitting on un-cracked and pre-cracked beams was studied too. The finite elements adopted by ANSYS were used in this study. The load-deflection plots obtained from the numerical study showed good agreement with the experimental plots. There was a difference in behavior between the un-cracked and the pre-cracked retrofitted beams though not significant.

In 2005, Islam et al [36] explored the prospect of strengthening structurally deficient deep beams by using an externally bonded fiber reinforced polymer (FRP) system. Six identical beams were

fabricated and tested up to failure. One of these beams was tested in its virgin condition to serve as a reference, while the remaining five beams were tested after being strengthened using carbon fiber wrap, strip or grids. Test results have shown that the use of a bonded FRP system leads to a much slower growth of the critical diagonal cracks and enhances the load-carrying capacity of the beam to a level quite sufficient to meet most of the practical upgrading requirements.

In 2005, Elgwady et al [37] examined six corbels strengthened by CFRP to study the effectiveness of using CFRP as an external strengthening method to increase the load carrying capacity of the corbel. Different configurations were used. The test results indicated that the proposed technique had potential in improving ultimate load carrying capacity of the short cantilever. The use of CFRP as diagonal strip increased the ultimate load carrying capacity of the corbel by 70 % of the control specimen. All other corbels tested had ultimate load carrying capacity higher than the control corbel with difference ranging from 8 % to 30 %.

In 2006, Al-Shmmary [38] presented a three-dimensional nonlinear finite element model suitable for the analysis of reinforced concrete beams strengthened in flexure with CFRP plates under static load. The ANSYS computer program has been used to investigate the behavior of the different composite CFRP reinforced concrete beams. The analytical results of load-deflection response along the examined beams have been compared with available experimental tests. In general, a good agreement between the finite element solutions and experimental results has been obtained with difference about (2 %). Parametric studies have been carried out to investigate the effect of some important material parameters. It was found that the flexural strengthening of RC beams with CFRP is effective with an increment in the ultimate load about (30-45) %.

In 2007, Ali [39] investigated the experimental and theoretical behavior of reinforced concrete beams, strengthened or repaired by CFRP for both flexural and shear. It was observed that the use

of CFRP sheet bonded to the tension side of beams could enhance the ultimate load capacity up to 160% in flexural over the ultimate load for the reference beam. The repaired beams reached 95% to 97% of ultimate load in comparison with the virgin beams. The shear group shows the use of CFRP sheet could enhanced the ultimate shear capacity up to 200% as compared with reference beam. ANSYS computer program was used to simulate a numerical model for reinforced concrete beam strengthened or repaired by CFRP. Full bond between the CFRP and concrete interface was considered. Comparison between the experimental and numerical results asserted the validity of the numerical analysis and the methodology developed.

In 2008, Nehdi et al [40] tested eight, seven, and four reinforced concrete short beams having $1.5<L_a/d<2.5$ strengthened with CFRP and GFRP sheets, respectively. Steel reinforced beams were used as control beams. For each parameter investigated in GFRP and CFRP strengthened beams, there was a corresponding steel reinforced control beam. The effects of the shear span to depth ratio L_a/d, effective depth d, axial stiffness of flexural reinforcement, and concrete compressive strength f'_c on the shear behavior of short RC beams were investigated. It was observed that the most important parameters affecting the efficiency factor of concrete struts in strut and tie models for FRP RC short beams are L_a/d, d, and the axial stiffness of the flexural reinforcement. The effect of the concrete compressive strength on the efficiency factor was found to be little to no significance.

In 2008, Izzet and Sarsam [41] tested seventeen specimens strengthened with CFRP sheets. The main variables were shear span to depth ratio L_a/d, the amount and distribution of CFRP. The experimental results indicated that the contribution of externally fixed CFRP strips to the shear capacity is significant and depends on the variables investigated. In all 16 beam specimens with end anchorage (steel plates and bolts, see Figure 2-9) the de-bonding was not observed. The

obtained enhancement in the ultimate shear capacity or the increase in the ultimate load was 0 %, 35 % and 40 % compared to the control beam with steel stirrups and 100 %, 170 % and 18 0% over that of the beam without steel stirrups. It was concluded that spacing of CFRP is a major factor in strength in shear.

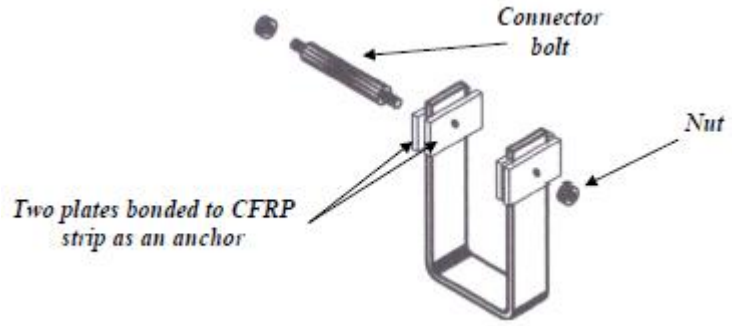

Figure 2-9 End anchorage made of steel plates and bolts [41]

In 2015, Rasheed et al [42] tested three T-beams and three rectangular beams in order to investigate the beneficial use of distributed U-wrap CFRP anchors to delay or shift the premature de-bonding of the RC beams in flexure. Results showed that the U-wrap anchorage successfully helped providing resistance to de-bonding by shear friction. The strengthened beam specimens with no anchorage failed by de-bonding while the strengthened beams with U-wraps anchorage failed in CFRP rupture. The increments in the ultimate load capacity were 30 % and 10 % over the unanchored beams for the T-beam and the rectangular beams, respectively. The reason for the lower percentage of increase in the rectangular beam is shifting the failure mode to concrete crushing.

In 2018, Zaki [43] tested three T-beams and three rectangular RC beams in order to introduce the effectiveness of two new flexural anchorage techniques using GFRP sidebars and GFRP side patches to anchor flexural CFRP sheets applied to strengthen these beams, see Figure 2-10. Test

results showed that these two anchorage techniques gave a fundamental improvement in the flexural behavior by achieving much higher levels of ultimate strength and deformability. The increase in flexural capacity of the T-beam with GFRP sidebar and GFRP side patch anchorage was 74 % and 58 % over the unanchored beams, respectively. Both of the anchorage devices were proven to achieve the full sectional capacity of the beam without any reduction due to premature de-bonding or bond slip. Moreover, the increase in the maximum deflection of these beams with GFRP sidebar and GFRP side patch anchorage was 76 % and 60 % over the unanchored beams.

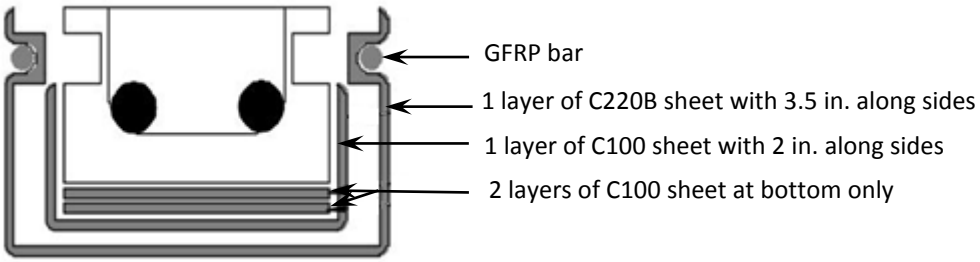

(a) GFRP side bar anchorage

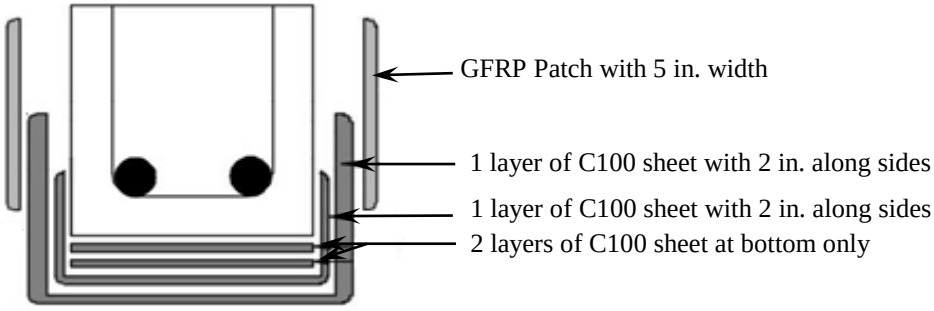

(b) GFRP side patch anchorage

Figure 2-10 New flexural anchorage techniques [43]

2.6 References

1. De Paiva, H.A. and Siess, C.P., 1965. Strength and behavior of deep beams in shear. *Journal of the Structural Division*, *91*(5), pp.19-41
2. Manuel, R.F., Slight, B.W. and Suter, G.T., 1971. Deep beam behavior affected by length and shear span variations. *Am Concrete Inst Journal & Proceedings*, *68*(12).
3. Kong, F.K. and Singh, A., 1972, August. Diagonal Cracking and Ultimate Loads of Lightweight Concrete Deep Beams deep beams,". In *Journal Proceedings* (Vol. 69, No. 8, pp. 513-521).
4. Smith, K.N. and Vantsiotis, A.S., 1982, May. Shear strength of deep beams. In *Journal Proceedings* (Vol. 79, No. 3, pp. 201-213).
5. Yang, K.H., Chung, H.S., Lee, E.T. and Eun, H.C., 2003. Shear characteristics of high-strength concrete deep beams without shear reinforcements. *Engineering structures*, *25*(10), pp.1343-1352.
6. Brown, M.D. and Bayrak, O., 2006. Minimum transverse reinforcement for bottle-shaped struts. *ACI Structural Journal*, *103*(6), p.813.
7. Mohamed, K.A., 2015. *Performance and Strut Efficiency Factor of Concrete Deep Beams Reinforced with GFRP Bars* (Doctoral dissertation, Université de Sherbrooke).
8. Tuchscherer, R., Birrcher, D., Huizinga, M. and Bayrak, O., 2011. Distribution of Stirrups across Web of Deep Beams. *ACI Structural Journal*, *108*(1).
9. Kani, G.N.J., 1964, April. The riddle of shear failure and its solution. In *Journal Proceedings* (Vol. 61, No. 4, pp. 441-468).

10. MacGregor, J.G. and Walters, J.R.V., 1967, October. Analysis of inclined cracking shear in slender reinforced concrete beams. In *Journal Proceedings* (Vol. 64, No. 10, pp. 644-653).
11. Hamadi, Y.D. and Regan, P.E., 1980. Behaviour in shear of beams with flexural cracks. *Magazine of Concrete Research*, *32*(111), pp.67-78.
12. Reineck, K.H., 1991. Ultimate shear force of structural concrete members without transverse reinforcement derived from a mechanical model (SP-885). *Structural Journal*, *88*(5), pp.592-602.
13. Chana, P.S., 1987. Investigation of the mechanism of shear failure of reinforced concrete beams. *Magazine of Concrete Research*, *39*(141), pp.196-204.
14. Vecchio, F.J. and Collins, M.P., 1986. The modified compression-field theory for reinforced concrete elements subjected to shear. *ACI J.*, *83*(2), pp.219-231.
15. Rahal, K.N., 2000. Shear Strength of Reinforced Concrete: Part 1-Membrane Elements Subjected to Pure Shear. *ACI Structural Journal*, *97*(1), pp.86-93.
16. Schlaich, J., Schäfer, K. and Jennewein, M., 1987. Toward a consistent design of structural concrete. *PCI journal*, *32*(3), pp.74-150.
17. Hsu, T.T., 1988. Softened truss model theory for shear and torsion. *Structural Journal*, *85*(6), pp.624-635.
18. Wight, J. K. and MacGregor, J. G., 2009. *Reinforced concrete: Mechanics and design* (5th edition). Upper Saddle River, NJ: Prentice Hall.
19. Schlaich, J. and Schafer, K., 1991. Design and detailing of structural concrete using strut-and-tie models. *Structural Engineer*, *69*(6), pp.113-125.

20. Latosh, F., 2014. *Structural behaviour of conventional and FRP-reinforced concrete deep beams* (Doctoral dissertation, Concordia University).

21. Quintero-Febres, C.G., Parra-Montesinos, G. and Wight, J.K., 2006. Strength of struts in deep concrete members designed using strut-and-tie method. *ACI Structural Journal*, *103*(4), p.577.

22. Brown, M.D., Bayrak, O., Yang, K.H., Ashour, A.F., Lin, C.H., Hwang, C.L., Lin, S.P., Liu, C.H., Yi, W.J., He, Q.F. and Xiao, Y., 2008. 395 Design of Deep Beams Using Strut-and-Tie Models-Part I: Evaluating US Provisions. *ACI Structural Journal*, *105*(4), p.2

23. Park, S. and Aboutaha, R.S., 2009. Strut-and-tie method for CFRP strengthened deep RC members. *Journal of Structural Engineering*, *135*(6), pp.632-643.

24. Mahmood, M.N., 1986. *Non-Linear Finite Element Analysis of Reinforced Concrete Deep Beams* (M.Sc. Thesis, University of Mousl, Iraq).

25. Aziz, O.Q.,1997. *Shear Strength Prediction of Crushed Stone Reinforced Concrete Deep Beams* (Doctoral dissertation, University of Technology, Iraq).

26. Al-Shraify, I.S., 2002. *Nonlinear Finite Element Analysis of Reinforced Concrete Continuous Deep Beams* **(**M.Sc. Thesis, Al-Nahrain Universty, Iraq).

27. Park, J.W. and Kuchma, D., 2007. Strut-and-tie model analysis for strength prediction of deep beams. *ACI Structural Journal*, *104*(6), p.657.

28. Zhang, N. and Tan, K.H., 2007. Size effect in RC deep beams: Experimental investigation and STM verification. *Engineering Structures*, *29*(12), pp.3241-3254.

29. Tan, K.H., Tang, C.Y. and Tong, K., 2003. A direct method for deep beams with web reinforcement. *Magazine of concrete research*, *55*(1), pp.53-63.

30. Berset, J.D., 1992. *Strengthening of reinforced concrete beams for shear using FRP composites* (Doctoral dissertation, Massachusetts Institute of Technology).
31. Farouk, I.A., 2008. *Retrofit of Shear Critical R.C Beam with Carbon Fiber Reinforced Polymer sheet* (Doctoral dissertation, University of Technology, Iraq).
32. Kachlakev, D.I., Miller, T.H., Potisuk, T., Yim, S.C. and Chansawat, K., 2001. *Finite element modeling of reinforced concrete structures strengthened with FRP laminates* (No. FHWA-OR-RD-01-XX). Oregon. Dept. of Transportation. Research Group.
33. Zhang, Z., Hsu, C.T.T. and Moren, J., 2004. Shear strengthening of reinforced concrete deep beams using carbon fiber reinforced polymer laminates. *Journal of Composites for Construction*, *8*(5), pp.403-414.
34. Hwang, S.J., Tu, Y.S., Yeh, Y.H. and Chiou, T.C., 2004. Reinforced concrete partition walls retrofitted with carbon fiber reinforced polymer. In *ANCER annual meeting: networking of young earthquake engineering researchers and professionals*.
35. Santhakumar, R., Chandrasekaran, E. and Dhanaraj, R., 2004. Analysis of retrofitted reinforced concrete shear beams using carbon fiber composites. *Electronic journal of structural engineering*, *4*(1), pp.66-74.
36. Islam, M.R., Mansur, M.A. and Maalej, M., 2005. Shear strengthening of RC deep beams using externally bonded FRP systems. *Cement and Concrete Composites*, *27*(3), pp.413-420.
37. Elgwady, M.A., Rabie, M. and Mostafa, M.T., 2005. Strengthening of corbels using CFRP an experimental program. *Cairo University, Giza, Egypt*, pp.1-9.

38. Al-Shmmary, T.M.H., 2006. *Nonlinear Finite Element Analysis of Reinforced Concrete Beams Flexural Strengthened with Carbon Fiber Reinforced Polymer Plates* (M.Sc. Thesis, University of Babylon).

39. Ali, D.D., 2007. *Experimental and Theoretical Investigation of The Behavior of Reinforced Concrete Beams Strengthened by Fiber Reinforced Polymer* (Doctoral dissertation, University of Baghdad, Iraq).

40. Nehdi, M., Omeman, Z. and El-Chabib, H., 2008. Optimal efficiency factor in strut-and-tie model for FRP-reinforced concrete short beams with (1.5< a/d< 2.5). *Materials and Structures*, *41*(10), pp.1713-1727.

41. Sarsam, K.F. and Izzet, A.F., 2009. Retrofit of Shear Critical RC Beams with Carbon Fiber Reinforced Polymers (CFRP). *Engineering and Technology Journal*, *27*(12), pp.2398-2410.

42. Rasheed, H.A., Decker, B.R., Esmaeily, A., Peterman, R.J. and Melhem, H.G., 2015. The influence of CFRP anchorage on achieving sectional flexural capacity of strengthened concrete beams. *Fibers*, *3*(4), pp.539-559.

43. Zaki, M., 2018. *Behavior of Reinforced Concrete Beams Strengthened Using CFRP Sheets with Superior Anchorage Devices* (Doctoral dissertation).

Chapter 3 - Experimental Work and Test Results

3.1 General

The main objective of the present work is to understand the behavior of reinforced concrete deep beams with and without flexural CFRP strengthening and the effect of an innovative anchorage devices on their capacities. This Chapter describes the material properties, the details of test specimens, and the experimental test procedure. Moreover, the general behavior and observation of tested deep beam specimens were reported and discussed.

3.2 Material Properties

3.2.1 Concrete

Ready-mix concrete supplied by a local concrete company was used for casting all deep beam specimens. Design nominal strength of the mix was 5000 psi (34.5 MPa), and all the beam specimens were cast in the same batch. Furthermore, six (4 in. x 8 in.) cylinders were casted on site simultaneously with all beam specimens. The six cylinders prepared and tested according to ASTM C39. Three cylinders were tested in compression after 7 days and the other three were tested in compression after 28 days. A typical mode of failure for the cylinders is shown in Figure 3-1. Table 3-1 shows the results of the cylinder tests.

Table 3-1 Concrete mix properties of test beams

Average compressive strength at 7 days	4.65 ksi
Average compressive strength at 28 days	5.30 ksi
Testing rate	350-450 lb/s
Slump	1.75 in.

(a) Before testing **(b)** After testing

Figure 3-1 Compression testing of the concrete cylinders

3.2.2 Steel Reinforcement

In this study, #3 and #5 diameter bars were used to make the steel caging of the tested beams. Three representative reinforcing steel specimens for each diameter were tested under tension by the research testing lab at Kansas Department of Transportation (KDOT) to evaluate the stress-strain characteristics of the steel bars.

Table 3-2 Test results of reinforcement bars

Specimens	No. 3		No. 5	
	F_y *(ksi)*	*E (ksi)*	F_y *(ksi)*	*E (ksi)*
Specimen #1	67.61	31360	68.50	28969
Specimen #2	68.95	28554	68.74	30668
Specimen #3	71.50	28000	72.50	29000
Average	69.35	29305	69.91	29545

The total length of the test specimens was 28 inches in length, see Figure 3-2. Table 3-2 summarizes the mechanical properties of the reinforcing bars. The stress-strain response for the steel bars is shown in Figure 3-3.

(a) No. 3

(b) No. 5

Figure 3-2 Steel tensile test

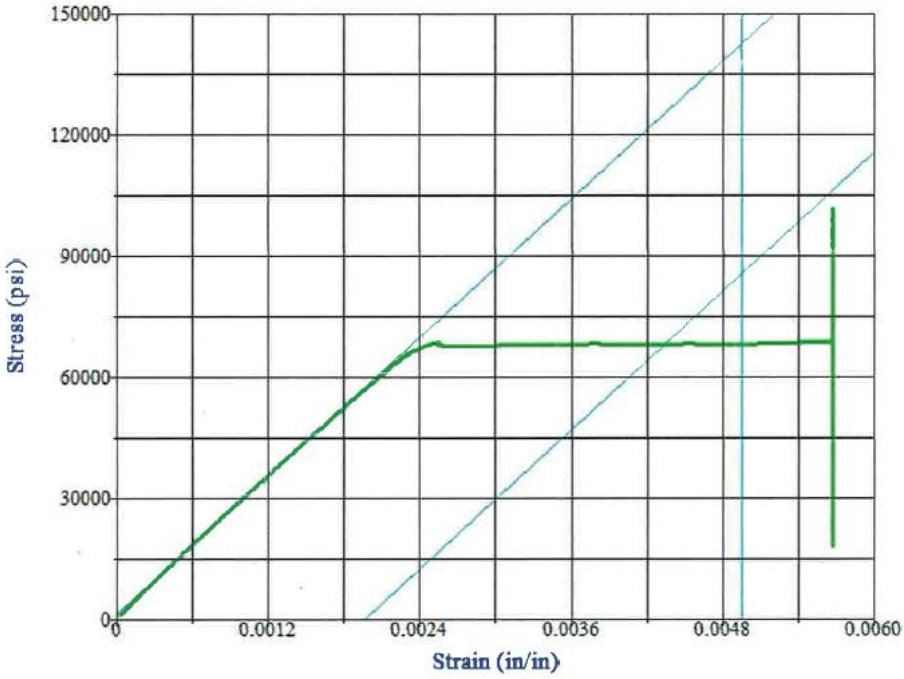

(a) No. 3

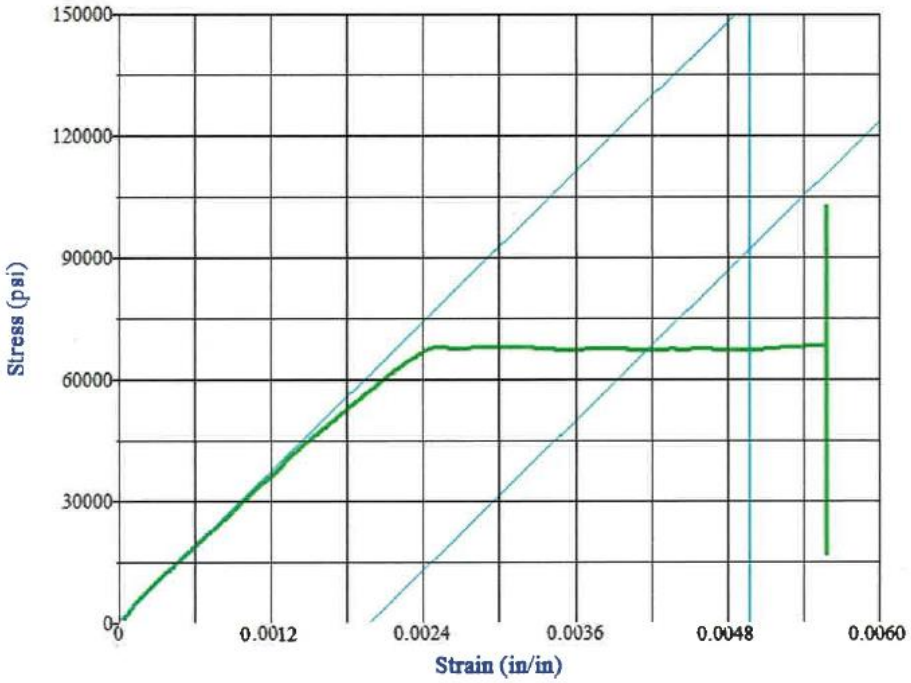

(b) No. 5

Figure 3-3 Stress-strain relationship for steel reinforcing bars

3.2.3 Fiber Reinforced Polymer (FRP)

Three different types of FRP materials were used for strengthening two of the tested beams.

(a) V-Wrap C100 **(b)** V-Wrap C220B **(c)** V-Wrap EG50-B

Figure 3-4 FRP sheets

The three types of FRP sheets are:

1. Uni-directional carbon fiber reinforced polymer (CFRP) identified as V-Wrap C100,
2. Bi-directional CFRP identified as V-Wrap C220B, and
3. Glass fiber reinforced polymer (GFRP) identified as EG-50B.

Figure 3-4 shows the FRP sheets used in this study. The mechanical properties of the FRP sheets used in this study, as reported by the manufacturers, are shown in Table 3-3.

Table 3-3 Mechanical properties of FRP sheets

Properties	0° Unidirectional CFRP (V-Wrap C100)	0/90° Bidirectional CFRP (V-Wrap C220B)	±45° Bidirectional GFRP (V-Wrap EG50-B)
Tensile Strength (Longitudinal)	140 ksi	155 ksi	40.5 ksi
Tensile Modulus (Longitudinal)	9600 ksi	14000 ksi	2697.70 ksi
Thickness (Cured Laminate)	0.023 in	0.020 in (each direction)	0.034 in (each direction)

3.2.4 Bonding Materials

Numerous studies show that the stress in FRP sheets is transferred to reinforced concrete beam via adhesive.

(a) **(b)**

Figure 3-5 Bonding Materials (a) Parts A and B of the epoxy; (b) Mixing of the epoxy

In this research, V-Wrap 770 epoxy resin is used for bonding CFRP sheets to the two of the tested reinforced concrete beams. This adhesive consists of two liquid components (A and B) that are mixed together with a mixing ratio of 3:1 by weight, according to manufacturer's proportions, see Figure 3-5. Table 3-4 shows the technical properties of the adhesive materials as supplied by the manufacturer.

Table 3-4 Technical properties of bonding materials

Physical properties	**psi**	**MPa**
Tensile Strength (ASTM D638)	8800	60.7
Tensile Modulus (ASTM D638)	400000	2760
Elongation at Break (ASTM D638	4.4%	4.4%
Flexure Strength (ASTM D790)	13780	95
Flexure Modulus (ASTM D790)	380000	2620
Compressive Strength (ASTM D695)	12450	85.8
Compressive Strength (ASTM D695)	387000	2670
Epoxy Shear Strength		

Density		**Packaging**		
		Volume	**Weight**	**Package**
Part A	9.7 lbs/gal (1.16 kg/L)	2.8 gal	27.3 lbs	5 gal pail
Part B	7.9 lbs/gal (0.95 kg/L)	1.15 gal	9.1 lbs	5 gal pail

3.3 Deep Beam Specimens

Three deep beams were obtained from healthy parts of 16-foot long specimens were previously tested in flexure under four-point bending to failure by Zaki (2018) **[2]**. These beams were prepared in the structural lab at Kansas State University with 42-inch length and cross sectional dimensions of 6-inch width by 12-inch height by using a gas power saw cut, see Figure 3-6. The flexural reinforcement of the beams consisted of 2-#5 tension bottom bars at the tension side, and 2-#3 top

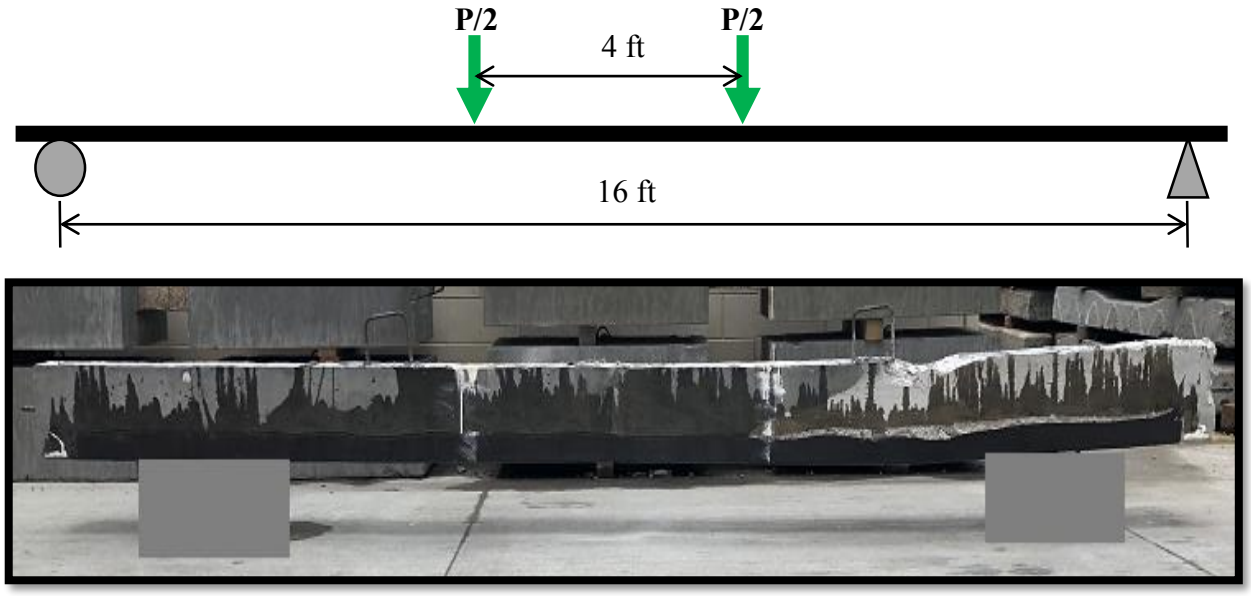

(a) Zaki's flexure specimens

(b) Preparation of the tested beams

(c) Cutting saw

Figure 3-6 History of the tested deep beam specimens

bars at the compression side. Moreover, the beams were reinforced for shear with #3 closed stirrups spaced at 5 inches on center along the span length. Figure 3-7 shows specimen dimensions, reinforcement details, support locations, and location of loading point.

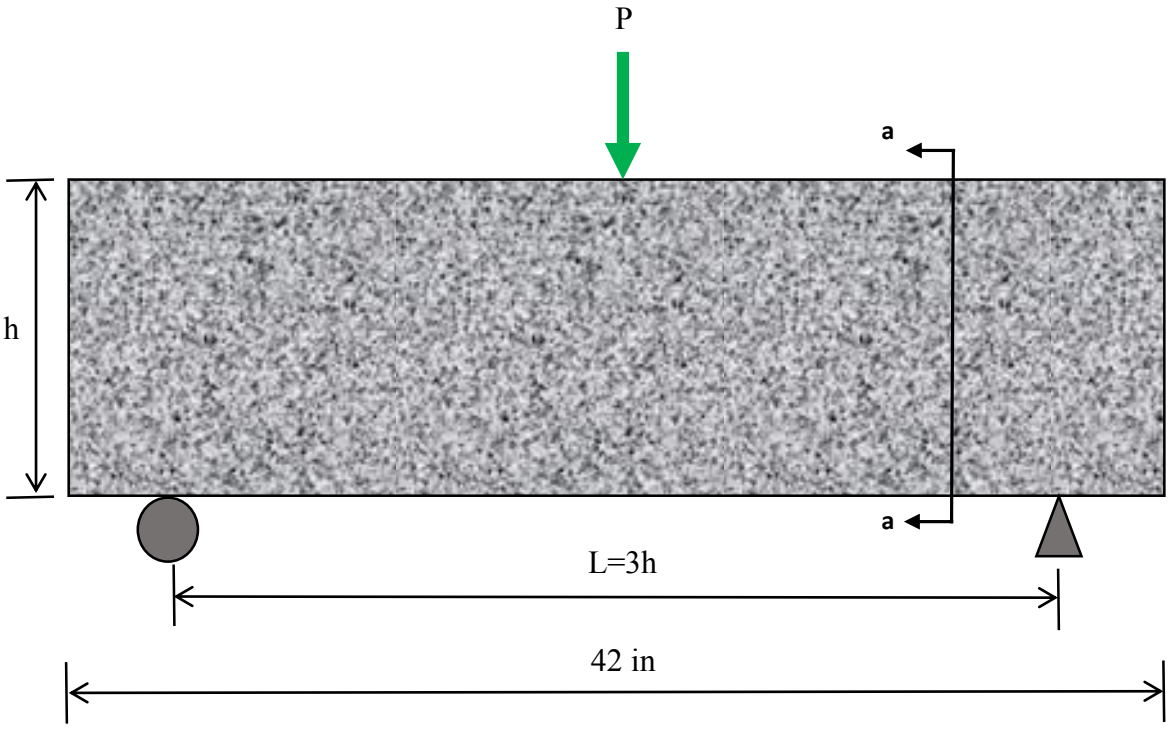

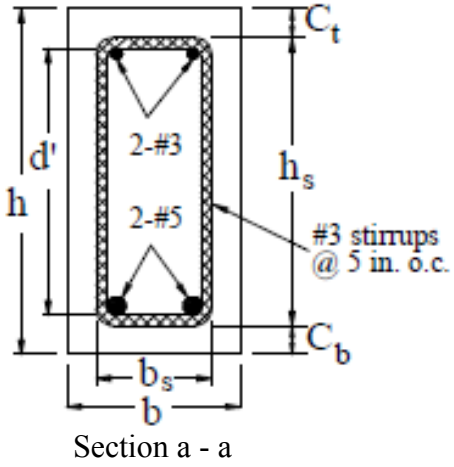

b	6 in. (153 mm)
h	12 in. (305 mm)
C_t	1 in. (25.4 mm)
C_b	1 in. (25.4 mm)
h_s	10 in. (254 mm)
b_s	4 in. (101.6 mm)
d'	9.25 in. (235 mm)

Figure 3-7 Geometry and reinforcement of the tested deep beam specimens

In order to identify the test beam specimens with different strengthening schemes and anchorage devices, the following designation system is used, see Table 3-5.

Table 3-5 Designation of the tested beam specimens

Symbol	Description
CON	**Con**trol
CSW	**C**FRP **S**hort **W**rap around beam sides
GSP	**G**FRP **S**ide **P**atch anchorage
GSB	**G**FRP **S**ide **Bar** anchorage

The first concrete beam specimen (**CON**) was tested without retrofitting and was considered as a control beam for comparison. The second-deep beam specimen (**CSW-GSP**) had four flexure layers of CFRP sheets installed at tension zone of the beam using external anchorage. These four flexural layers were three layers of unidirectional CFRP (V-Wrap C100) and one layer of bidirectional CFRP (V-Wrap C220B). The external anchorage used for this specimen consists of side ±45° bidirectional GFRP (V-Wrap EG50-B) patches with 5 inches width along the beam length. Figure 3-8 shows the strengthening scheme of this deep beam specimen.

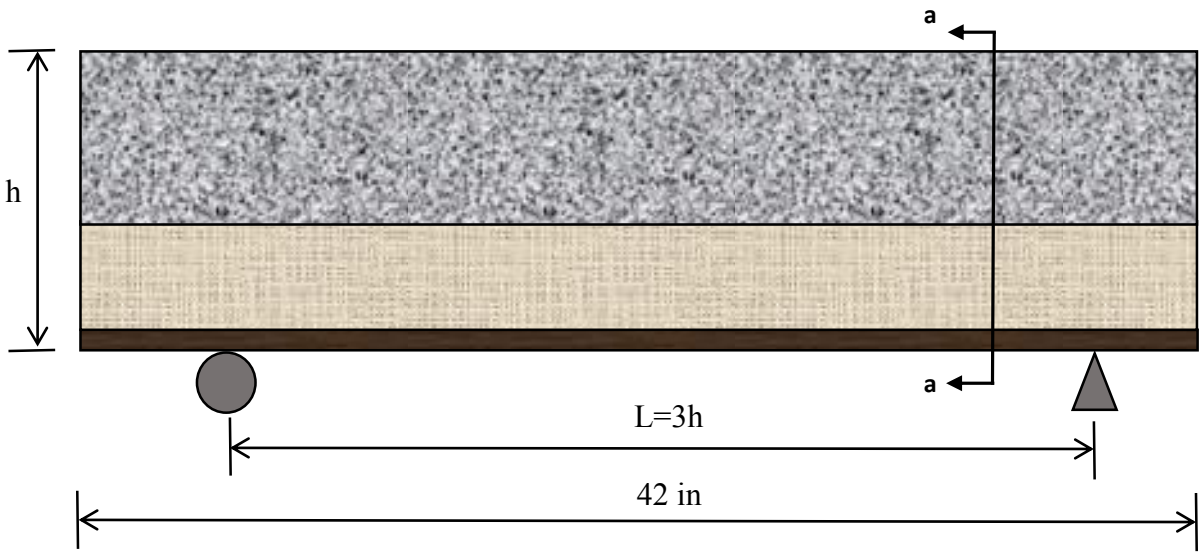

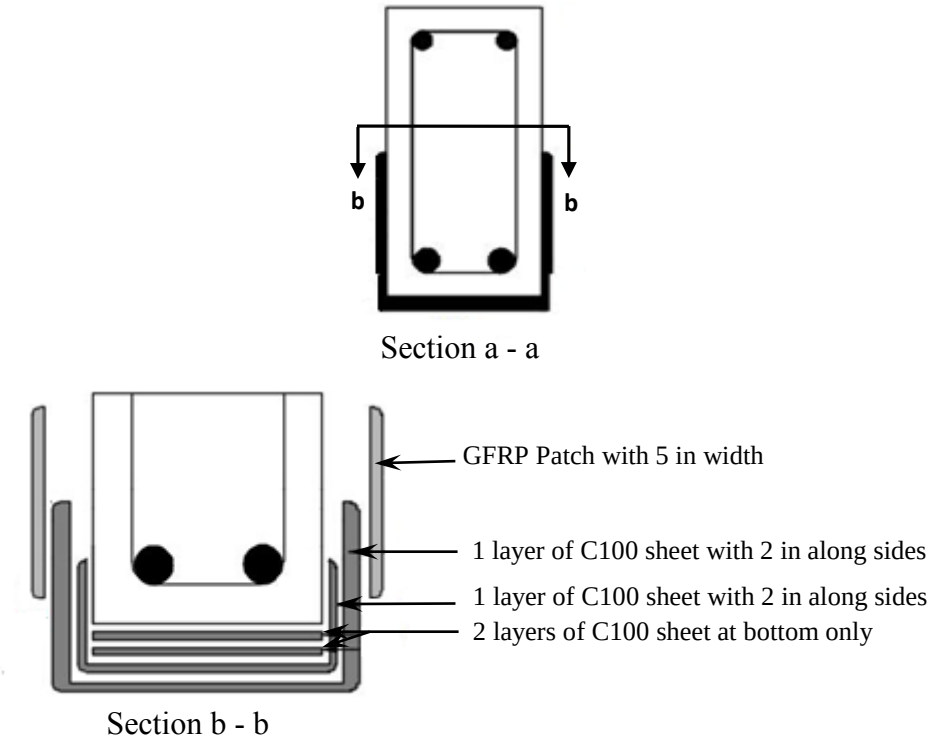

Figure 3-8 Geometry and details of specimen (CSW-GSP)

The third-deep beam specimen (**CSW-GSB**) had the same three layers of unidirectional CFRP (V-Wrap C100) and one layer of bidirectional CFRP (V-Wrap C220B). But, the bidirectional layer of C220B was inserted into premade side grooves (1 inch by 1 inch) along the beam length.

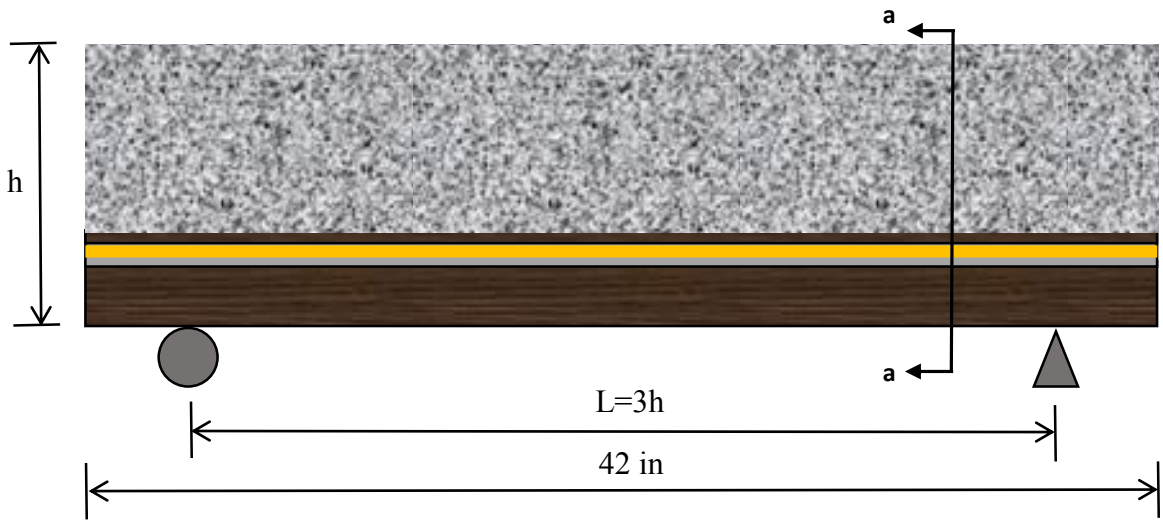

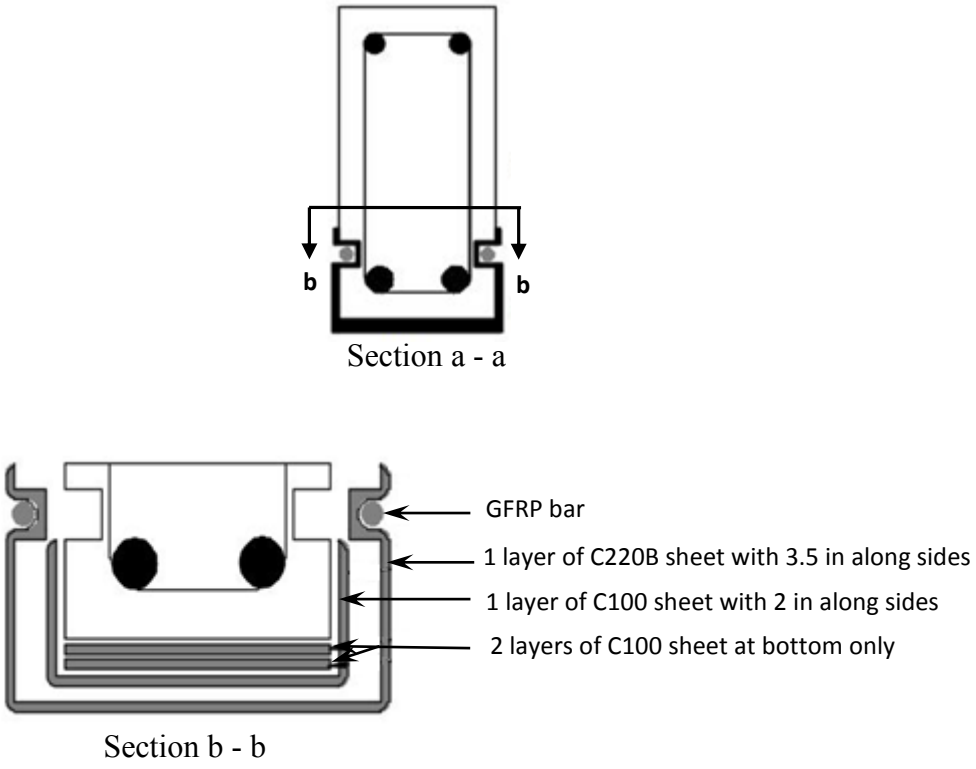

Figure 3-9 Geometry and details of specimen (CSW-GSB)

A GFRP bars with diameter of 0.5 inches was inserted into each groove that were filled with high strength of epoxy putty filler. Figure 3-9 shows the strengthening schemes of this deep beam specimen.

Casting of the beam specimens, preparation of concrete surface, and the installation of FRP materials can be found in Zaki (2018) **[2]**.

3.4 Test Setup and Instrumentation

All beams were tested up to failure as simply supported by three 1 in. diameter steel rollers. A steel bearing plate of (4 in. x 6 in. x 1 in.) inserted between the concrete and steel rollers to prevent localized failure at the supporting and loading point. All beams had a total clear span length of 36 inches., and the CFRP sheets were cut using a hand saw machine to have the CFRP

sheets cover 85% of the full span in order not to extend under the beam supports, see Figure 3-10.

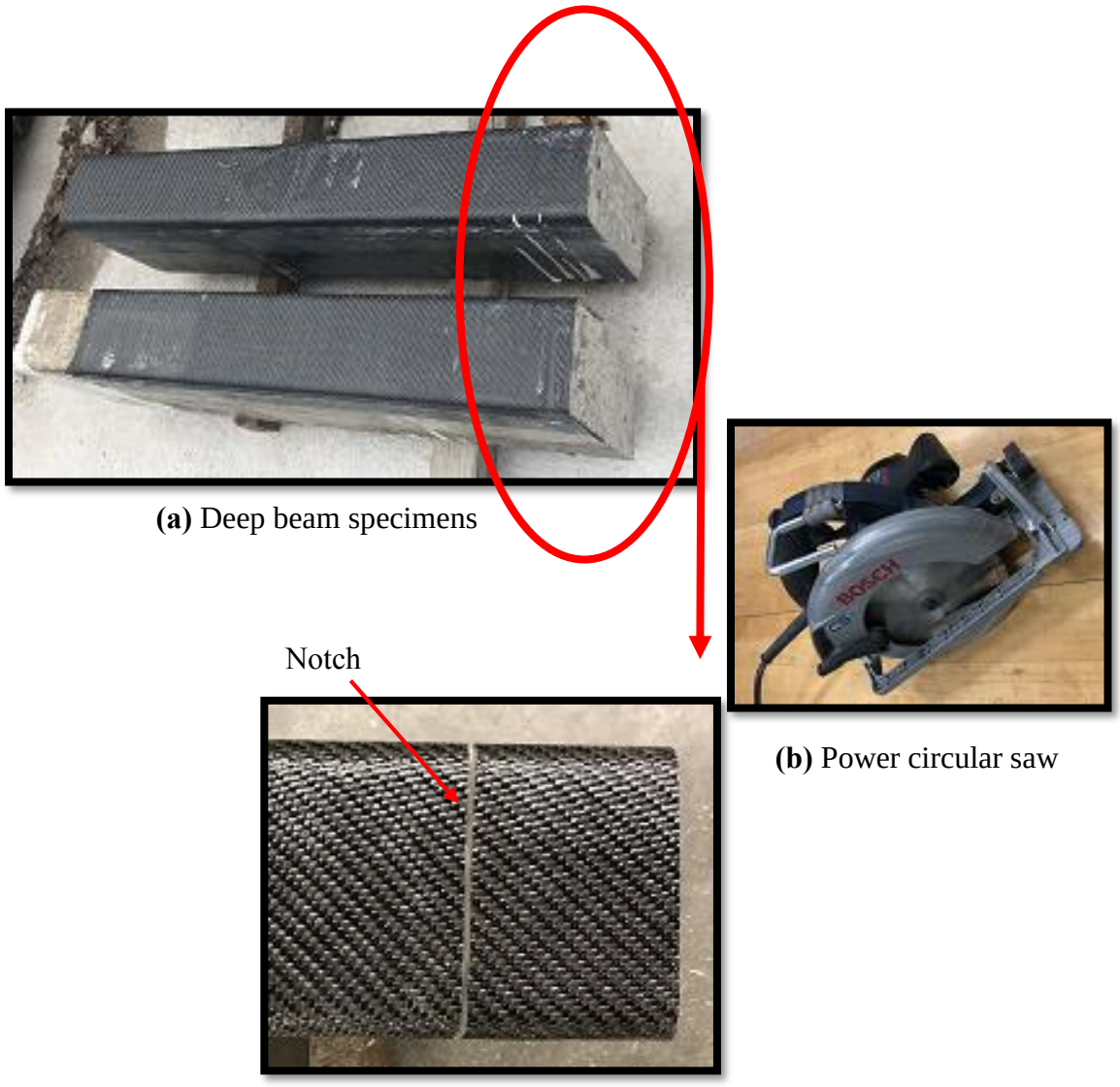

(a) Deep beam specimens

(b) Power circular saw

(c) CFRP sheet notch

Figure 3-10 Introduction of notches on the CFRP sheets

The deep beams were tested in the structural testing laboratory at Kansas State University using a 150 kips capacity hydraulic actuator, see Figure 3-11. The loading rate applied on the beam was 0.025 in./min. The beam deflection was measured at mid-span. Two FRP strain gages per specimen

were bonded to beam soffit of the strengthened beams in order to measure the strain in the CFRP sheets. Moreover, four more FRP strain gages (two per shear span) were installed on side patch anchorage of specimen **CSW-GSP** in order to record the FRP transverse strain on the failure side as shown in Figure 3-12. The beams were white-painted to facilitate crack viewing, and the appearance of first cracks and their propagation were detected visually.

Figure 3-11 Laboratory test setup

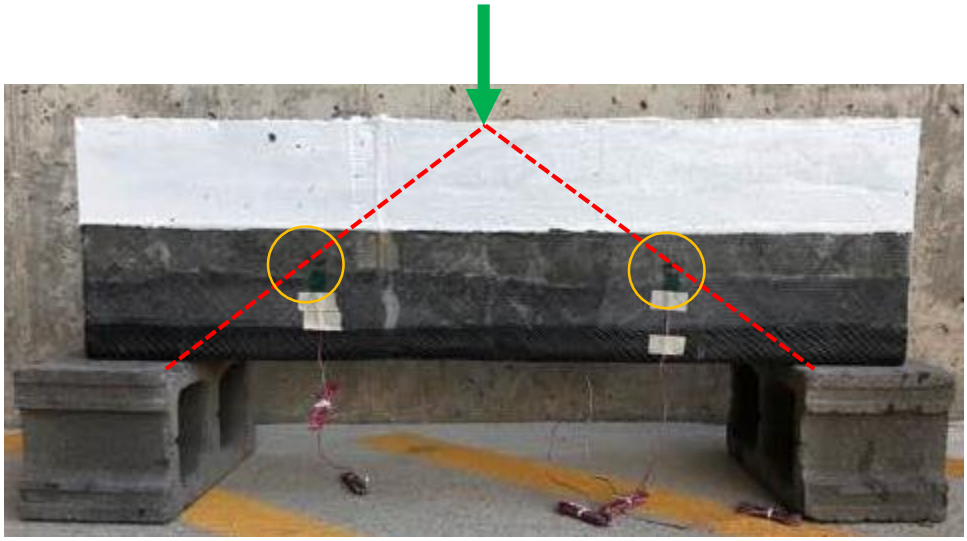

Figure 3-12 Location of side FRP strain gages of specimen (CSW-GSP)

3.5 Test Results and Discussion

Test results were analyzed based on cracking load, ultimate load, vertical mid-span deflection, failure mode and vertical mid-span strain on the FRP sheets at the beam's soffit. It also presents the gain in shear capacity due to the application of the CFRP sheets with the anchorage devices.

The cracks pattern of the specimen **CON** is shown in Figure 3-13.

Figure 3-13 Cracks pattern of beam specimen (CON)

First crack was observed at an applied load of 22 kips at the right hand side of the beam. Then, some flexural small cracks along the beam bottom appeared and got wider rapidly as the load was increased. Some of the small shear cracks merged and developed into the inclined crack. The collapse happened by crushing of the horizontal strut at the left hand side of the beam at load of 87.44 kips. Figure 3-14 shows the load-deflection curve for the beam specimen **CON**.

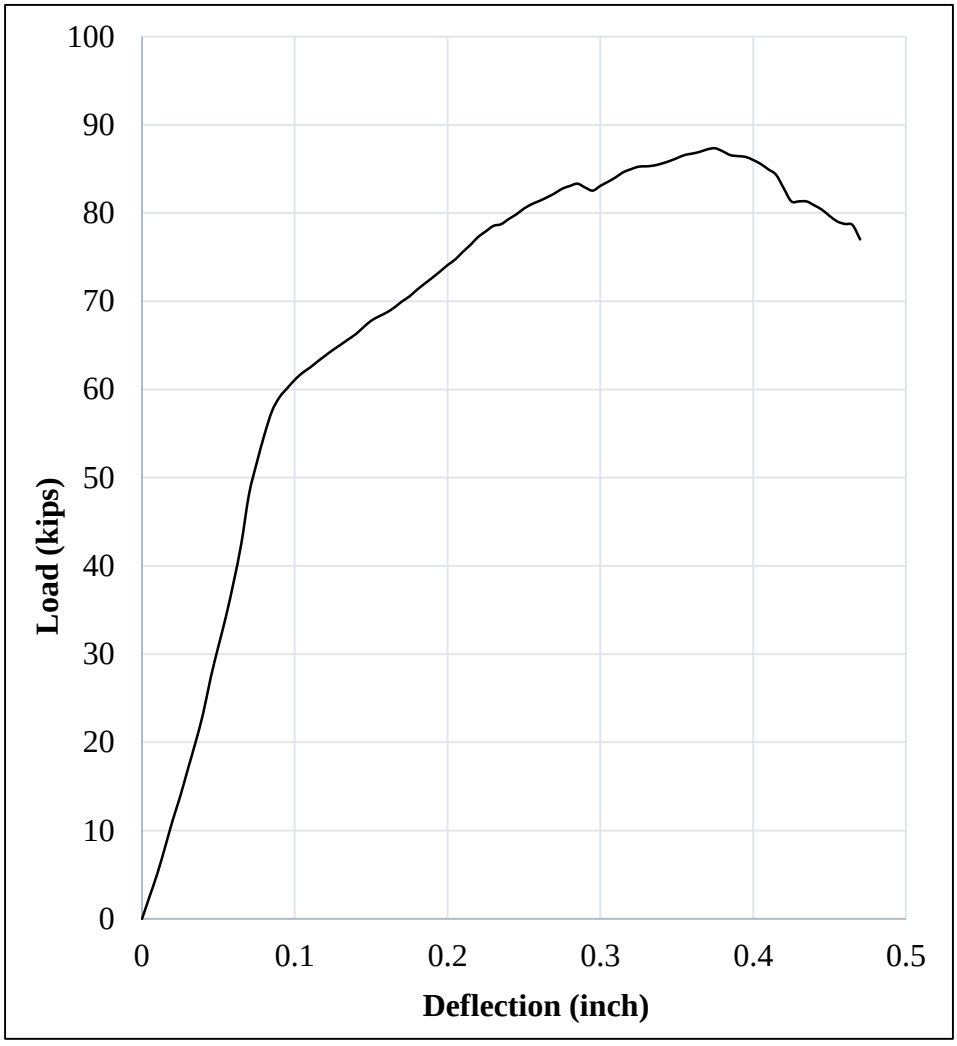

Figure 3-14 Load vs. mid-span deflection for beam specimen (CON)

The cracks pattern of the beam specimen (**CSW-GSP**) is shown in Figure 3-15. First crack is delayed and was observed at an applied load of 58 kips, and the beam failed at an ultimate

applied load of 107.63 kips with an increase in strength of about 23.09 % with respect to un-strengthened beam specimen **CON.** Figure 3-16 shows the comparison of load and mid-span deflection of beam specimens **CON** and **CSW-GSP**. The beam failed due to inclined crack at the right hand side of the beam. This crack initiated from the support and propagated towards the point of applied loads, which led to de-bonding of the GFRP side patches from the concrete surface. The maximum measured FRP strain was 0.00322 at the the beam's soffit (see Figure 3-17) and 0.001404 at side patches of the failure side (Figure 3-18).

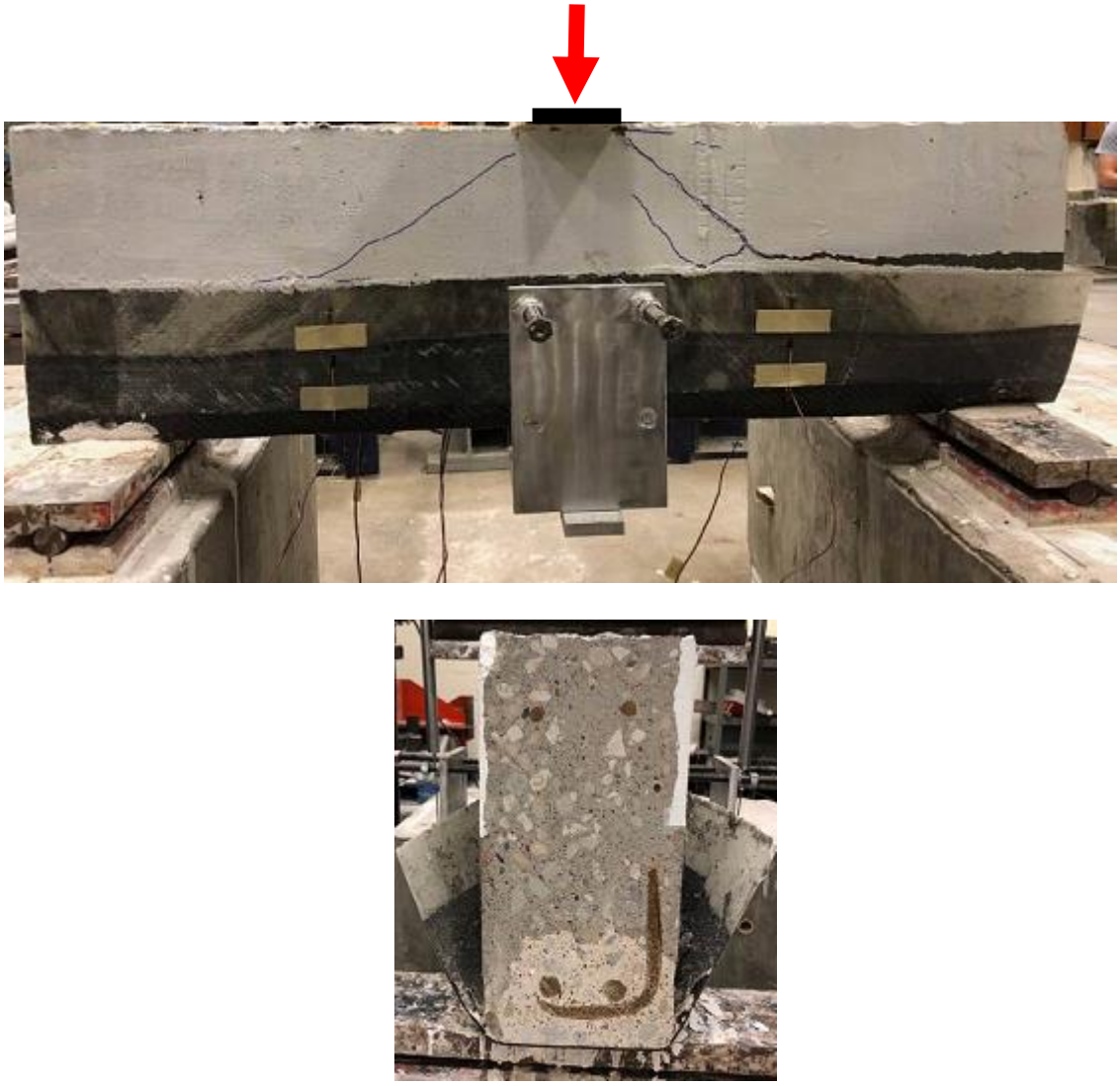

Figure 3-15 Cracks pattern of beam specimen (CSW-GSP)

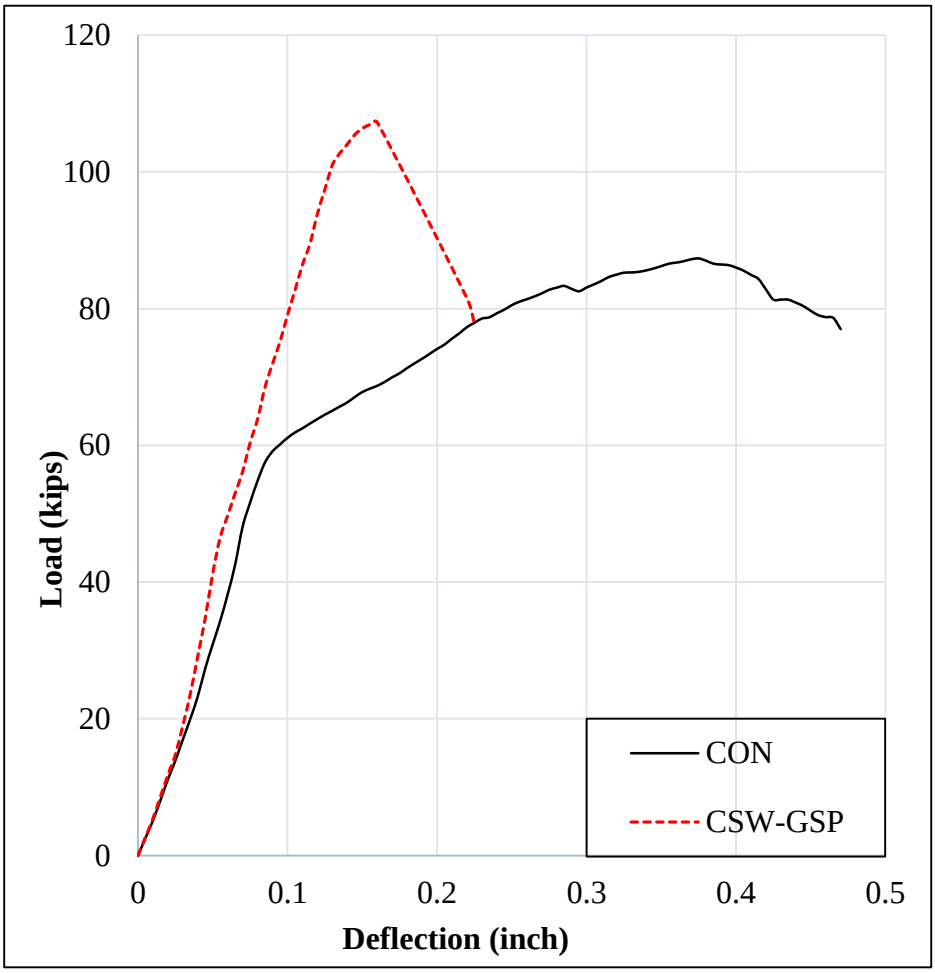

Figure 3-16 Load vs. mid-span deflection for beam specimen (CSW-GSP)

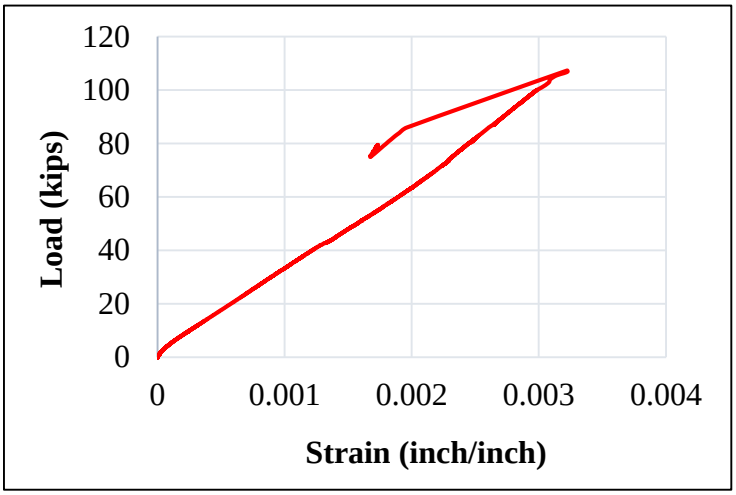

Figure 3-17 Load vs. mid-span FRP strain for beam specimen (CSW-GSP)

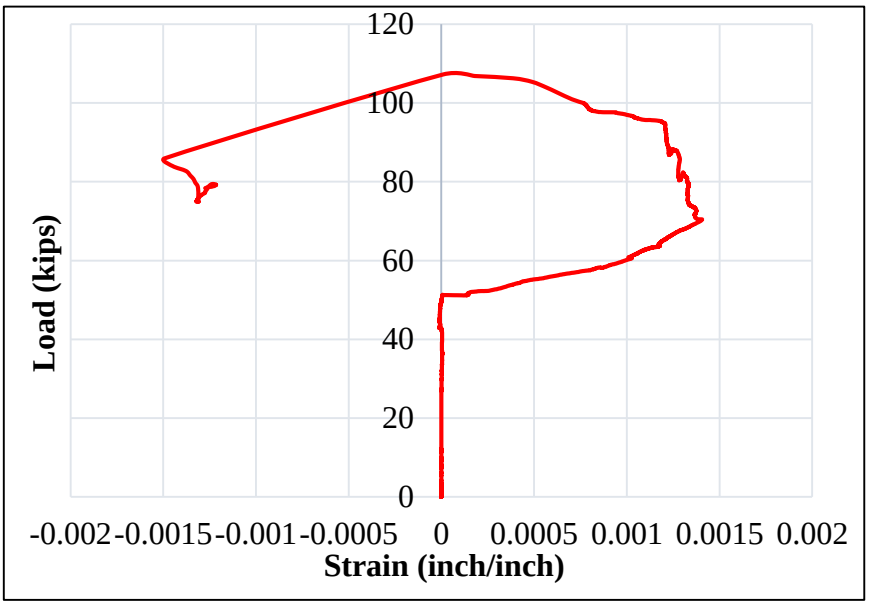

Figure 3-18 Load vs. GFRP patch strain at the failure for beam specimen (CSW-GSP)

The crack pattern of the beam specimen (**CSW-GSB**) is shown in Figure 3-19. First crack is delayed and was observed at an applied load of 32 kips, and the beam failed at an ultimate applied load of 58.10 kips with a decrease in strength of about 33.55 % with respect to un-strengthened beam specimen **CON.** Figure 3-20 shows the comparison of load and mid-span deflection of beam specimens **CON** and **CSW-GSB**.

The beam failed due to an inclined crack initiated from the GFRP side bar anchorages and propagated towards the point of applied load. Although the side GFRP bar anchors showed a significant increase in the capacity of the flexural beam specimens of Zaki 2018 **[2]**, test results showed that the mechanism of this anchorage in case of deep beams is not valid. The reason for this decrease in the capacity is that the GFRP side bars works as additional longitudinal ties which lead to decrease the effective depth of such beams. The max. measured FRP strain was 0.00125 at the the beam's soffit, see Figure 3-21.

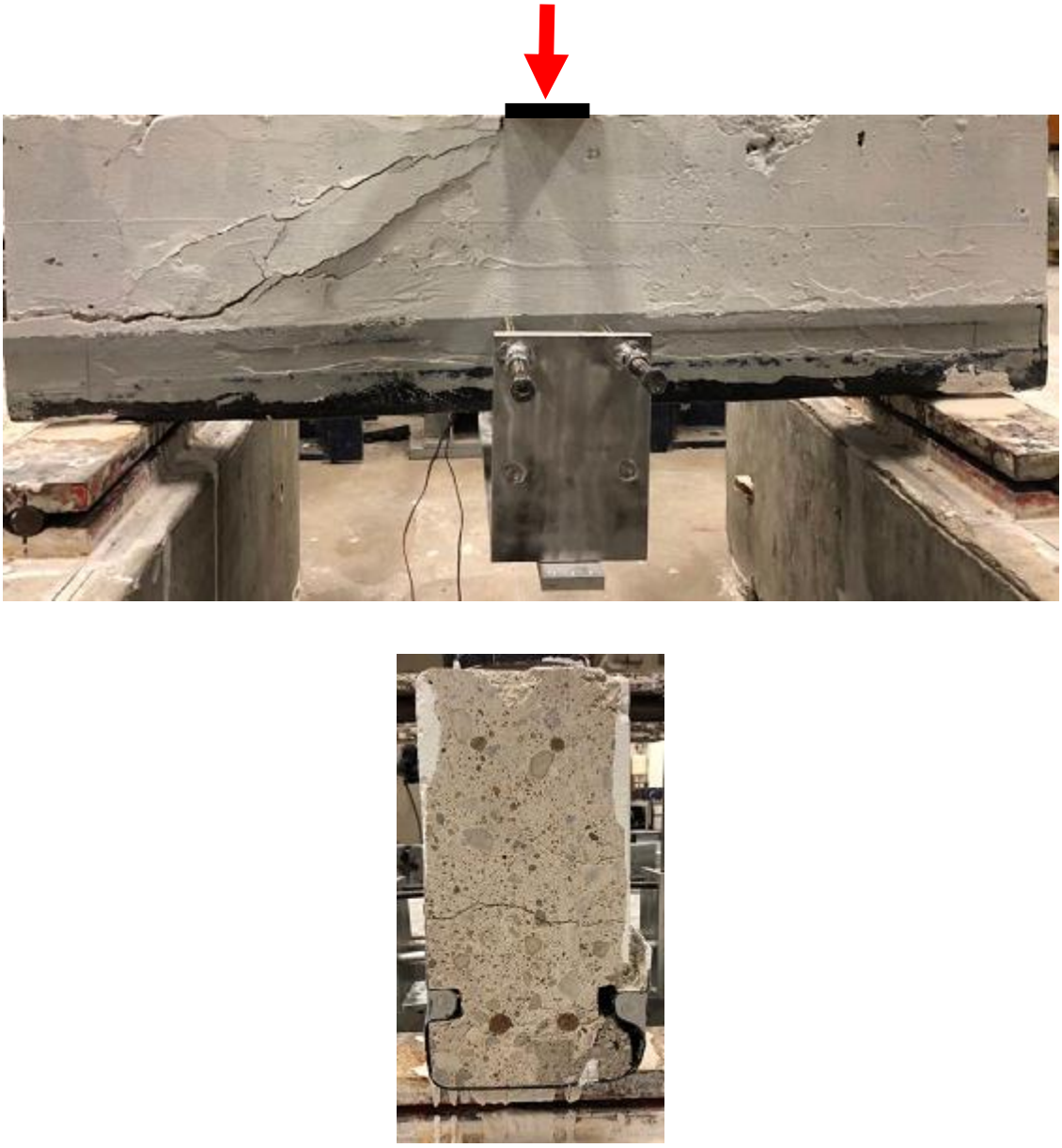

Figure 3-19 Cracks pattern of beam specimen (CSW-GSP)

The load-deflection comparison of the control beam, and the strengthened beam specimens are shown in Figure 3-22. Table 3-6 summarizes the experimental findings of all tested specimens.

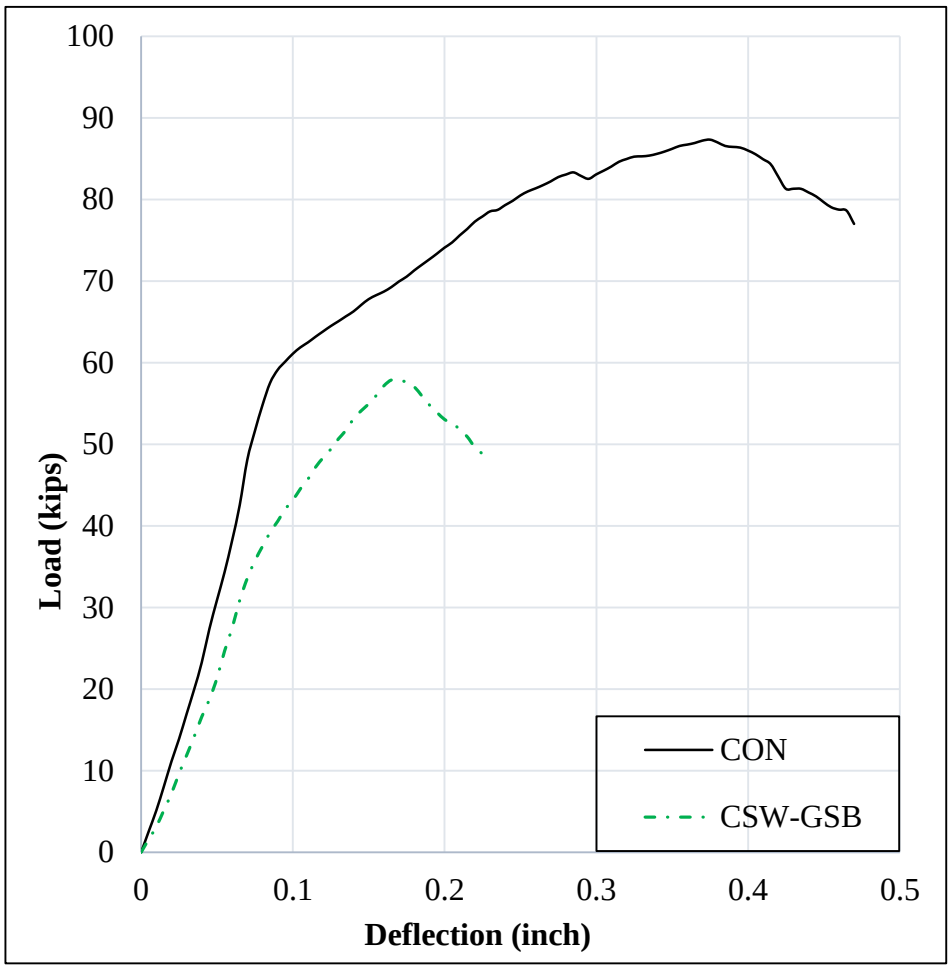

Figure 3-20 Load vs. mid-span deflection for beam specimen (CSW-GSP)

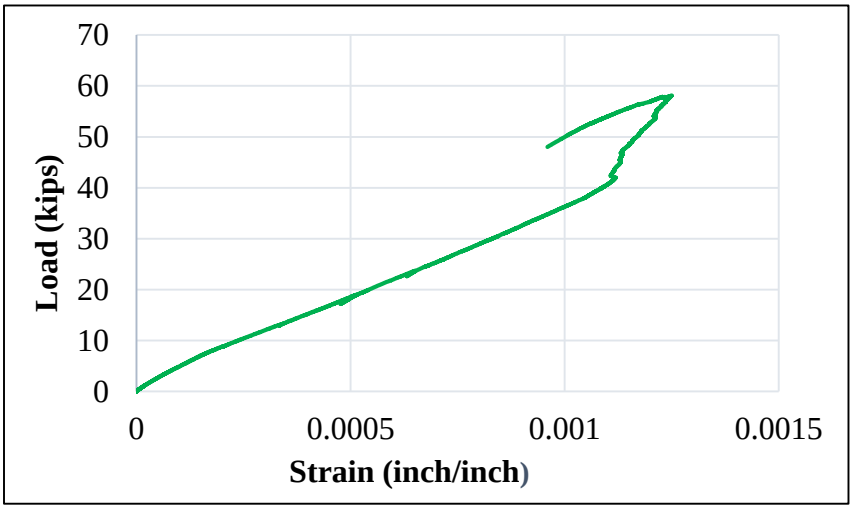

Figure 3-21 Load vs. mid-span FRP strain for beam specimen (CSW-GSP)

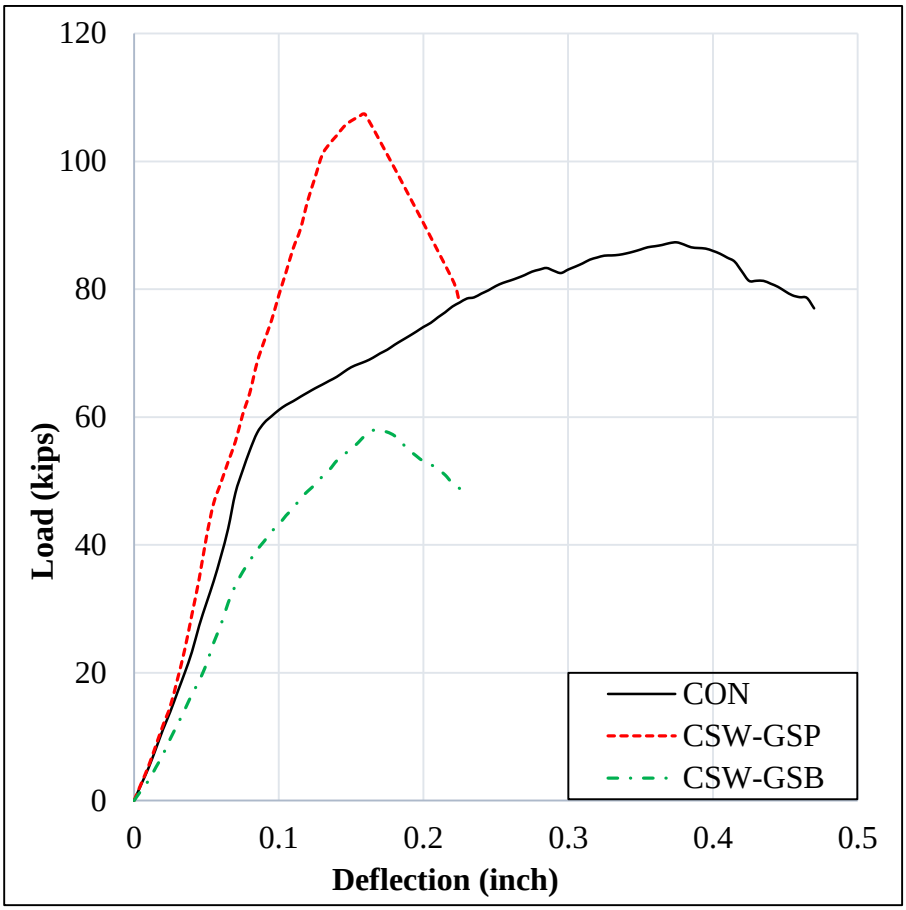

Figure 3-22 Load vs. mid-span deflection for all tested deep beam specimens

Table 3-6 Summary of results of the tested beam specimens

Specimen	Cracking load (kips)	P_u (kips)	% P_u Increase over CON	Maximum Deflection (in.)	Strut angle (deg.)	Failure mode [a]
CON	22	87.44	-	0.39	49	A
CSW-GSP	58	107.63	+23.09	0.15	53	B
CSW-GSB	36	58.10	-33.55	0.17	45	C

[a] **A** is Shear-flexural crack followed by horizontal strut failure; **B** is Diagonal strut failure plus FRP debonding; **C** is Diagonal strut failure.

3.6 References

1. American Society for Testing and Materials. Committee C-9 on Concrete and Concrete Aggregates, 2011. *Standard test method for compressive strength of cylindrical concrete specimens*. ASTM International.
2. Zaki, M., 2018. *Behavior of Reinforced Concrete Beams Strengthened Using CFRP Sheets with Superior Anchorage Devices* (Doctoral dissertation).

Chapter 4 - Analytical Work and Prediction Results

4.1 General

In this Chapter, a rational approach to predict the response of reinforced concrete deep beams with and without flexural CFRP strengthening is proposed based on the truss analogy method. Verification, against experimental results, is done in order to check the validity and accuracy of the proposed approach. The accuracy of the approach is determined by ensuring that the ultimate load is reasonably predicted in comparison with the experimental values. Furthermore, comparison of the load-deflection curves between the experimental and analytical findings is made for the tested deep beams and tested beams from literature.

4.2 Assumptions and Analytical Procedure

1. 2D truss structure is used to analyze rectangular deep beams following the ACI rules for STM as defined in Chapter Two.
2. The full response of deep beams is simplified with two loading stages by assuming the stress-strain relationships for the concrete in compression and the reinforcement steel are independent of each other. The concrete compressive stress-strain relationship is assumed to follow the Hognestad's curve, and a bilinear behavior is assumed for steel reinforcement. Typical stress-strain curve for concrete and steel are shown in Figure 4-1 and Figure 4-2, respectively. The two loading stages are:

Stage 1$(\mathbf{P_y}$ vs. $\mathbf{\Delta_y})$: ends with the yielding of the main tension reinforcement and uses the secant (total) stiffness approach with virtual work method to compute the mid span deflection, as following

***Tie Force*:**

$$F_t = \sigma_s \cdot A_s = \left(E_s * \varepsilon_{sy}\right) \cdot A_s \qquad (4.1)$$

Inclined Strut Force:

$$F_{ist} = \sigma_c \cdot A_{ist} = (E_c * \varepsilon_{ce}) \cdot A_{ist} \quad (4.2)$$

Horizontal Strut Force:

$$F_{hst} = \tilde{\sigma}_C \cdot A_{hst} \quad (4.3)$$

The three forces above (F_t, F_{ist}, F_{hst}) will be equated to their corresponding force values from standard truss analysis in terms of (P_y). The smallest value of (P_y) computed will be selected as the yielding force of the beam. The mid-span deflection of the beam at yielding will be computed by virtual work method as in Equation (4.4)

$$\Delta_y = \sum_{i=1}^{m} \frac{n_i^2 P_y L_i}{A_i E_i} \quad (4.4)$$

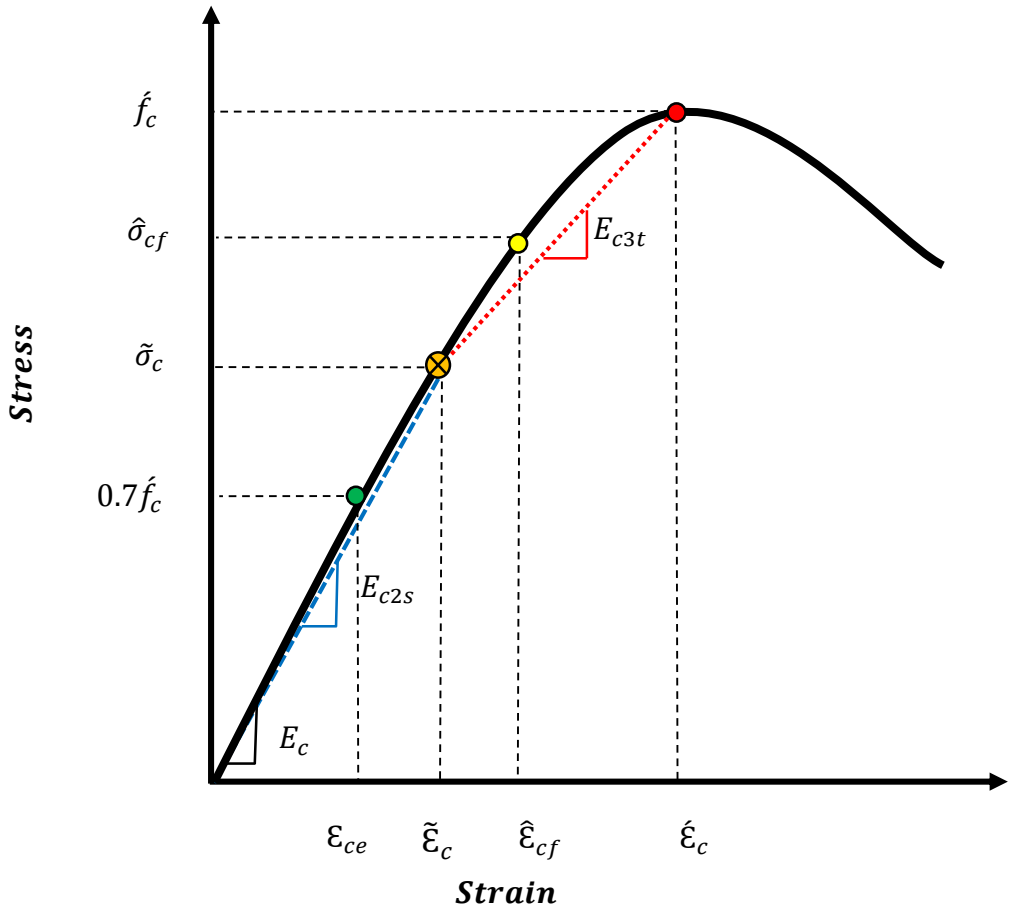

Figure 4-1 Concrete stress-strain curve

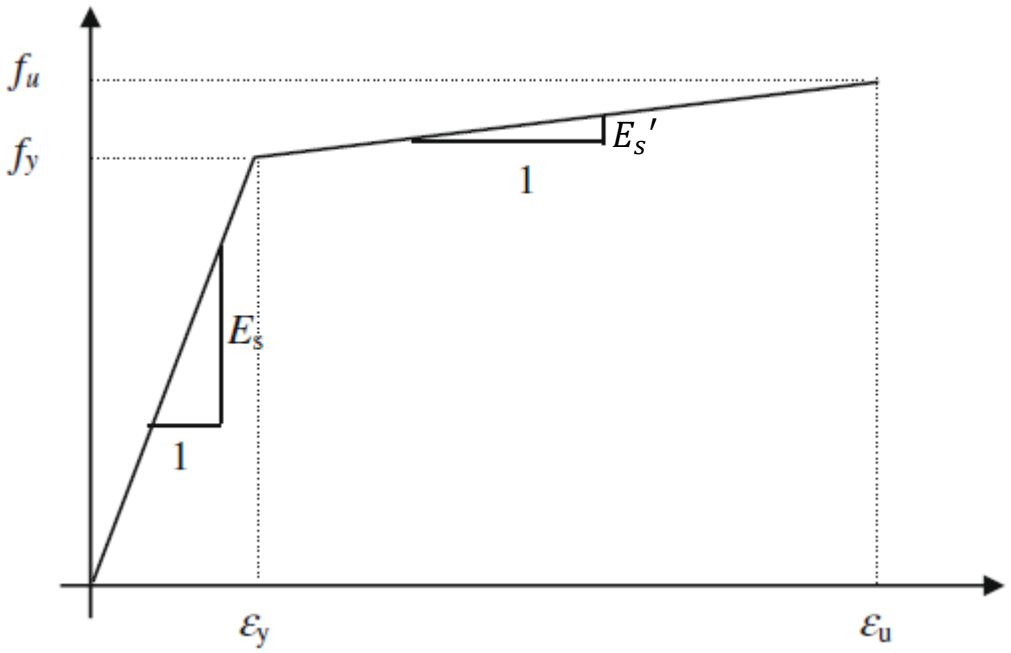

Figure 4-2 Steel bilinear stress-strain relationship

Stage 2 $(\boldsymbol{\Delta P_u}$ **vs.** $\boldsymbol{\Delta_{y-u}})$: ends with the ultimate point and uses the tangent (incremental) stiffness approach with virtual work method to compute the mid-span deflection, as following:

Tie Force Increment:

$$\Delta F_t = \Delta\sigma_s \cdot A_s = \left(\acute{E}_s * (\varepsilon_{su} - \varepsilon_{sy}\right) \cdot A_s \tag{4.5}$$

Inclined Strut Force Increment:

$$\Delta F_{ist} = \Delta\sigma_c \cdot A_{ist} = \left(E_{c2t} * (\hat{\varepsilon}_{cf} - \varepsilon_{ce}\right) \cdot A_{ist} \tag{4.6}$$

Where $E_{c2t} = \frac{\hat{\sigma}_{cf} - 0.7\acute{f}_c}{\hat{\varepsilon}_{cf} - \varepsilon_{ce}}$

Horizontal Strut Force Increment:

$$\Delta F_{hst} = \Delta\sigma_{cf} \cdot A_{hst} = \left(E_{c3t} * (\acute{\varepsilon}_c - \tilde{\varepsilon}_c\right) \cdot A_{hst} \tag{4.7}$$

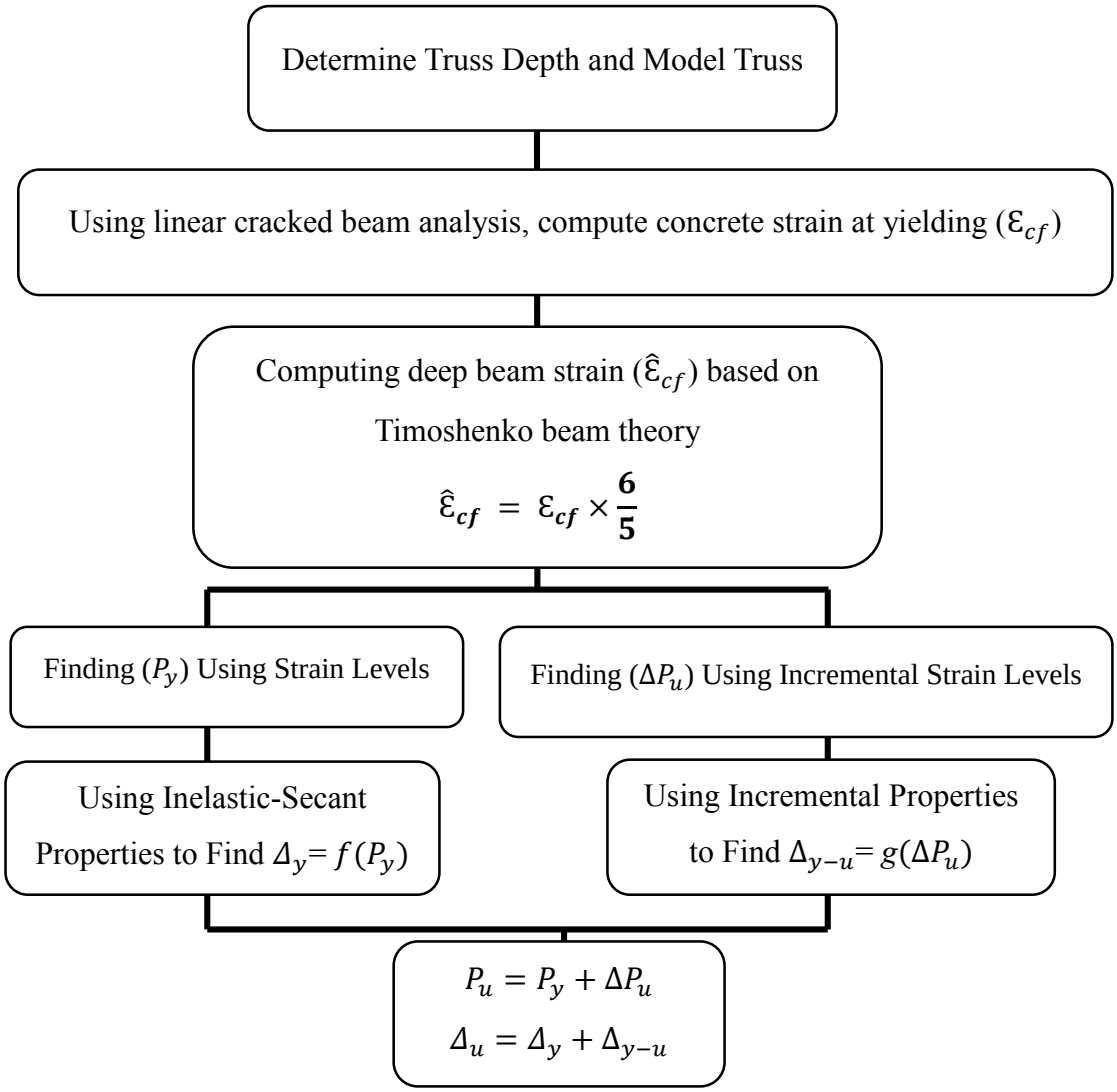

Figure 4-3 Flowchart of proposed approach for unstrengthened deep beam

The three force increments ($\Delta F_t, \Delta F_{ist}, \Delta F_{hst}$) above will be equated to their corresponding force increment values from standard truss analysis in terms of (ΔP_u). The smallest value of (ΔP_u) computed will be selected as the yielding-ultimate force in the deep beam. The mid-span deflection of the beam as the yielding-ultimate deflection in the deep beam will be computed by virtual work method as in Equation (4.8).

$$\Delta_{y-u} = \sum_{i=1}^{m} \frac{n_i^2 \Delta P_u L_i}{A_i E_i} \quad (4.8)$$

From the two loading stages above, the ultimate load capacity and mid span deflection of the RC deep beams are computed from Equation (4.9) and Equation (4.10), respectively

$$P_u = P_y + \Delta P_u \tag{4.9}$$

$$\Delta_u = \Delta_y + \Delta_{y-u} \tag{4.10}$$

Figure 4-3 illustrates solution steps of the proposed approach to predict the full response of unstrengthened deep beam.

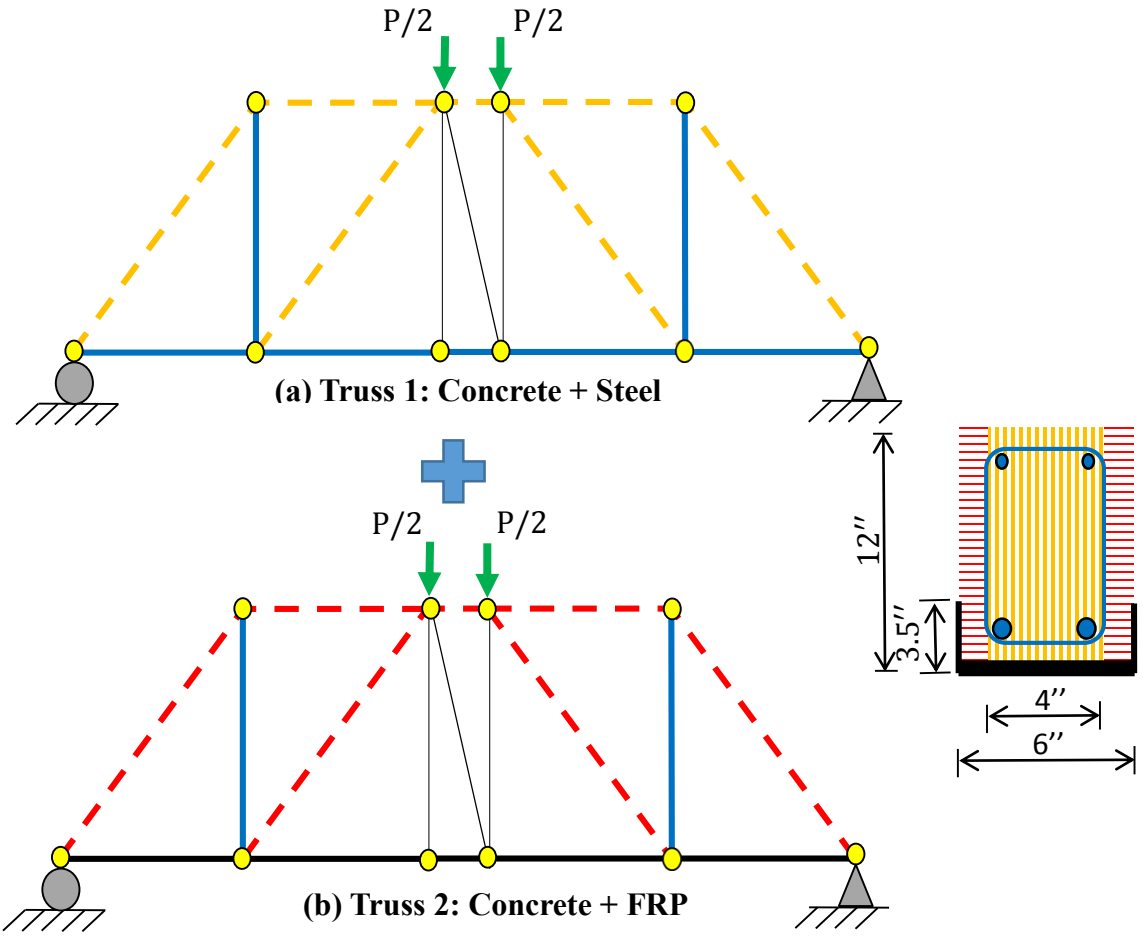

Figure 4-4 Two parallel trusses for a deep beam strengthened in flexure with CFRP

3. A strengthened deep beam is assumed to be composed of two parallel trusses. The first truss consists of the concrete core plus the steel tie and half of the steel stirrups since the concrete core is taken to the centroid of the stirrups. The second truss consists of the side concrete cover plus the FRP tie and the other half of the steel stirrups since the concrete cover is taken to the centroid of the stirrups, see Figure 4-4. The two loading stages are also used to compute the full response of the strengthened deep beam. Moreover, a compatibility equation at the maximum deflection node is applied to equate the two parallel trusses at that location. The compatibility equation is used to find the unknown shares of the two trusses at both loading stages. Figure 4-5 illustrates solution steps of the proposed approach to predict the full response of strengthened deep beam.

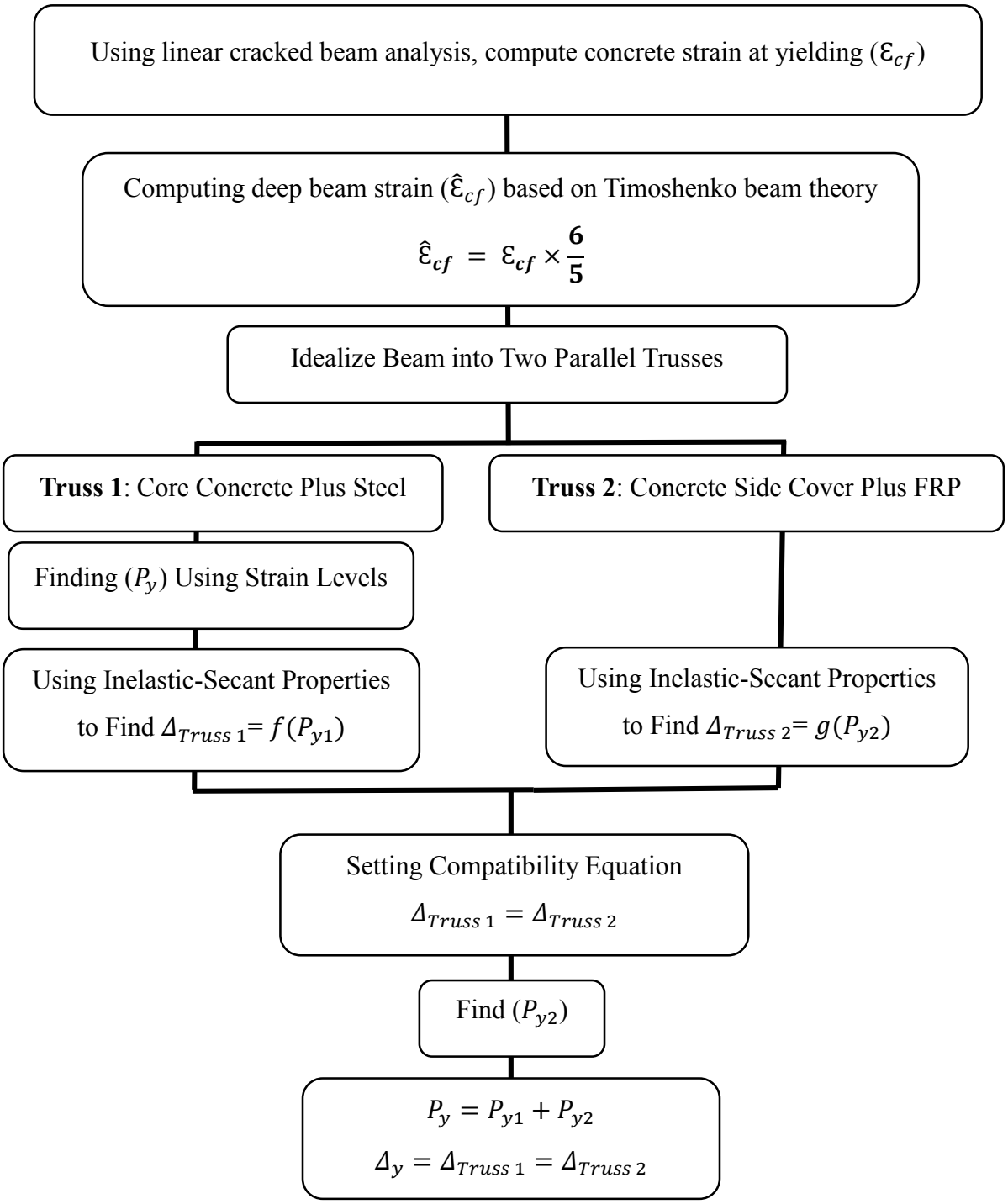

(a) Stage 1: $(P_y$ vs. $\Delta_y)$

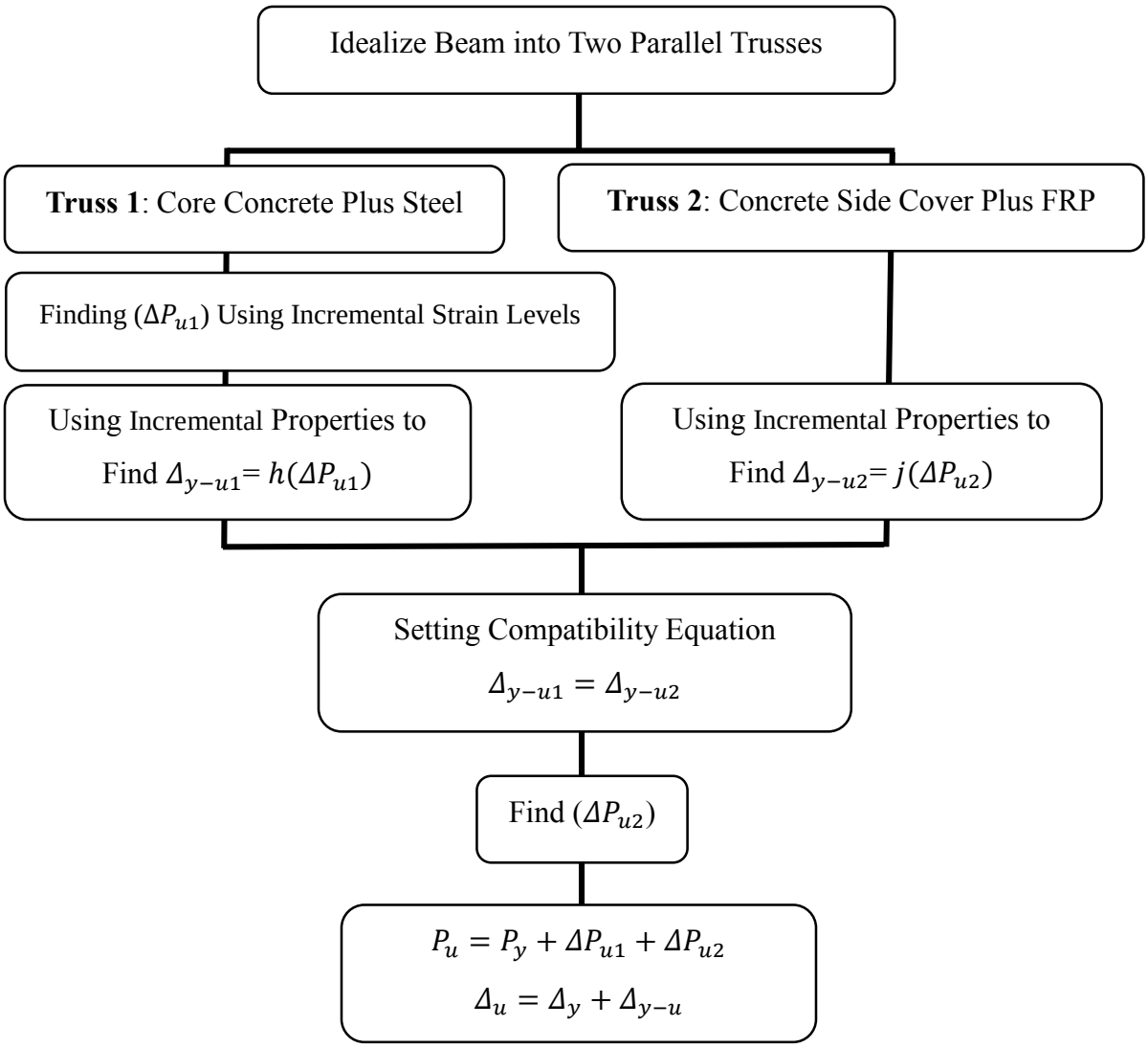

(b) Stage 2: $(\Delta \mathbf{P_u}$ vs. $\mathbf{\Delta_{y-u}})$

Figure 4-5 Flowchart of proposed approach for strengthened deep beam

4.3 Confirmation Examples

4.3.1 Beams from Experimental Program

In this section, beams (**CON**) and (**CSW-GSP**) are used to compare their analytical response of against the experimental results. The calculation steps are illustrated below:

4.3.1.1 Beam (CON)

Truss dimensions:

$T_n = A_s \cdot F_y = 2 * 0.31 * 70 = 43.4^k$

$T_n = C_n \Rightarrow 43.4 = (0.85 \cdot B_n \cdot f'_c \cdot y_c \cdot b_w) + A'_S \cdot f_y$

$43.4 = (0.85 * 1 * 5 * y_c * 6) + (0.11 * 2 * 70) \Rightarrow y_c = 1.098\ in$

$y_t = 2\left[cover + d_{stirrup} + \frac{d_b}{2}\right] = 2\left[1 + 0.375 + \frac{0.625}{2}\right] = 3.375\ in$

$j_d = h - 0.5y_c - 0.5y_t = 9.765\ in$

Using two truss panels per shear span, see Figure 4-6:

$$Strut\ angle\ (\theta) = tan^{-1}\left[\frac{9.765}{\frac{18-4}{2}}\right] = 54.36°$$

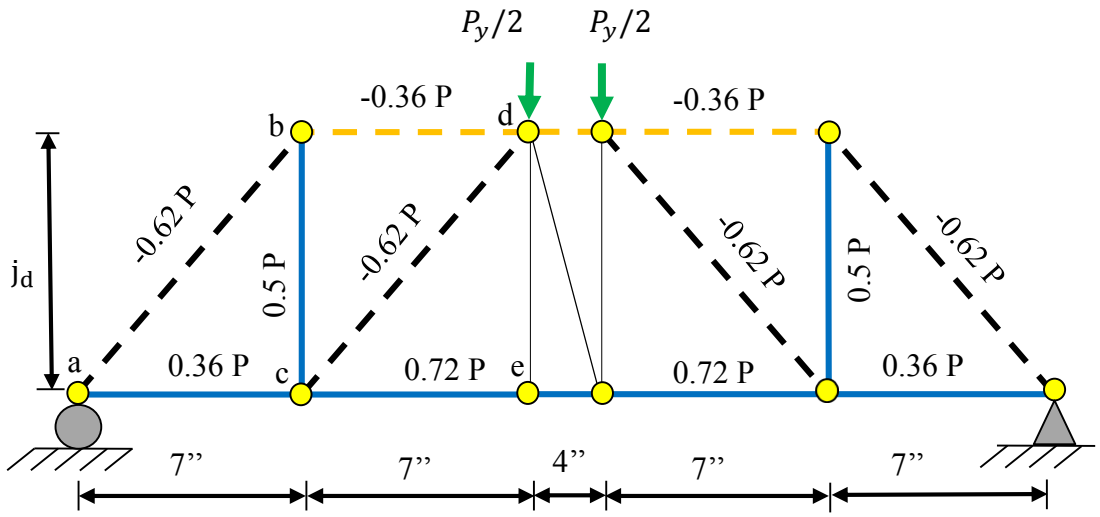

Figure 4-6 Truss model of specimen beam (CON)

Assuming linear cracked beam analysis:

$k = \sqrt{(n\rho)^2 + 2n\rho} - n\rho = 0.314 \Rightarrow kd = c = 3.24\ in$

From strain compatibility ($\varepsilon_{sy} = 0.0024$ and c = 3.24 in), this leads to $\varepsilon_{cf} = 0.0011$. This strain is for shallow beams, which does not take into account the contribution of shear deformation.

Thus, ε_{cf} is adjusted to $\hat{\varepsilon}_{cf}$ as follows:

$$\hat{\varepsilon}_{cf} = \varepsilon_{cf} \times \frac{6}{5} = 0.00132$$

Finding concrete stress at extreme fiber (σ_c):

$\acute{\varepsilon}_c = 1.7 \frac{5}{57\sqrt{5000}} = 0.0021$ strain at f'_c

$$\hat{\varepsilon}_{cf} = 0.00132 \Rightarrow \hat{\sigma}_{Cf} = 5\left[\frac{2 * 0.00132}{0.0021} - \left(\frac{0.00132}{0.0021}\right)^2\right] \Rightarrow \hat{\sigma}_{Cf} = 4.31\ ksi$$

Finding concrete elastic strain limit:

$$\sigma_{ce} = 0.7\acute{f}_c = 3.5 = \acute{f}_c\left[\frac{2\varepsilon_{ce}}{0.0021} - \left(\frac{\varepsilon_{ce}}{0.0021}\right)^2\right] \Rightarrow \varepsilon_{ce} = 0.000947$$

Finding (E_{C2}):

$\tilde{\sigma}_c = \frac{4.31+3.5}{2} = 3.905\ ksi$ and $\tilde{\varepsilon}_c = 0.001134 \Rightarrow E_{c2s} = \frac{3.905}{0.001134} = 3445.1\ ksi$

Stage 1: $(\boldsymbol{P_y\ vs.\ \Delta_y})$

$E_s = 29000\ ksi,\ E_c = 4030.51\ ksi\ ,\ E_{c2s} = 3445.1\ ksi$

From the linear secant truss analysis, see Figure 4-6:

Tie:

$$F_t = \sigma_s \cdot A_s = (E_s \cdot \varepsilon_s) \cdot A_s = 0.72P_y = (29000 * 0.0024) * 0.62 = 43.2 \Rightarrow P_y = 59.934^k$$

Inclined Strut:

Inclined strut width = Minimum (top width, bottom width), see Figure 4-7:

At top of the strut: $w_{ab} = 4" \cdot sin\theta + y_c \cdot cos\theta \Rightarrow w_{ab} = 3.9\ in$

At Bottom of the strut: $w_{ba} = 4" \cdot Sin\theta + y_t \cdot Cos\theta \Rightarrow w_{ab} = 5.2\ in$

Inclined strut capacity: $F_{ist} = \sigma_{ce} \cdot A_{dst} = (3.5) * (3.9 * 6) \Rightarrow 0.62P_y = 81.9 \Rightarrow P_y = 132.1^k$

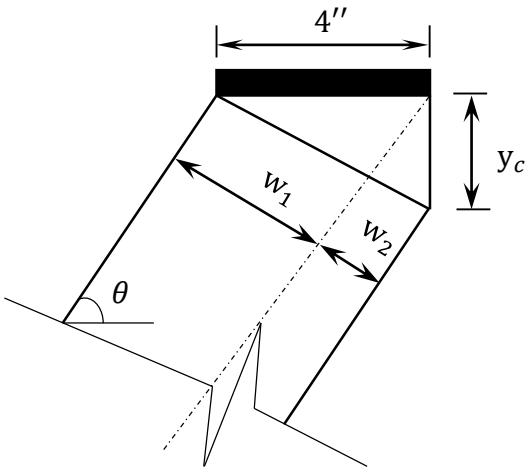

Figure 4-7 Top nodal zone of specimen beam (CON)

Horizontal Strut

Horizontal strut capacity: $F_{hst} = \tilde{\sigma}_c \cdot A_{hst} = 3.905 * (1.098 * 6) \Rightarrow 0.36P_y = 25.73 \Rightarrow P_y = 71.46^k$

Calculating (Δ_y):

$P_y = 59.934^k$

$L_{ab} = \sqrt{(9.764)^2 + 7^2} = 12.014\ in,\ L_{ac} = 7\ in$

$A_{ab} = Inclined\ strut\ depth *\ b_w = 23.34\ in^2$

$A_{bd} = Horizontal\ strut\ depth * b_w = 6.588\ in^2$

$A_{ac} = 0.31 * 2 = 0.62\ in^2$

Lumping all the stirrup areas into one vertical truss member:

$$A_{bc} = A_v * \frac{18"}{Spacing\ (5")} = 0.11 * 2 * 3.6 = 0.79\ in^2$$

$E_{c1s} = \frac{3.5}{0.000947} = 3695.9\ ksi$ and $E_{c2s} = 3445.1\ ksi$ and $E_s = 29000\ ksi$

$$\Delta_y = P_y \left[\frac{0.62^2 * L_{ab}}{A_{ab} * E_{C1s}} \times 4 + \frac{0.36^2 * L_{bd}}{A_{bd} \cdot E_{C2s}} \times 2 + \frac{0.5^2 * L_{bc}}{A_{bc} \cdot E_s} \times 2 + \frac{0.36^2 * L_{ac}}{A_{ac} \cdot E_s} \times 2 \right.$$

$$\left. + \frac{0.72^2 * L_{ce}}{A_{ce} \cdot E_s} \times 2 + \frac{0.36^2 * 4}{A_{bd} \cdot E_{c2s}} + \frac{0.72^2 * 4"}{A_{ce} \cdot E_s} \right] = 0.0678\ in$$

Stage 2: $(\boldsymbol{\Delta P_u\ vs.\ \Delta_{y-u}})$

$E_s' = 0.03E_s$ =870 ksi Rasheed (1990) **[1]**, and $\sigma_{su} = 101.5\ ksi$ (from experimental testing)

$E_{c3t} = \frac{5-3.905}{0.021-0.001134} = 1133.54\ ksi$, and $E_{c2t} = \frac{4.31-3.5}{0.00132-0.000947} = 2172\ ksi$

Tie:

$F_t = \Delta\sigma_s \cdot A_s = \left[E_s' \cdot \left(\varepsilon_{su} - \varepsilon_y\right)\right] \cdot A_s$

$F_t = [870 * (0.0386 - 0.0024)] * 0.62 \Rightarrow 0.72\Delta P_u = 19.53 \Rightarrow \Delta P_u = 27.12^k$

Inclined Strut:

Inclined strut capacity:

$F_{ist} = \Delta\sigma_c \cdot A_{ist} = \left[E_{c2t} * (\hat{\varepsilon}_{cf} - \varepsilon_{ce})\right] \cdot (w_s \cdot b)$

$F_{dst} = [2172 * (0.00132 - 0.000947)] * (3.9 * 6) = 0.62\Delta P_u = 18.91 \Rightarrow \Delta P_u = 30.498^k$

Horizontal Strut:

Horizontal strut capacity

$F_{hst} = \Delta\sigma_{cf} \cdot A_{hst} = \left[\left(E_{c3t} * (\acute{\varepsilon}_c - \tilde{\varepsilon}_c\right)\right] * (y_c \cdot b)$

$F_{hst} = [1133.54 * (0.0021 - 0.001134)] * (1.098 * 6) = 0.36\Delta P_u = 7.21 \Rightarrow \Delta P_u = 20.04^k$

$\Delta P_u = Minimum\ (\Delta P_u) =\ 20.04^k$

Calculating (Δ_u)***:***

$$\Delta_{y-u} = \Delta P_u' \left[\frac{0.62^2 * L_{ab}}{A_{ab} * E_{c2t}} \times 4 + \frac{0.36^2 * L_{bd}}{A_{bd} \cdot E_{c3t}} \times 2 + \frac{0.5^2 * L_{bc}}{A_{bc} \cdot E_s} \times 2 + \frac{0.36^2 \times 4"}{A_{bd} \cdot E_{c3t}} + \frac{0.36^2 * L_{ac}}{A_{ac} \cdot E_s} \right.$$

$$\left. \times 2 + \frac{0.72^2 * L_{ce}}{A_{ce} \cdot E_s'} \times 2 + \frac{0.72^2 * 4"}{A_{ce} \cdot E_s'} \right] = 0.407\ in$$

$\Delta_u = \Delta_y + \Delta_{y-u} = 0.0678 + 0.407 = 0.475\ in$

$P_u = P_y + \Delta P_u = 59.934 + 20.04 = 79.974^k$

Based on the calculations above, the full analytical response is compared with the experimental load-deflection curve showing very good correspondence, Figure 4-8.

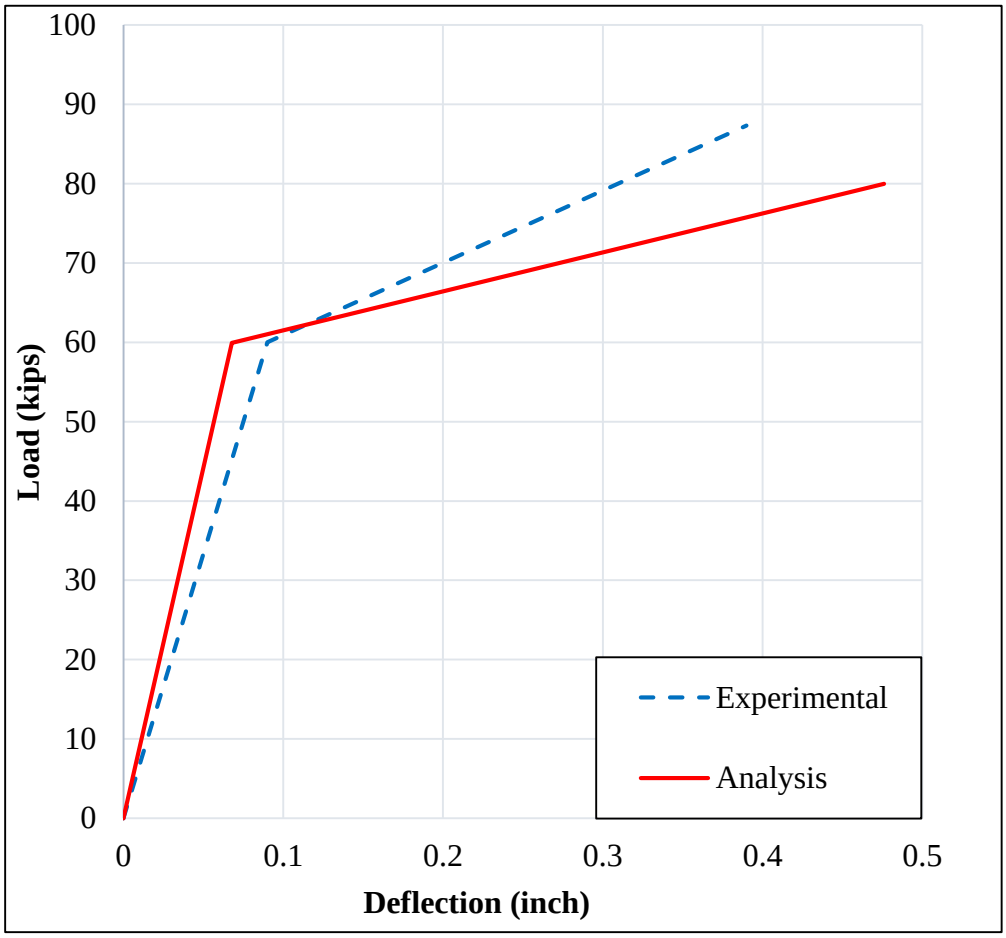

Figure 4-8 Load-deflection comparison of beam specimen (CON)

4.3.1.2 Beam (CSW-GSP)

Following the flowchart steps in Figure 4-5a to compute the yielding load of truss 1 (Figure 4-9)

$b_{w1} = 6 - 2 \times 1 - 2 \times \frac{1}{2} \times \frac{3}{8} = 3.625\ in$, and

$j_{d1} = h - 0.5 \times y_c - 0.5 \times y_{ts} = 9.404\ in$

Based on Figure 4-9:

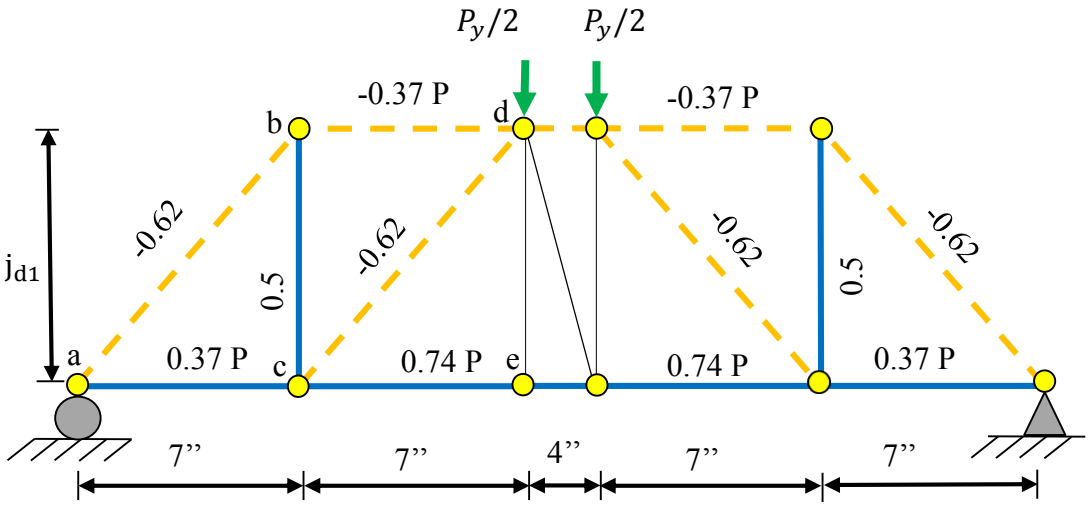

Figure 4-9 Truss 1 (concrete + steel) model of beam specimen (CSW-GSP)

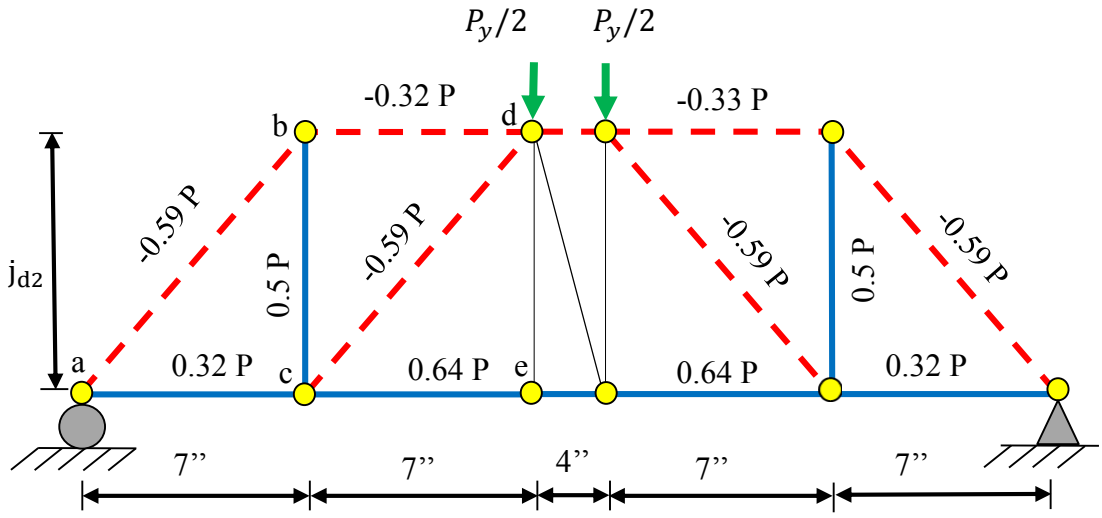

Figure 4-10 Truss 2 (concrete + CFRP) model of beam specimen (CSW-GSP)

Tie Force: $P_{y1} = 58.30^k$

Inclined Strut Force: $P_{y1} = 96^k$

Horizontal Strut Force: $P_{y1} = 75.62^k$

The yielding force of truss 1 = $P_{y1} = 58.30^k$

The second truss (Figure 4-10) has the following parameters:

$b_{w2} = 2 \times 1 + 2 \times \frac{1}{2} \times \frac{3}{8} = 2.375\ in$, and

$j_{d2} = h - 0.5 \times y_c - 0.5 \times y_{tf} = 10.935\ in$

Where $y_{tf} = 2(h - d_f) = 1.02\ in$

Based on Figure 4-9 and Figure 4-10, the compatibility equation is applied at node (d) for the two trusses:

$\Delta_{y1} = \Delta_{y2}$

Where:

$$\Delta_{y1} = P_{y1}\left[\frac{0.62^2 * L_{ab1}}{A_{ab1} * E_{c1s}} \times 4 + \frac{0.37^2 * L_{bd1}}{A_{bd1} \cdot E_{c2s}} \times 2 + \frac{0.5^2 * L_{bc1}}{A_{bc1} \cdot E_s} \times 2 + \frac{0.37^2 * L_{ac1}}{A_{ac1} \cdot E_s} \times 2 + \frac{0.74^2 * L_{ce1}}{A_{ce1} \cdot E_s} \times 2 + \frac{0.37^2 * 4}{A_{bd1} \cdot E_{c2s}} + \frac{0.74^2 * 4"}{A_{ce1} \cdot E_s}\right] = 1.53 \times 10^{-3}\ P_{y1}$$

$$\Delta_{y2} = P_{y2}\left[\frac{0.59^2 * L_{ab2}}{A_{ab2} * E_{c1s}} \times 4 + \frac{0.32^2 * L_{bd2}}{A_{bd2} \cdot E_{c2s}} \times 2 + \frac{0.5^2 * L_{bc2}}{A_{bc2} \cdot E_s} \times 2 + \frac{0.32^2 * L_{ac2}}{A_{ac2} \cdot E_f} \times 2 + \frac{0.64^2 * L_{ce2}}{A_{ce2} \cdot E_f} \times 2 + \frac{0.32^2 * 4}{A_{bd2} \cdot E_{c2s}} + \frac{0.64^2 * 4"}{A_{ce2} \cdot E_f}\right] = 2.29 \times 10^{-3}\ P_{y2}$$

$P_{y2} = 0.67\ P_{y1} = 39.06^k$

$P_y = 58.3 + 39.06 = 97.36^k$

$\Delta_y = \Delta_{y1} = 1.53 \times 10^{-3} P_{y1} = 0.09\ in$

For the second stage of loading, the incremental procedure is applied as illustrated in Figure 4-5b:

Based on Figure 4-9:

Tie Force: $\Delta P_{u1} = 1.30^k$

Inclined Strut Force: $\Delta P_{u1} = 37.61^k$

Horizontal Strut Force: $\Delta P_{u1} = 13^k$

The incremental ultimate force of truss 1 = $\Delta P_{u1} = 1.30^k$

Based on Figure 4-9 and Figure 4-10, the compatibility equation is applied at node (d) for the two trusses:

$\Delta_{y-u1} = \Delta_{y-u2}$

$$\Delta_{y-u1} = \Delta P_{u1}\left[\frac{0.62^2 * L_{ab1}}{A_{ab1} * E_{c2t}} \times 4 + \frac{0.37^2 * L_{bd1}}{A_{bd1} \cdot E_{c3t}} \times 2 + \frac{0.5^2 * L_{bc1}}{A_{bc1} \cdot E_s} \times 2 + \frac{0.37^2 * L_{ac1}}{A_{ac1} \cdot E_s} \times 2 + \frac{0.74^2 * L_{ce1}}{A_{ce1} \cdot \acute{E}_s} \times 2 + \frac{0.37^2 * 4}{A_{bd1} \cdot E_{c3t}} + \frac{0.74^2 * 4"}{A_{ce1} \cdot \acute{E}_s}\right] = 0.0244\ \Delta P_{u1}$$

$$\Delta_{y-u2} = \Delta P_{u2}\left[\frac{0.59^2 * L_{ab2}}{A_{ab2} * E_{c2t}} \times 4 + \frac{0.32^2 * L_{bd2}}{A_{bd2} \cdot E_{c3t}} \times 2 + \frac{0.5^2 * L_{bc2}}{A_{bc2} \cdot E_s} \times 2 + \frac{0.32^2 * L_{ac2}}{A_{ac2} \cdot E_f} \times 2 + \frac{0.64^2 * L_{ce2}}{A_{ce2} \cdot E_f} \times 2 + \frac{0.32^2 * 4}{A_{bd2} \cdot E_{c3t}} + \frac{0.64^2 * 4"}{A_{ce2} \cdot E_f}\right] = 3.544 \times 10^{-3}\ \Delta P_{u2}$$

$\Delta P_{u2} = 6.88\ \Delta P_{u1} = 8.944^k$

$\Delta P_u = 1.3 + 8.944 = 10.244^k$

$P_u = P_y + \Delta P_u = 97.36 + 10.24 = 107.60^k$

$\Delta_{y-u} = \Delta_{y-u1} = 0.03\ in$

$\Delta_u = \Delta_y + \Delta_{y-u} = 0.09 + 0.03 = 0.12\ in$

Based on the calculations above, the full analytical response is compared with the experimental load-deflection curve showing very good correspondence, Figure 4-11.

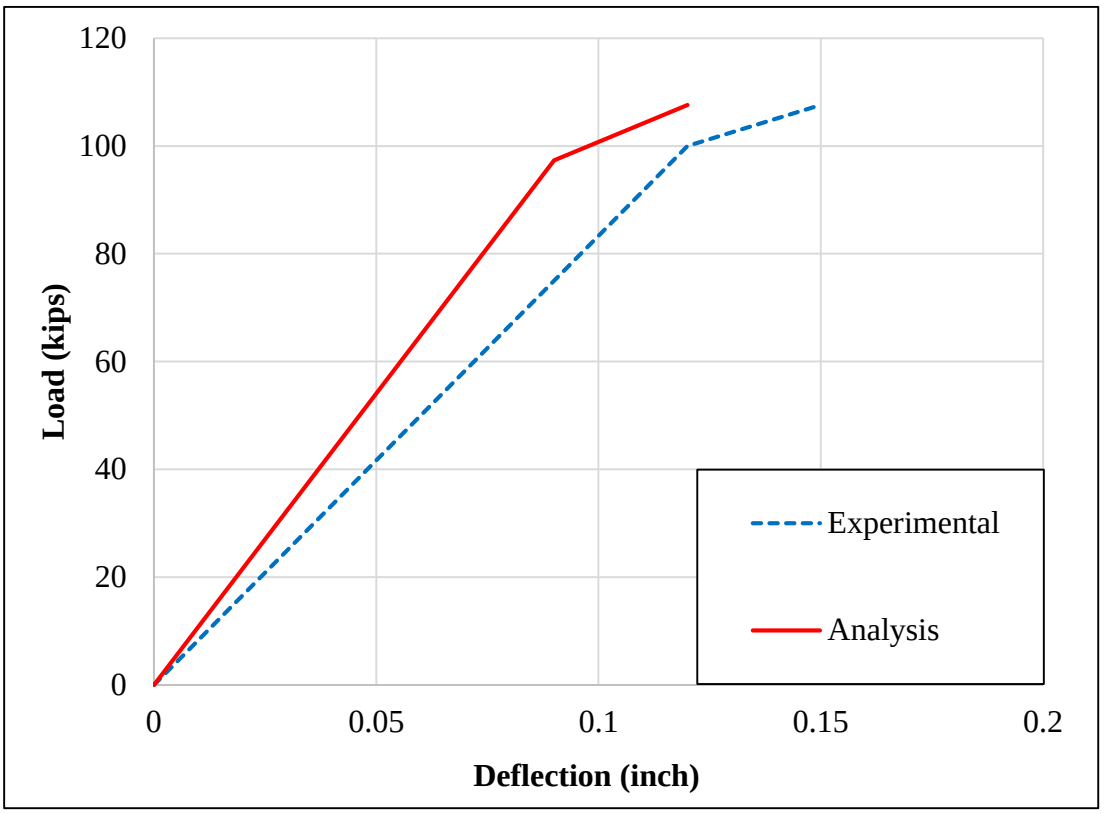

Figure 4-11 Load-deflection comparison of beam specimen (CSW-GSP)

Comparison between prediction results and experimental findings is summarised in Table 4-1.

Table 4-1 Prediction and experimental results of experimental program beams

Specimen	Experimental results				Prediction results				Comparison	
	$^{(1)}P_y$ (kips)	$^{(2)}\Delta_y$ (in.)	$^{(3)}P_u$ (kips)	$^{(4)}\Delta_u$ (in.)	$^{(5)}P_y$ (kips)	$^{(6)}\Delta_y$ (in.)	$^{(7)}P_u$ (kips)	$^{(8)}\Delta_u$ (in.)	(1)/(5)	(3)/(7)
CON	60	0.09	87.44	0.4	59.93	0.07	80	0.47	1.00	1.09
CSW-GSP	100	0.13	107.63	0.15	97.36	0.09	107.60	0.12	1.03	1.00

4.3.2 Beams from Literature

In this section, an unstrengthed beam (**Control**) and a strengthen beams (**S1**) that were tested by Pham and Al-Mahadi (2004) **[2]** are used to check the validity of the analytical approach. Typical beam setup, reinforcement details, and section properties are shown in Figure 4-12.

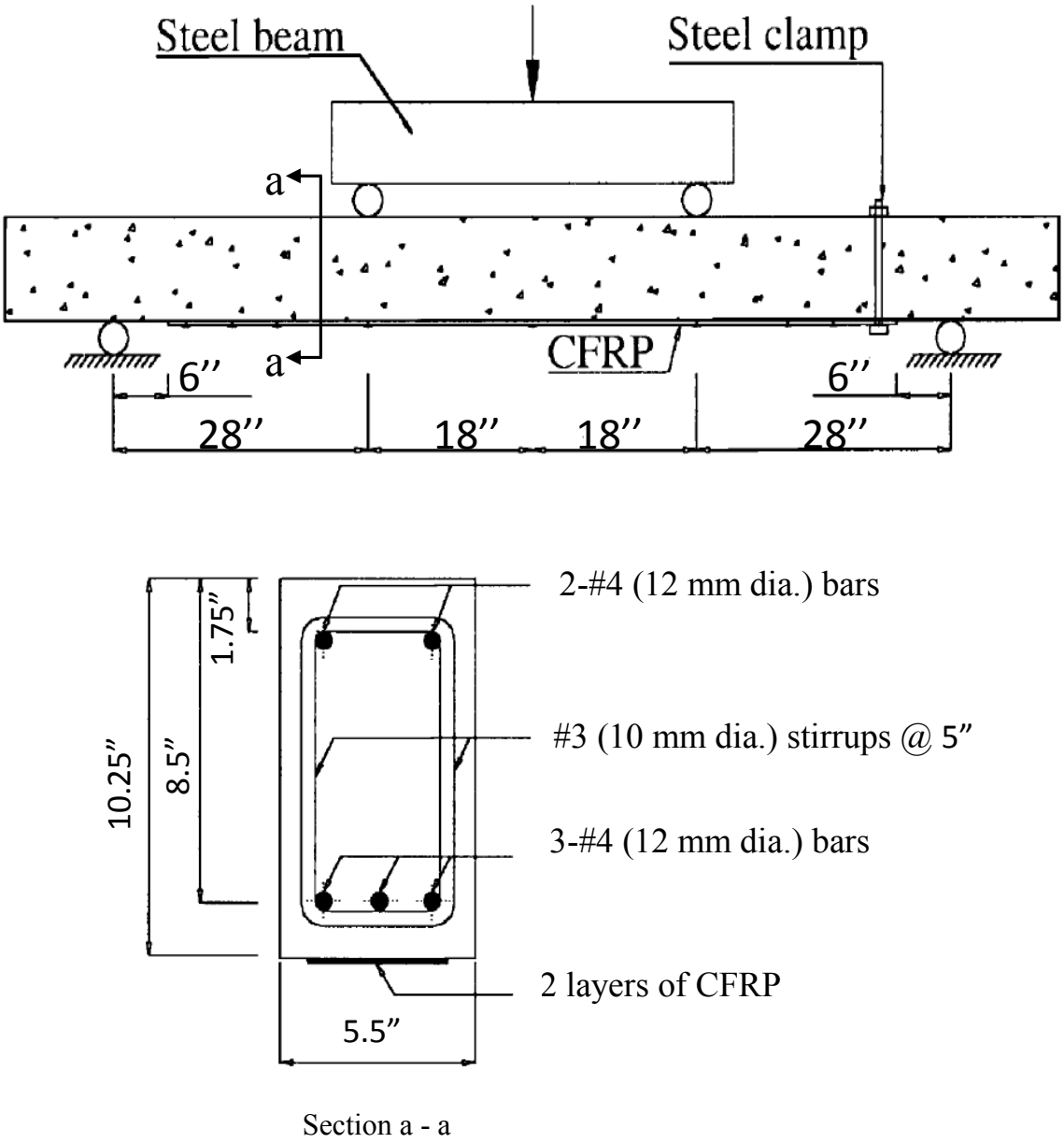

Figure 4-12 Typical beam dimensions of the literature beams

4.3.2.1 Unstrengthened Beam (Control)

Following the flowchart steps in Figure 4-3:

Stage 1: $(\boldsymbol{P_y\ vs.\ \Delta_y})$

Tie Force: $P_y = 23.66^k$

Inclined Strut Force: $P_y = 93.21^k$

Horizontal Strut Force: $P_y = 22.03^k$

Calculating $(\boldsymbol{\Delta_y})$***:***

The yielding force of the beam $(P_y) = 22.03^k$

$\Delta_y = 0.39\ in$

Stage 2: $(\boldsymbol{\Delta P_u\ vs.\ \Delta_{y-u}})$

Tie Force: $\Delta P_u = 2.07^k$

Inclined Strut Force: $\Delta P_u = 10.40^k$

Horizontal Strut Force: $\Delta P_u = 7.03^k$

Calculating $(\boldsymbol{\Delta_u})$***:***

$\Delta P_u = Minimum\ (\Delta P_u) = 2.07^k$

$\Delta_{y-u} = 0.82\ in$

$\Delta_u = \Delta_y + \Delta_{y-u} = 0.39 + 0.82 = 1.214\ in$

$P_u = P_y + \Delta P_u = 22.03 + 2.07 = 24.11^k$

Based on the calculations above, the full analytical response is compared with the experimental load-deflection curve showing very good correspondence, Figure 4-13.

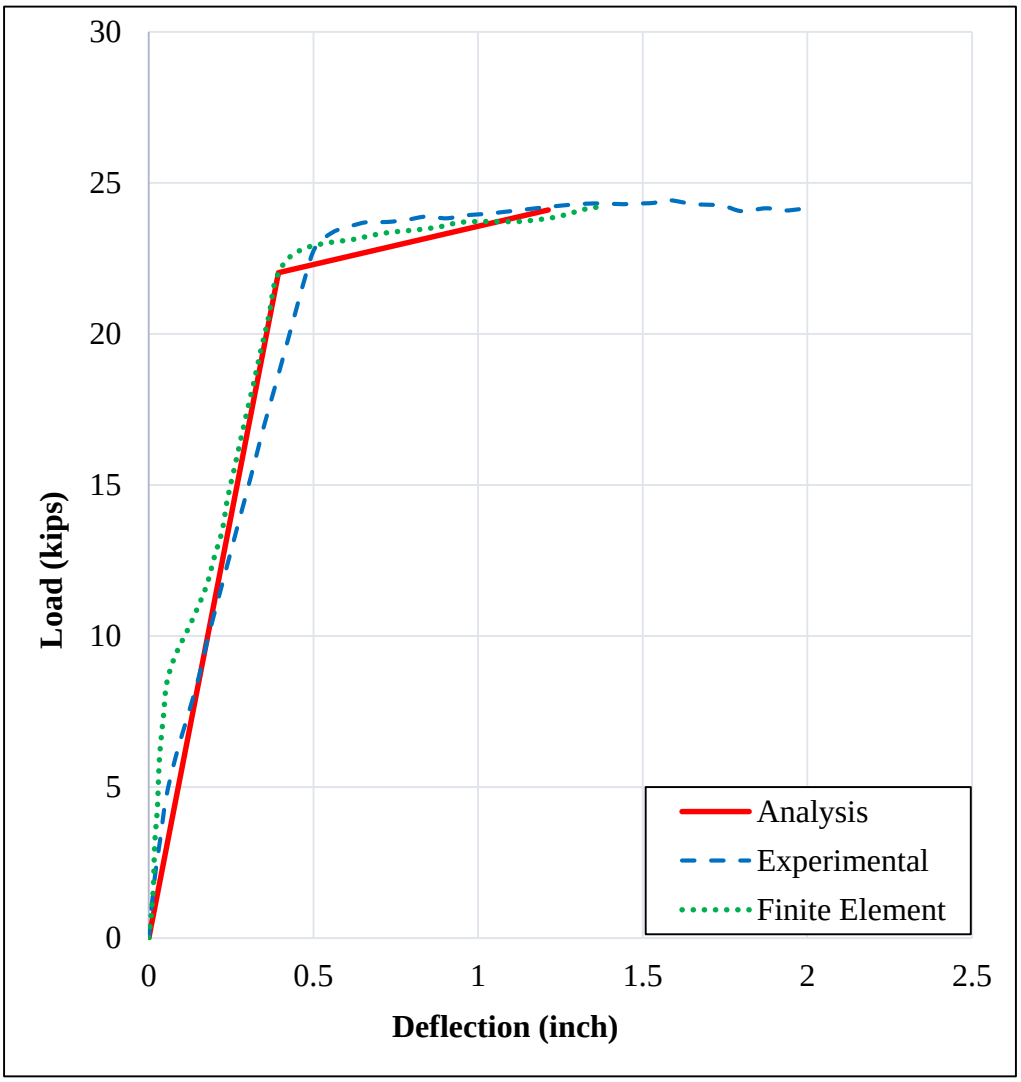

Figure 4-13 Load-deflection comparison of unstrengthened beam (Control)

4.3.2.2 Strengthened Beam (S1)

Following the flowchart steps in Figure 4-5a to compute the yielding load of truss 1:

Tie Force: $P_{y1} = 23.38^k$

Inclined Strut Force: $P_{y1} = 90.21^k$

Horizontal Strut Force: $P_{y1} = 22.76^k$

The yielding force of truss 1 = $P_{y1} = 22.76^k$

From second truss parameters, we can set the compatibility equation at the loading node for the two trusses:

$\Delta_{y1} = \Delta_{y2}$

$\Delta_{y1} = 0.019\ P_{y1}$

$\Delta_{y2} = 0.136\ P_{y2}$

$P_{y2} = 0.14\ P_{y1} = 3.19^{k}$

$P_y = P_{y1} + P_{y2} = 25.94^{k}$

$\Delta_y = \Delta_{y1} = 0.019\ P_{y1} = 0.43\ in$

For the second stage of loading, the incremental procedure is applied as illustrated in Figure 4-5b:

Tie Force: $\Delta P_{u1} = 2.18^{k}$

Inclined Strut Force: $\Delta P_{u1} = 10.61^{k}$

Horizontal Strut Force: $\Delta P_{u1} = 10.61^{k}$

The incremental ultimate force of truss 1 = $\Delta P_{u1} = 2.18^{k}$

From second truss parameters, we can set the compatibility equation at the loading node for the two trusses:

$\Delta_{y-u1} = \Delta_{y-u2}$

$\Delta_{y-u1} = 0.408\ \Delta P_{u1}$

$\Delta_{y-u2} = 0.176\ \Delta P_{u2}$

$\Delta P_{u2} = 2.312\ \Delta P_{u1} = 5.05^{k}$

$\Delta P_u = \Delta P_{u1} + \Delta P_{u2} = 7.23^{k}$

$P_u = P_y + \Delta P_u = 33.18^{k}$

$\Delta_{y-u} = \Delta_{y-u1} = 0.89\ in$

$\Delta_u = \Delta_y + \Delta_{y-u} = 1.32\ in$

Based on the calculations above, the full analytical response is compared with the experimental load-deflection curve showing very good correspondence, Figure 4-14.

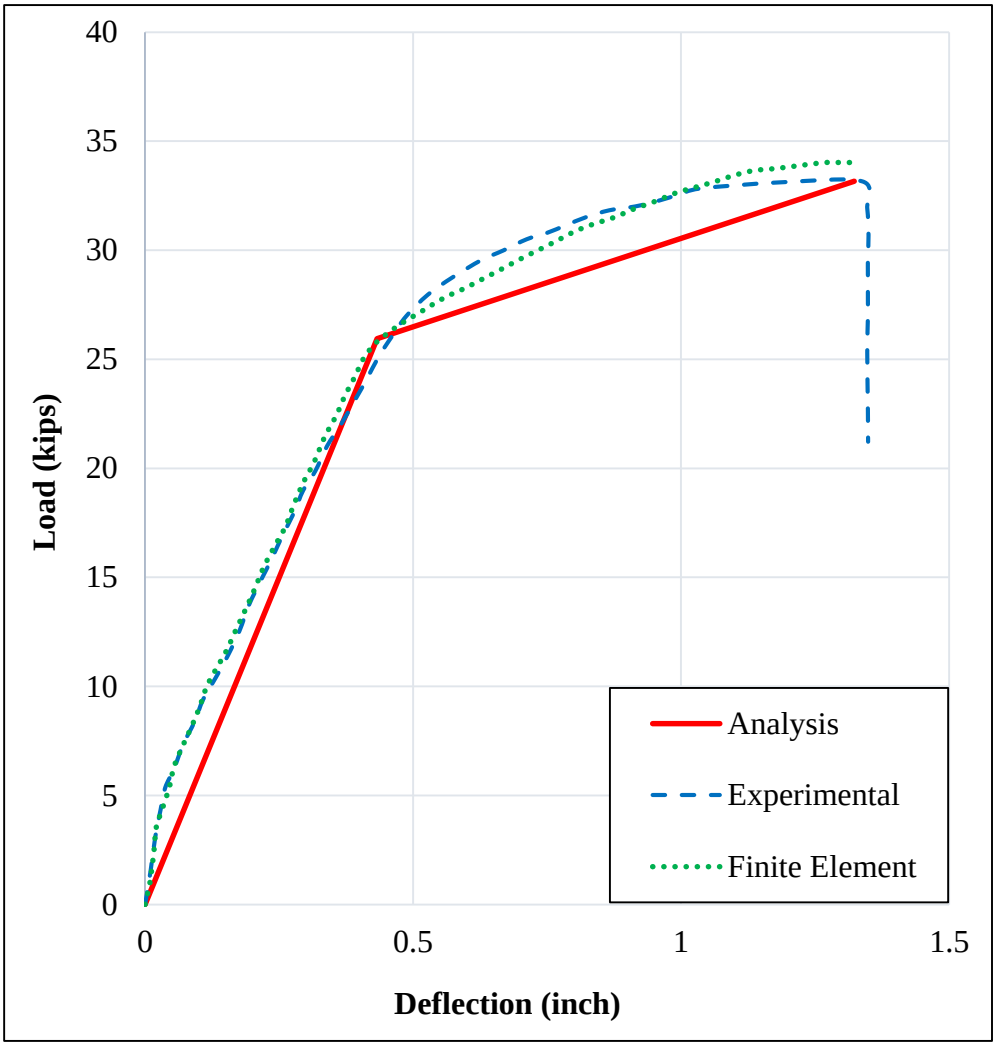

Figure 4-14 Load-deflection comparison of strengthened beam (S1)

Comparison between prediction results and experimental findings of the beams from the literature is summarised in Table 4-2.

Table 4-2 Prediction and experimental results of literature beams

Specimen	Experimental results				Prediction results				Comparison	
	$^{(1)}P_y$ (kips)	$^{(2)}\Delta_y$ (in.)	$^{(3)}P_u$ (kips)	$^{(4)}\Delta_u$ (in.)	$^{(5)}P_y$ (kips)	$^{(6)}\Delta_y$ (in.)	$^{(7)}P_u$ (kips)	$^{(8)}\Delta_u$ (in.)	(1)/(5)	(3)/(7)
Control	22.9	0.50	24.4	1.57	22	0.39	24.1	1.21	1.04	1.01
S1	27	0.47	33.2	1.34	25.9	0.43	33.2	1.32	1.04	1.00

4.4 References

1. Rasheed, H. A., 1990. *Inelastic Behavior of Reinforced Concrete Frame Structures* (M.Sc. Thesis, University of Baghdad, Iraq).
2. Pham, Huy, and Riadh Al-Mahaidi. "Experimental investigation into flexural retrofitting of reinforced concrete bridge beams using FRP composites." Composite structures 66, no. 1-4 (2004): 617-625.

Chapter 5 - Conclusions and Recommendations

5.1 General

The objective of this dissertation is to study the behavior of RC deep beams with and without flexural CFRP strengthening and the effect of an innovative anchorage devices on their capacities. This research includes an experimental program and an analytical approach. The analytical approach is extended from STM in order to predict the full response (load-deformation) and the failure capacity of these tested beams as well as to identify the failure mode involved. The analytical approach is further verified against another set of tested beams from literature. Good agreement is shown between the experimental and analytical results indicating that the flexural strengthening scheme is effective in increasing the shear capacity and improving the structural behavior of RC deep beams.

In this Chapter, conclusions obtained from experimental and analytical results are given, as well as some recommendations and suggestions for future work are presented.

5.2 Conclusions

Based on the present experimental and analytical results of reinforced concrete deep beams with and without flexural CFRP sheets made from normal strength concrete, the following conclusions can be drawn:

5.2.2 Conclusions from Experimental Work

1. It has been observed from the behavior of the tested beam specimens that the addition of well-anchored CFRP flexural sheets increase the shear capacity of the deep beams tested.
2. The reinforced concrete deep beams strengthened in flexure with CFRP sheets show a lower deflection at corresponding loads in comparison with unstrengthened beam due to the presence of CFRP sheets.

3. An increase in cracking load was observed when using flexural CFRP sheets. This increase is 160 % for reinforced concrete deep beam externally strengthened with flexural CFRP sheets and GFRP side patches as external anchorages over shear spans.
4. Experimental test results show that GFRP side bars as external anchorages are not valid anchorage devices for deep beams. The side bars work as additional longitudinal ties which lead to a decrease in the effective depth of such beams.

5.2.2 Conclusions from Analytical Work

1. The analytical approach in this study is capable of predicting for the first time the full response (load-deflection) of unstrengthened and flexure strengthened reinforced concrete deep beams with a very acceptable accuracy.
2. The present analytical model of bilinear response was sufficient in accurately tracing the shear load-deflection behavior.
3. The introduction of the deformation calculations using truss analogy was a powerful contribution of this work.
4. The comparison between the analytical and the experimental results asserted the validity of the proposed approach and the methodology developed. The maximum error in the ultimate load prediction was less than 10 %. On the other hand, the maximum error in the ultimate deflection is within 20 % since the truss does not completely represent the full beam mass.

5.3 Limitations of The Study

1. The size effect on the behavior of deep beams is not studied.
2. The applicability of the present analytical approach has been tested for beams with (L_a/d) ratios equal to 1.75 and 3.25 only.

5.4 Recommendations for Future Work

Based on the findings and conclusions of the current study, the following recommendations are made for future research work:

1. Further studies should focus on wide range of deep beam geometry, concrete cover, and different amounts of internal steel reinforcement.
2. Predicting the shear strength of RC deep beams with web skin reinforcement.
3. Studying the effect of concrete compressive strength on the behavior of lightweight aggregate concrete deep beams.
4. Experimental investigation of the behavior of RC continuous deep beams strengthened by CFRP.